DISSERTATION

In vitro differentiated osteoclasts from human induced pluripotent stem cells as a disease model for *CLCN7*-related autosomal recessive osteopetrosis

In vitro-Differenzierung von Osteoklasten aus humanen induziert pluripotenten Stammzellen als ein Krakheitsmodell für *CLCN7*-Autosomal Rezessive Osteopetrose

zur Erlangung des akademischen Grades
Doctor of Philosophy (PhD)

vorgelegt der Medizinischen Fakultät
Charité – Universitätsmedizin Berlin

von
Uta Rössler

Erstbetreuung: Prof. Dr. rer. nat. Uwe Kornak

Datum der Promotion: 28.Februar 2025

Table of contents

List of figures

List of abbreviations

aa	amino acids
ATP	adenosine triphosphate
bp	base pairs
BMP4	bone morphogenetic protein 4
CD	cluster of differentiation
cDNA	complementary deoxyribonucleic acid
CDX2	caudal-type homeobox 2
c-fms	colony-stimulating factor 1 receptor
ClC-7	chloride channel 7 protein
CLCN7	chloride channel 7 gene
c-Myc	myelocytomatosis oncogene
CRISPR	clustered regularly interspaced palindromic repeats
CSF1R	colony stimulating factor 1 receptor
CTSK	cathepsin K
DAPI	4',6-diamidino-2-phenylindole
DMEM	Dulbecco's Modified Eagle Medium
DNA	deoxyribonucleic acid
dNTP	deoxynucleoside triphosphate
EDTA	ethylenediamine tetraacetic acid
FACS	fluorescence-activated cell sorting
FCS	fetal calf serum
GAPDH	glyceraldehyde 3-phosphate dehydrogenase
gDNA	genomic DNA
h	human
HAND1	heart and neural crest derivates expressed 1
hiPSC	human induced pluripotent stem cell
IL	interleukin
Klf4	Krüppel-like factor 4
LAMP1	lysosomal-associated membrane protein 1
MAF	macrophage activating factor
MCFC	myeloid cell-forming complex
M-CSF	macrophage colony-stimulating factor
MEM	minimum essential medium
MMP	matrix metalloproteinases
NFATC 1	nuclear factor of activated T cells 1
OCT4	octamer-binding transcription factor 4
OSTM1	osteopetrosis-associated transmembrane protein 1
PBMCs	peripheral blood mononuclear cells
PBS	phosphate buffered

	saline
PCR	polymerase chain reaction
RT-PCR	reverse transcription polymerase chain reaction
RANK	receptor activator of nuclear factor-κB
RANKL	receptor activator of nuclear factor-κB ligand
RNA	ribonucleic acid
RT	room temperature
SCF	stem cell factor
Sox2	sex determining region Y-box 2
TBXT	T-box transcription factor T
TCIRG1	T cell immune regulator gene 1
TRAcP	tartrate-resistant acid phosphatase
VEGF	vascular endothelial growth factor
v-type H^+-ATPase	vacuolar-type ATP-driven proton pump
WT	wild type

1 Abstract

Autosomal recessive osteopetrosis (ARO) is a rare genetic bone disorder characterised by an increase in bone mass resulting in symptoms such as anaemia, recurrent infections, growth retardation and variable central nervous system defects. Without a curative treatment with hematopoietic stem cells, patients die within the first decade of life. ARO can be caused by mutations in the *CLCN7* gene coding for the Cl^-/H^+ exchanger ClC-7, which is highly expressed in bone resorbing osteoclasts. Loss of ClC-7 function causes an impairement of the acidification of the osteoclast's resorption lacuna, which is essential for the bone remodelling process. As patient material for diagnostic and research purpose is scarce, an adequate human disease model is of high importance.

Patient-derived human induced pluripotent stem cells (hiPSCs) have great potential for modelling diseases as they provide an unlimited source of patient cells, which can be differentiated into disease-relevant cell types. For modelling ARO, a novel and simplified osteoclast differentiation technique was developed, and the obtained cells were characterised at every differentiation step. The differentiation of hiPSCs starts with embryoid body formation to obtain mesodermal cells and the hematopoietic specification induces the continuous production of monocyte-like cells for up to nine weeks providing enough cells for several osteoclast cultures and follow-up investigations. Comparing primary blood monocytes with hiPSC-derived monocyte-like cells demonstrated a monocytic gene and surface marker expression in both cell types. Terminally differentiated osteoclasts showed the characteristic morphology, multinucleation, TRAcP expression and functionality as they were able to resorb bone and dentine. In comparison to osteoclasts differentiated from peripheral blood mononuclear cells, hiPSC osteoclasts were larger in size with a slightly higher number of nuclei and minimal changes in the resorption pattern were evident.

To demonstrate the ARO disease phenotype *in vitro*, patient-derived hiPSCs harbouring compound heterozygous mutations in the *CLCN7* gene were differentiated into osteoclasts, which were enlarged compared to hiPSC osteoclasts from healthy donors and not able to resorb any bone or dentine. Additional functional analyses of ARO hiPSCs and the mutated ClC-7 protein revealed an enhanced level of the autophagy marker LC3-II in ARO hiPSCs and strongly reduced ion currents in the mutated chloride channel despite the physiological localisation of mutated ClC-7 in lysosomes. Hence, it is

assumed that patient-specific mutations result in a loss-of-function effect responsible for the severe phenotype and the death of the patient.

Overall, osteopetrotic hiPSCs and this innovative osteoclast differentiation technique provide a good disease model system for ARO and could also be utilised to examine osteoclasts morphology and function in other diseases when applying to a patient-specific hiPSC line.

2 Zusammenfassung

Autosomal-rezessive Osteopetrose (ARO) ist eine schwere genetische Knochenerkrankung, die sich durch eine erhöhte Knochenmasse auszeichnet und zu Symptomen wie Anämie, wiederkehrenden Infektionen, Wachstumsverzögerung und verschiedenen Defekten des zentralen Nervensystems führt. Falls keine kurative allogene Stammzelltransplantation erfolgt, verläuft die Krankheit innerhalb der ersten zehn Lebensjahre tödlich. ARO kann durch Mutationen im *CLCN7*-Gen verursacht werden, das für den Cl^-/H^+-Austauscher ClC-7 codiert. Dieser ist an der Bürstensaummembran von knochenresorbierenden Osteoklastenzellen hoch exprimiert und Mutationen beeinträchtigen den Ansäuerungsprozess der Resorptionslakune, welcher lebensnotwendig ist für den kontinuierlichen Knochenumbauprozess. Da primäres Patientenmaterial oft sehr limitiert ist, wird ein geeignetes ARO-Krankheitsmodell benötigt.

Vom Patienten stammende humane induzierte pluripotente Stammzellen (hiPS) stellen eine unbegrenzte Quelle von patientenspezifischen Zellen dar und können in krankheitsrelevante Zelltypen differenziert werden. Es wurde eine neuartige Methode zur hiPS-Osteoklastendifferenzierung entwickelt und detailiert charakterisiert. Die hiPS-Differenzierung wird über die Bildung von Embryoid Bodies initiiert und in die mesodermale Richtung geleitet, um anschließend mit Hilfe einer hämatopoetischen Spezifizierung die kontinuierliche Freisetzung von monozytenähnlichen Zellen hervorzurufen. Diese bis zu neun Wochen lange kontinuierliche Zellproduktion ermöglicht eine Vielzahl von experimentellen Untersuchungen. Die differenzierten hiPS-Osteoklasten zeigten die zelltypischen Merkmale: a) eine hohe Anzahl an Zellkernen, b) eine positive TRAcP-Färbung und c) die Resorption von Knochen. In einem detaillierten Vergleich mit aus zirkulierenden Monozyten differenzierten Osteoklasten waren die hiPS-Osteoklasten vergrößert, wiesen eine leicht erhöhte Anzahl von Zellkernen auf und zeigten ein leicht verändertes Resorptionsmuster.

Um den osteopetrotischen Phänotyp *in vitro* zu demonstrieren, wurden hiPS eines ARO-Patienten mit compound heterozygoten Mutationen im *CLCN7*-Gen zu Osteoklasten differenziert, die im Vergleich zu hiPS-Osteoklasten gesunder Spender vergrößert waren und kein Knochen resorbieren konnten. Funktionale Analysen der ARO hiPS und dem

mutierten ClC-7-Protein ergaben eine erhöhte Konzentration des Autophagiemarkers LC3-II sowie stark reduzierte Ionenströme im mutierten Chloridkanal obwohl eine physiologische Lokalisierung des mutierten ClC-7 in Lysosomen detektiert wurde. Es wird daher angenommen, dass die patientenspezifischen Mutationen im *CLCN7*-Gen zu einem Loss-of-Function-Effekt führten, der für den schweren Phänotypen und den Tod des Patienten verantwortlich war. Insgesamt ist diese innovative Osteoklastendifferenzierungstechnik in Verbindung mit einer Patienten-hiPS Linie ein gutes *in vitro* Krankheitsmodell für die ARO und könnte auch bei weiteren osteoklastenbasierten Krankheiten Verwendung finden.

3 Introduction and current state of research

The bone is a rigid and yet dynamic tissue and comes in a variety of shapes and sizes within the body of vertebrate animals. It supports the body, protects organs, and enables movement. Furthermore, the bone plays a crucial role in hematopoiesis and provides the bone marrow “niche” for hematopoietic stem cell maintenance. The bone itself consists of a flexible organic bone matrix mainly composed of collagen fibres and a mineral called calcium hydroxyapatite. The three main bone cells responsible for bone growth, bone remodelling and fracture healing are osteocytes, osteoblasts, and osteoclasts. The osteoblast is responsible for bone matrix formation and mineralisation, whereas the osteoclast resorbs old or damaged bone. The osteocyte receives as well as transduces mechanical stimuli and regulates the differentiation and function of osteoblasts and osteoclasts (Freemont, 1993; Seeman and Delmas, 2006).

3.1 The bone remodelling process and osteoclast biology

Bone undergoes a lifelong remodelling process to maintain its strength and mineral homeostasis. An initiating remodelling signal is sensed by osteocytes and causes the recruitment of osteoclast precursor cells from the circulation (Bonewald, 2007), which start to differentiate into large multinucleated cells and get activated. They migrate and attach to the bone surface after removal of the bone lining cells, which are quiescent osteoblasts. By secreting hydrogen ions and enzymes such as matrix metalloproteinases and cathepsin K, the organic bone matrix is digested, and the bone mineral is dissolved (see figure 1). After bone resorption, monocytes, osteocytes and pre-osteoblasts are recruited for bone formation (Katsimbri, 2017). Differentiated osteoblasts start to synthesise new matrix mostly consisting of type I collagen, which fills up the cavity. During bone mineralisation, osteoblasts become quiescent bone lining cells covering the newly made bone surface. Buried osteoblast cells terminally differentiate into osteocytes. Engulfed in the bone matrix, osteocytes change shape into dendritic-like cells, which build up a canalicular network for interacting with other osteocytes and bone lining cells on the surface (Katsimbri, 2017).

The bone-resorbing osteoclast was identified as being of hematopoietic origin (Walker, 1975). After differentiating from the monocyte-macrophage lineage, mononuclear osteoclast precursor cells fuse into large multinucleated cells. This process is based on the signalling through c-fms, which binds M-CSF (macrophage colony stimulating factor) secreted by osteoblasts. The presence of M-CSF triggers the expression of the receptor RANK (receptor activator of nuclear factor-κB) on the osteoclast precursor cell surface (Arai et al., 1999). When RANKL (RANK ligand) binds to its receptor, the maturation and fusion of osteoclast precursors into multinucleated osteoclasts is induced. The two cytokines M-CSF and RANKL are crucial for osteoclast survival, differentiation and expansion (Boyle et al., 2003; Mellis et al., 2011). A mature osteoclast needs to fulfill specific properties to be defined as such: multinucleation, the expression of tartrate-resistant acid phosphatase (TRAcP), the formation of an actin ring and the ability to resorb bone and mineralised matrix, which is unique, as osteoclasts are the only bone-resorbing cells in the body (Cappariello et al., 2014; Katsimbri, 2017).

For osteoclast-mediated bone resorption, the osteoclast needs to become polarised by binding to the bone matrix. Podosomes, consisting of an actin core surrounded by integrins and cytoskeletal proteins (see figure 1), are formed, first as single foot-like stuctures and later as a podosome belt sealing the osteoclast to the bone surface (sealing zone) (Cappariello et al., 2014; Katsimbri, 2017; Saltel et al., 2008). The cell membrane facing the bone surface is called a ruffled border, which possesses an outer “fusion zone” and the inner “uptake zone” (see figure 1) (Mulari et al., 2003). The resorption mechanism takes place extracellularly through the secretion of acids and enzymes into the resorption lacuna, which is tightly sealed by the sealing membrane (Cappariello et al., 2014). The ruffled border is densely packed with membrane proteins such as v-type H^+-ATPase (vacuolar-type adenosine triphosphate driven proton pump), which releases protons into the resorption lacuna (Chatterjee et al., 1992; Forgac, 1999; Frattini et al., 2000), and the chloride channel 7 (ClC-7) together with its β-subunit OSTM1 (osteopetrosis-related transmembrane protein 1) which exchange chloride ions with protons (Graves et al., 2008; Kornak et al., 2001; Lange et al., 2006) (see figure 1). This acidification of the resorption lacuna demineralises the bone matrix and exposes the organic components like collagen type I. In order to degrade the organic bone components, lysosomes fuse with the cell membrane in the fusion zone of the ruffled border and release lysosomal enzymes mainly composed of cathepsin K, TRAcP and matrix metalloproteinases into

the resorption lacuna (Baron et al., 1988; Cappariello et al., 2014) (see figure 1). Decomposed collagen fragments as well as calcium and phosphate are endocytosed via the "uptake zone" (Mulari et al., 2003), transported through the osteoclast by transcytosis and released again through the "functional secretory domain" into the extracellular space (Cappariello et al., 2014; Katsimbri, 2017; Stenbeck and Horton, 2004) (see figure 1).

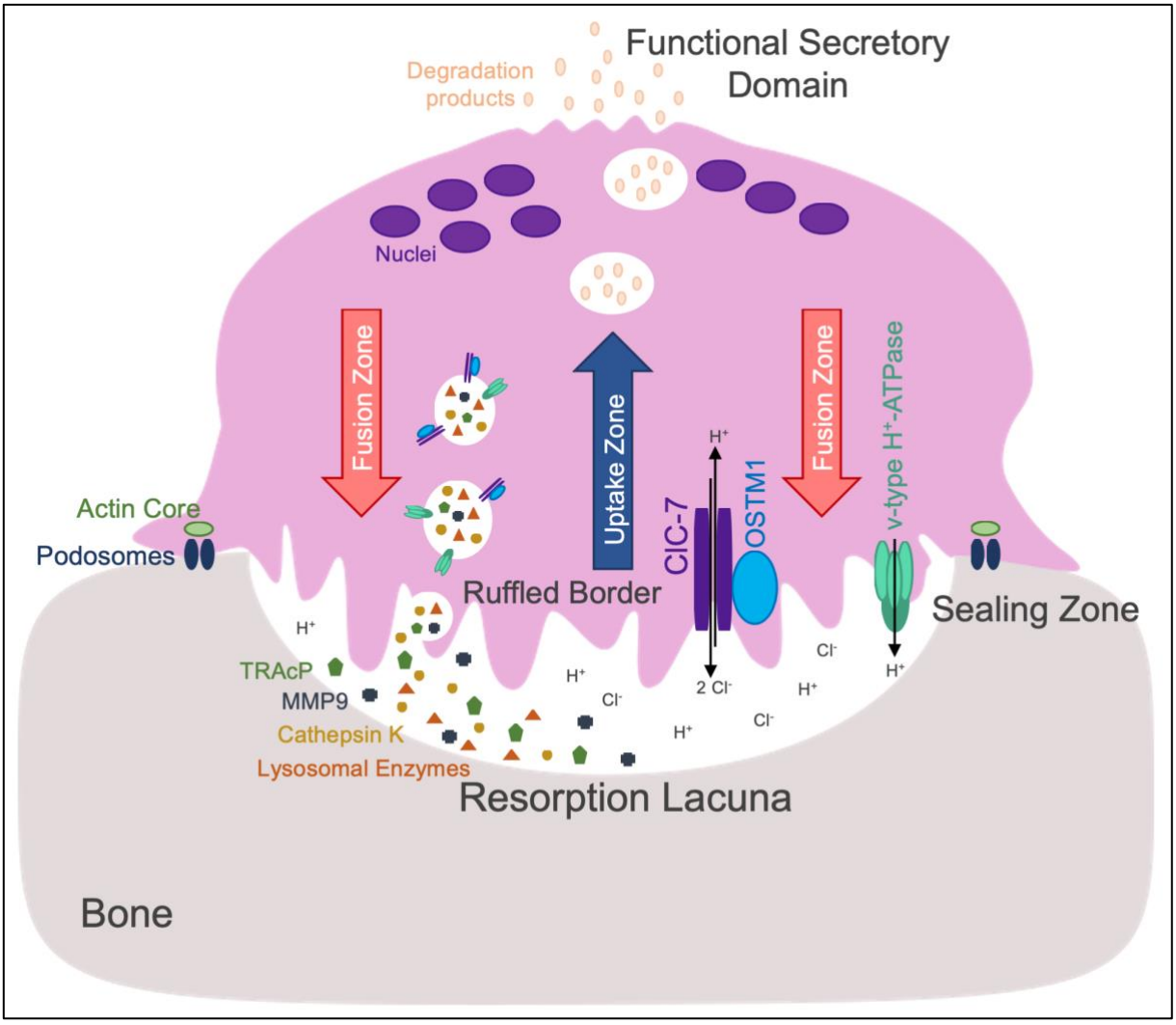

Figure 1: Schematic illustration of bone resorption by an osteoclast.

The osteoclast is attached to the bone via a podosomal belt forming the sealing zone. Acidification of the bone takes place within the resorption lacuna. In the fusion zone lysosomal enzymes are released and protons and chloride ions are transported by v-type H^+-ATPase and the ClC-7/OSTM1 complex. Degradation products of the inorganic and organic bone matrix are shuttled through the osteoclast (uptake zone) and released at the functional secretory domain. (in accordance to Cappariello et al., 2014; Coudert et al., 2015)

Two main bone resorption patterns of osteoclasts exist. Round excavations are called pits and can occur either as single pit or as a cluster of several pits adjacent to each other.

Osteoclasts in “pit mode” build up a sealing zone surrounding the ruffled border, secrete resorption factors and take up resorption products before they rearrange their cytoskeleton and migrate to the next resorption side, leaving behind a pit in the bone surface (Georgess et al., 2014; Lakkakorpi and Väänänen, 1991; Søe and Delaissé, 2017). However, osteoclasts also form elongated continuous resorption cavities referred to as trenches. The osteoclast in “trench mode” moves over the bone surface during its resorption activity. Despite the movement, the sealing zone is continuously displaced but not disrupted or rebuilt at any time. For lateral resorption, the ruffled border is orientated to the front wall of the cavity, where resorption and uptake takes place (Søe and Delaissé, 2017). The “trench mode” is the more aggressive way of resorption, as it is faster, trenches are deeper and the expression of cathepsin K is higher (Merrild et al., 2015; Søe et al., 2013; Søe and Delaissé, 2017). Whether or not osteoclasts use pit formation or trench formation as the preferred resorption mode depends on several factors, including the presence of other cells in the osteoclast microenvironment, the cathepsin K expression, collagenolytic activity, the skeletal site, as well as age and gender of the individual (Merrild et al., 2015; Søe et al., 2013). In functionally impaired osteoclasts, a third type of resorption can be observed, which is only superficial, shows no defined edges and is called pseudoresorption (Howaldt et al., 2020).

3.2 Autosomal recessive osteopetrosis

Osteopetrosis is a group of rare genetic skeletal diseases characterised by impaired bone resorption. Depending on the disease-causing mutation, the mode of inheritance, the severity, and the age of onset, different forms of osteopetrosis are distinguished. The most frequent autosomal dominant type (also called Albers-Schönberg disease) usually displays a skeletal sclerosis, a modelling defect, an onset in childhood, and complications arise in only a subset of affected individuals (Bénichou et al., 2000; Albers-Schönberg, 1904). The more severe form is autosomal recessive osteopetrosis (ARO), which is typically diagnosed within the first months of life and is lethal when left untreated. Patients suffer from a variety of complications. Due to bone resorption failure, bones show an increase in mass and at the same time extreme brittleness. Growth retardation, recurrent infections and anaemia are characteristic symptoms, however these common symptoms are coupled with neurological defects caused by cranial nerve compression, leading to

deafness and progressive loss of vision. The bone marrow failure results from the reduction of the bone marrow space in the long bones of the patients (Coudert et al., 2015; Sobacchi et al., 2013). So far, a hematopoietic stem cell (HSC) transplantation is the only curative treatment option, as defective osteoclasts differentiate from the hematopoietic lineage (Walker, 1975). Donor cells can repopulate the bone marrow and thereby rescue the disease phenotype, if performed early in life. For this, it is necessary to identify the disease-causing mutation and the associated pathomechanism, as mutations affecting the osteoclast differentiation process indirectly, for example all *RANKL*-related types of ARO, cannot be overcome by a transplantation of HSCs (Penna et al., 2019; Sobacchi et al., 2013).

At least seven different genes are known to cause autosomal recessive osteopetrosis when mutated (Coudert et al., 2015; Sobacchi et al., 2013). The most prevalent mutated gene is called *TCIRG1* (T cell immune regulator gene 1) coding for a subunit of the v-type H^+-ATPase, which is highly expressed at the ruffled border of osteoclasts and transports protons into the resorption lacuna. This loss-of-function mutation hampers the acidification process and thus disrupts the balance of the bone remodelling cycle (Frattini et al., 2000). About 10% to 15% of all ARO cases are caused by a mutation in the *CLCN7* gene and 2% to 5% are associated with mutations in the *OSTM1* gene. OSTM1 is a β-subunit for ClC-7 and due to its highly glycosylated N-terminus it is protected from degradation by lysosomes (Lange et al., 2006). Both proteins together form a $2Cl^-/H^+$ antiporter (Graves et al., 2008), which is highly expressed in lysosomes and late endosomes, as well as in the acid-secreting ruffled border of osteoclasts due to the exocytic insertion of lysosomal membranes (Kornak et al., 2001). Mutations in each protein result in osteopetrosis as the absence of chloride ions in the resorption lacuna impairs the acidification of bone matrix. Furthermore, studies in mice showed that the osteoclasts' ruffled border of *Clcn7*-knockout mice is underdeveloped (Kornak et al., 2001), suggesting that defective lysosomal trafficking and fusion contribute to the osteopetrotic phenotype (Jentsch and Pusch, 2018).

In some patients, mutations in *CLCN7* and *OSTM1* are additionally associated with neuronopathic symptoms such as seizures, developmental delay, hypotonia and primary retinal atrophy as sequelae of primary neurodegeneration (Sobacchi et al., 2013). Different *Clcn7*-knockout mouse models show an osteopetrotic phenotype together with a progressive neurodegeneration in the brain and retina (Kornak et al., 2001; Lange et

al., 2006). Further studies revealed a lysosomal storage disease characterised by storage material and accumulations of mitochondrial ATP synthase in lysosomes, as well as neuronal cell loss in various brain regions accompanied by inflammatory responses in the brain (Kasper et al., 2005). Even though ClC-7/OSTM1 are involved in maintaining the acidic pH in lysosomes, *Clcn7*-knockout mouse cells display no changes in lysosomal pH (Kasper et al., 2005; Steinberg et al., 2010). However, lysosomal protein degradation is impaired, and it is assumed that not just the pH, but that the chloride itself has an impact on lysosomal enzyme activity. Furthermore, a trafficking problem between endosomal and lysosomal compartments is suspected (Wartosch and Stauber, 2010). Overall, these studies in mice lead to the assumption that the resulting severe neurological problems can shorten life expectancy not only of the knockout mice but also of ARO patients harbouring mutations in the *CLCN7* or *OSTM1* gene. A hematopoietic stem cell transplantation can save the patient's life, but in this specific subtype of osteopetrosis, may not prevent blindness and neurodegeneration (Kasper et al., 2005).

3.3 Human induced pluripotent stem cells and their differentiation into osteoclasts

The detection of the Yamanaka factors revolutionised the world of medical research. In the year 2006, Shin'ya Yamanaka discovered that with the transient expression of the four transcription factors c-Myc (myelocytomatosis oncogene), Klf4 (Krüppel-like factor 4), Oct4 (octamer-binding transcription factor 4) and Sox2 (sex determining region Y-box 2) a non-pluripotent somatic cell could be converted into a pluripotent stem cell, which is called an induced pluripotent stem cell (iPSC) (Takahashi and Yamanaka, 2006). The process is called reprogramming and today, the most common technique uses a Sendai virus for transducing the cells with the Yamanaka factors. iPSCs have many valuable features in common with embryonic stem cells, such as the potential for infinite cell division and the differentiation into a large number of cell types. Hence, iPSCs are a source of cells that can be used not only to study the mechanism of disease, but also to test therapeutic approaches, to repair damaged tissue or even to replace whole organs in the far future.

Human induced pluripotent stem cells (hiPSCs) can be generated from many primary cells. Most commonly used are leukocytes, skin fibroblasts, and urine sediment cells.

Patient-specific hiPSCs can be used for studying disease mechanisms and developing therapy strategies if it is possible to differentiate hiPSCs into disease-relevant cell types. As autosomal recessive osteopetrosis is caused by dysfunctional osteoclasts, the use of patient-derived hiPSC depends on methods for their differentiation into osteoclasts allowing for studies of their resorption behavior and the ARO pathomechanism *in vitro*. Differentiation techniques for generating osteoclasts from blood-derived monocytes are well established. However, only a few protocols for differentiating osteoclast from hiPSCs have been published and some of the procedures are very complex with up to seven steps including a number of time-consuming selection processes. The described protocols utilise multiple expensive differentiation media, cytokines and small molecules (Chen et al., 2017; Choi et al., 2009; Cui et al., 2019; Grigoriadis et al., 2010). Additionally, the efficiencies of the differentiation procedures were either not specified at all or were rather low. For example, Cui et al. (2019) presented a very low osteoclast differentiation efficiency of 1.5%.

3.4 Aim of this PhD project

As autosomal recessive osteopetrosis is usually diagnosed within the first year of life, primary patient material is often scarce. Also, primary monocytes cannot be propagated *in vitro* and transport of blood samples over long distances affects the viability and differentiation potential of the cells. Due to these limitations, only a limited number of experiments are possible, being mostly performed for diagnostic purposes. Furthermore, the use of animal models is limited due to ethical reasons and species differences. The aim of this study was to develop a disease model system for autosomal recessive osteopetrosis using hiPSCs to overcome these limitations and gain more insights into the pathomechanism of *CLCN7*-related osteopetrosis.

To create a disease model for osteopetrosis, an hiPSC-based osteoclast differentiation protocol needed to be established first. Already published osteoclast differentiation protocols were time-consuming, labour intensive, expensive, and inefficient in terms of osteoclast yield. Lachmann et al. published a macrophage differentiation protocol which included a large-scale monocyte-like cell production step (Lachmann et al., 2015) and a similar procedure starting with a feeder-free hiPSC culture was shown by Buchrieser et al. (Buchrieser et al., 2017). Based on these two publications, a new hiPSC-derived

osteoclast differentiation technique was to be developed aiming for a high differentiation efficiency, a feasible procedure, and the least possible use of expensive components. The differentiated cells were to be characterised with regard to their differentiation status at different stages of development and the resulting hiPSC osteoclasts were to be compared to primary monocyte-derived osteoclasts.

I contributed to the generation of an ARO hiPSC line from patient-derived blood cells habouring mutations in the *CLCN7* gene in cooperation with the BIH iPS Core Facility (Hennig et al., 2019). As this osteopetrosis patient showed a particular severe course of the disease, functional investigations of the ARO hiPSCs were performed to get insights into the cellular dysfunctions caused by the patient-specific mutations. The most striking defect in osteopetrosis is the inability of osteoclasts to resorb the bone matrix. Hence, ARO hiPSCs were differentiated into hiPSC-derived osteoclasts and characterised in comparison to hiPSC osteoclasts from healthy individuals.

4 Methodology

In the following, an overview is given about the principles of the methods and protocols used in my PhD project. For a detailed description and listing of materials see the publication “Efficient generation of osteoclasts from human induced pluripotent stem cells and functional investigations of lethal *CLCN7*-related osteopetrosis” itself and supplementary information provided by the Journal of Bone and Mineral Research.

4.1 Maintenance and osteoclast differentiation of hiPSCs

For osteoclast differentiation experiments and characterisation a total of eight different hiPSC lines were used. BIHi001-A, BIHi004-A, 10211.EURCC, isWT1.14 and isWT7.21 were generated from healthy control donors, whereas BIHi002-A, BIHi002-B and BIHi002-C originated from an osteopetrosis patient harbouring compound heterozygous mutations in the *CLCN7* gene (Hennig et al., 2019). These hiPSC lines belong either to the BIH Stem Cell Core Facility (Harald Stachelscheid) in Berlin or the Stem Cell Unit (Lukas Cyganek) at University Medical Center Göttingen. All hiPSC lines were cultured in Essential 8 medium in Geltrex-coated dishes in a humified normoxic incubator at 37 °C and 5% CO_2 and passaged in colonies using 0.5 mM EDTA following standard procedures (for detailed description see Rössler et al., 2021).

At least three days prior to the differentiation, cells were transferred from Essential 8 to mTeSR™1 medium (Stemcell Technologies). The first step of differentiation, the formation of embryoid bodies, was induced by harvesting single cells with TrypLE™ Select (Life Technologies) enzyme treatment and seeding 1.25 x 10^4 cells per 96-well into an ultra-low-attachment plate. After four days of mesodermal induction using the cytokines hSCF (human stem cell factor, 20 ng/mL), hBMP4 (human bone morphogenetic protein 4, 50 ng/mL) and $hVEGF_{165}$ (human vascular endothelial growth factor-165, 50 ng/mL) and 10 μM Rock-inhibitor Y-27632, embryoid bodies were harvested and seeded into cell culture dishes in X-VIVO 15 medium supplemented with hIL3 (human interleukine 3, 25 ng/mL), hM-CSF (human macrophage colony stimulating factor, 100 ng/mL) and 55 μM 2-mercaptoethanol. The embryoid bodies transformed into myeloid cell-forming complexes (MCFCs), which in turn, secreted monocyte-like cells into

the medium as suspension cells. Monocyte-like cells were harvested weekly and terminally differentiated into osteoclasts by culturing them in α-MEM (minimum essential medium) Eagle medium supplemented with 50 ng/mL each of hsRANKL (human soluble receptor activator of nuclear factor-κ B ligand) and hM-CSF (for detailed description see Rössler et al., 2021).

4.2 Isolation and osteoclast differentiation of primary blood monocytes

For the comparison with hiPSC-derived monocyte-like cells and osteoclasts, primary monocytes were isolated from human peripheral blood of healthy donors and differentiated into osteoclasts. For this purpose, blood cells were separated using density gradient centrifugation. Peripheral blood mononuclear cells were extracted and monocytic cells were enriched by magnetic cell separation (human Pan Monocyte Isolation Kit from Miltenyi Biotec). Primary blood monocytes were either further characterised or terminally differentiated into osteoclasts using hsRANKL and hM-CSF (50 ng/mL each) in an α-MEM Eagle medium.

4.3 Staining of osteoclasts and resorption assay

Differentiated hiPSC-derived or primary osteoclasts were characterised by a combination of different stainings. In the final differentiation step, as several macrophages fuse together to form osteoclasts, a number of three and more nuclei per cell define an osteoclast. Hence, fixed osteoclasts were stained with DAPI for detection of the number of cell nuclei. Additionally, the formation of a podosome belt (actin ring) is crucial for osteoclasts being able to stick to the bone surface and resorb the bone matrix. Therefore, the actin rings in osteoclasts were stained using fluorescently labelled phalloidin representing another osteoclast characteristic. The third part of the staining shows the TRAcP activity of osteoclast cells. Naphtol AS-MX phosphate disodium salt and Fast Red Violet LB salt were used to stain TRAcP-positive osteoclasts.

Osteoclasts are able to resorb bone matrix by acid and enzyme secretion into the resorption lacunae, which is the ultimate proof of their successfull differentiation. For *in vitro* resorption assays, differentiated osteoclasts were detached with 10 minutes accutase enzyme treatment and reseeded onto either dentine or cortical bovine bone

slices (boneslices.com). After cultivation for another five days, the dentine and bone slices were washed with distilled water and stained with black ink or toluidine solution in order to visualise resorption pits and trenches. To evaluate the resorption behaviour, resorption cavities were classified according to their shape, the depth of the cavitation and the presentation of the edges (Merrild et al., 2015). The evaluation of the resorption was carried out by Kent Søe and his colleagues.

4.4 Flow cytometry analysis of monocytic marker expression

To gain further insights into the nature of the suspension cells released by the myeloid cell forming complexes, typical monocytic surface markers were labelled via specific antibodies bound to fluorescent dyes. Via flow cytometry, stained cells were analysed through a laser beam measuring their physical and chemical properties. The cell population released during the hiPSC differentiation process was compared to primary monocytes freshly isolated from peripheral blood of healthy donors (see section 4.2). For the identification of human monocytes, fluorescently labelled antibodies against CD45, CD11b, CD14 were used. As negative controls, antibodies against CD34 and CD66b were chosen, as they are typical markers for hematopoietic stem cells ($CD34^+$) and eosinophiles ($CD66b^+$). All antibodies were combined into one panel together with an Fc block in order to prevent unspecific binding of the antibodies to the cells. Compensation was performed to avoid a fluorescence spillover of the multiple fluorochromes.

4.5 Quantitative reverse transcription PCR for determination of the differentiation status

hiPSCs differentiation from hematopoietic cells to osteoclasts could be subdivided into four main stages. Each differentiation stage was determined by the relative expression level of marker genes. For this purpose, ribonucleic acid (RNA) was extracted at defined points of the differentiation process and reversely transcribed into complementary deoxyribonucleic acid (cDNA). Using the quantitative polymerase chain reaction (PCR), the expression levels were determined. *SOX2* (sex determining region Y-box 2)*, NANOG,* and *OCT4* (octamer-binding transcription factor 4) were markers for undifferentiated hiPSCs. *CD34, TBXT* (T-box transcription factor T)*, HAND1* (heart and neural crest

derivatives expressed 1) and *CDX2* (caudal-type homeobox 2) expression rises during the mesodermal priming in embryoid body formation and *MAF* (macrophage activating factor) and *CSF1R* (colony stimulating factor 1 receptor) represent monocytic markers. Differentiated osteoclasts were characterised by high expression of *CTSK* (cathepsin K) and *MMP9* (matrix metalloproteinases 9).
Furthermore, the level of *CLCN7* and *OSTM1* gene expression was determined in undifferentiated ARO hiPSCs and three control hiPSC lines to compare the RNA levels to the corresponding protein levels by immunoblot analysis.

4.6 Quantitative analysis of hiPSC-derived osteoclasts

hiPSC-derived osteoclasts were further evaluated regarding their cell size as well as their nuclei number, in comparison to primary monocyte-derived osteoclasts. Additionally, ARO osteoclasts were compared to osteoclasts derived from control hiPSC lines. To determine the differentiation efficiency, the number of hiPSC osteoclasts per mm^2 and the area covered by osteoclasts were assessed. This analysis was based on three independent differentiation experiments and multiple images acquired by the Opera Phenix high content screener, which were then evaluated by the Cell Profiler image analysis software, including a manual step for defining osteoclast borders.

4.7 Lysosomal pH measurement of ARO hiPSCs

ClC-7 is ubiquitously expressed in most cell types and resides intracellularly in the membrane of lysosomes (Brandt and Jentsch, 1995). The acidic luminal pH of lysosomes depends on the functioning of ion channels and proton pumps. Defects in these proteins have numerous adverse effects on lysosomal degradation of cellular materials. Hence, undifferentiated ARO and control hiPSCs were analysed to determine the pH in lysosomes using the dual-excitation ratio fluorescence imaging. After targeting lysosomes using dextran conjugated to a fluorophore, which is sensitive to pH variation, the excitation was measured at 440 nm and 480 nm and emission at 516 to 556 nm. After background subtraction, the mean intensity ratio of 480 and 440 nm was calculated (Weinert et al., 2010). As the fluorochrome is much less pH-sensitive at 440 nm than at 480 nm, the calculation of the ratio automatically corrects variations in the experimental

procedure. For each experiment, an *in situ* pH calibration curve was generated in order to convert measured fluorescence ratios into absolute pH values (Canton and Grinstein, 2015). The lysosomal pH measurement and its analysis was conducted by our collaboration partners Tobias Stauber and Shroddha Bose.

4.8 Immunostaining for localization of mutated ClC-7

To investigate the localisation of mutated ClC-7, HeLa cells were transfected with plasmids coding for fluorescently labelled OSTM1 and either wildtype (WT) ClC-7 or mutated ClC-7 harbouring one of the osteopetrotic mutations (p.(G292E) or p.(R403Q)). Immunostaining was performed using antibodies specific for the target protein and a second fluorescently labelled antibody to detect mutated or WT ClC-7 in combination with LAMP-1 (lysosomal-associated membrane protein 1) in late endosomes and lysosomes by fluorescence microscopy. A second immunostaining was conducted to check for the co-localisation of both, wildtype and mutated ClC-7 with OSTM1. The described immunostainings were performed by Tobias Stauber and Shroddha Bose.

4.9 Electrophysiology analysis of mutated ClC-7

HEK-293 cells were transfected with plasmids coding for wildtype or mutated ClC-7 (Leisle et al., 2011) and OSTM1. Additional mutations were introduced to delete the lysosomal targeting motif and redirect both proteins to the cell membrane (Stauber and Jentsch, 2010). Whole-cell patch-clamp recordings of transfected cells were used to investigate the ion current through the $2Cl^-/H^+$ antiporter (ClC-7 and OSTM1) and the influence of osteopetrotic mutations (p.(G292E) or p.(R403Q)) on its functionality. To this end, transfected cells were brought into close contact with a micropipette touching the cell membrane. This micropipette contained an electrolyte solution and together with a second electrode only touching the surrounding solution, an electrical circuit was induced. Differences in the current traces could be attributed back to the alteration of mutated ion channels expressed in these cells. All electrophysiologic experiments were performed by our collaboration partners Giovanni Zifarelli, Michael Pusch and their colleagues.

4.10 Western blot analysis of LC3 and ClC-7 expression

As the lysosomal localisation of ClC-7 might affect the process of autophagy, autophagy markers and the autophagic flux in ARO hiPSCs were analysed and compared to control hiPSCs. In western blot analysis, proteins of cell lysates were separated according to their size and visualised by specific antibodies and fluorescently labelled secondary antibodies. LC3-I and LC3-II were investigated in undifferentiated hiPSCs in a normal growth medium or in a Krebs-Ringer solution, the latter inducing autophagy in the cells due to a starvation effect. In addition, treatment with the autophagy inhibitor chloroquine blocked the conversion of LC3-I into LC3-II. To calculate the autophagic flux representing the dynamic process of autophagy, densitometrically quantified relative LC3-II levels obtained without chloroquine were subtracted from LC3-II levels acquired with chloroquine (Klionsky et al., 2016).

Western blot analysis was also applied to test the protein expression of ClC-7 in ARO hiPSCs and two additional control hiPSC lines.

5 Essential results

In this PhD project a simple, robust, and efficient differentiation protocol was developed to transform hiPSCs into osteoclasts. Each differentiation step was intensively studied to identify the differentiation status of the cells. Differentiated osteoclasts were characterised in detail using multiple techniques and experiments. Furthermore, patient-derived ARO hiPSCs were used to investigate disease-causing mutations and their consequences in depth. Finally, ARO hiPSCs were differentiated into osteoclasts and examined, demonstrating that this novel differentiation procedure is a valuable disease model to further study the pathology and therapy of osteopetrosis.

5.1 Osteoclast differentiation of hiPSCs and the detailed characterisation of the differentiation procedure

In the first part of my PhD project, I developed a novel osteoclast differentiation protocol for hiPSCs and this formed the basis of all follow-up experiments and the publication presented here (see chapter 11). Osteoclast differentiation protocols that had been published before were either complicated and time consuming or involved expensive amounts of media and cytokines (Chen et al., 2017; Choi et al., 2009; Grigoriadis et al., 2010). Moreover, the efficiency of published osteoclast differentiation procedures was rarely evaluated in detail, but appeared rather low (Jeon et al., 2016). The osteoclast differentiation technique introduced here consisted of only three steps and started from a feeder-free hiPSC culture growing in colonies. In the first step, embryoid bodies were generated by transferring hiPSCs as single cells into ultra-low attachment cell culture plates (see figure 2). The differentiation of the embryoid bodies into a mesodermal direction was induced using the cytokines hSCF, hVEGF and hBMP4. Quantitative reverse transcription PCR (RT-PCR) of specific marker genes was applied to evaluate the differentiation status of the cells. This analysis not only proved the pluripotent state of undifferentiated hiPSCs by the high expression of *SOX2* and *OCT4,* but also the mesodermal induction in embryoid bodies by the rising expression of *CD34* and *HAND1* as well as the decreased expression of the pluripotency marker. In the second step, attached embryoid bodies were transformed into myeloid cell-forming complexes (MCFCs) by plating them onto gelantine-coated cell culture plates and exposing them to

a cell culture medium containing a cytokine cocktail of hIL-3 and hM-CSF (see figure 2). After a few days MCFCs started a continuous production of monocyte-like cells for up to 9 weeks. The monocytic character of the suspension cells was shown by the detection of typical surface marker expression (CD45, CD14 and CD11b) in flow cytometry experiments, in comparison to primary monocytes freshly isolated from blood of healthy donors. Additionally, the gene expression of monocytic markers like *CSF1R* and *MAF* was demonstrated in quantitative RT-PCR. Overall, there were no significant differences detected between the released suspension cells and primary monocytes. The hiPSC-derived monocyte-like cells were harvested from MCFCs and further differentiated into macrophages by treating them with hM-CSF and finally into osteoclasts by adding hsRANKL (see figure 2). Again, marker expression of osteoclasts like *CTSK* and *MMP9* were demonstrated via quantitative RT-PCR.

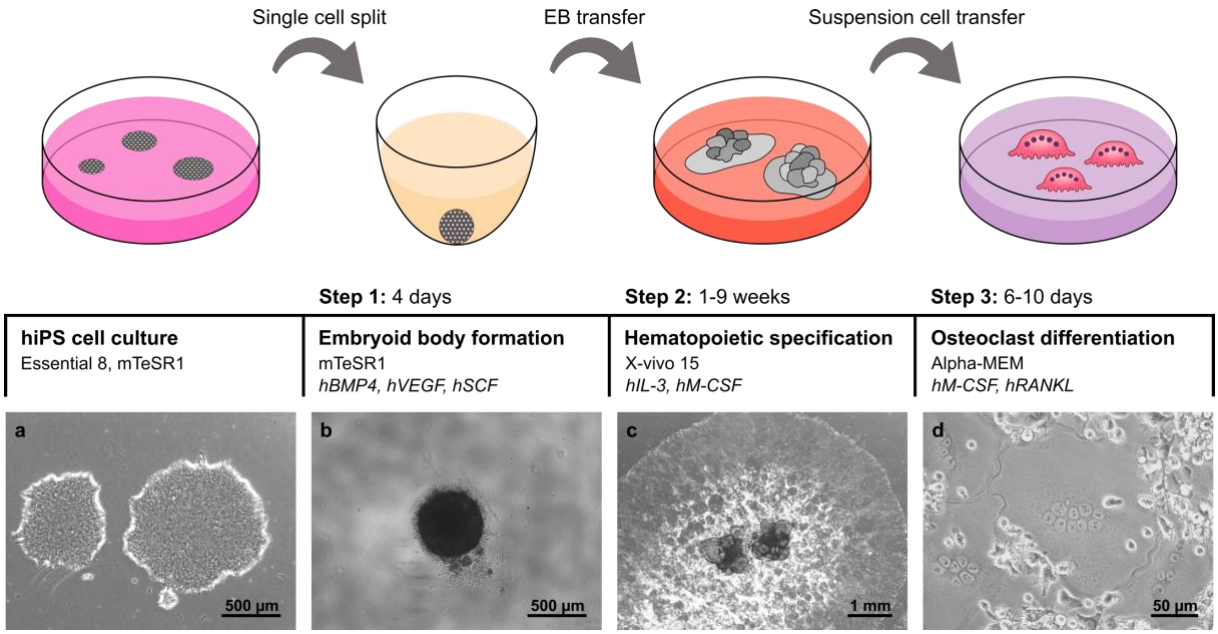

Figure 2: Scheme and workflow of the hiPSC osteoclast differentiation procedure.

Step 1: Embryoid body (EB) formation. Step 2: Transformation of EBs into myeloid cell forming complexes (MCFC) and monocyte-like cell production. Step 3: Osteoclast differentiation. Phase contrast images of hiPSC colonies (a), an embryoid body (b), MCFC (c) and osteoclasts (d). (in accordance to Figure 1, Rössler et al., 2021)

The continuous release of monocytic suspension cells over up to 9 weeks, enabled the differentiation of more than 4,000 osteoclasts (nine nuclei on average) from a single hiPSC within 3 months, demonstrating the high efficiency of our protocol. The resulting

average osteoclast density of 41% in the cell culture dish was very high and, in some experiments, reached even maximal levels of 73%.

Differentiated osteoclasts were further characterised, showing giant cells with several hundred micrometers in diameter in phase contrast images, and fluorescence staining revealed actin ring formation as well as multinucleated TRAcP-positive cells (see figure 3). The high gene expression of *CTSK* and *MMP9* proved the successful differentiation of hiPSCs into osteoclasts. This was shown not only by quantitative RT-PCR, but also by transcriptome analysis via RNA sequencing. The comparison of global expression signatures unveiled high similarities between PBMC-derived osteoclasts and hiPSC osteoclasts and a clear distinction from monocytes. Besides, hiPSC osteoclasts not only showed the morphological characteristics like primary osteoclasts and typical gene expression, but also resorption activity. They were able to produce both types of resorption, pits and trenches, on bovine cortical bone as well as on dentine chips (see figure 3). When looking at the osteoclast size and number of nuclei in hiPSC-derived osteoclasts in more detail, it was observed that osteoclasts grew slightly bigger and harboured a higher number of nuclei compared to osteoclasts differentiated from primary blood monocytes. The analysis of the resorption pattern showed little differences in comparison with primary osteoclasts. hiPSC-derived osteoclasts had the tendency to form a higher proportion of trenches and more pseudoresorption, but the total amount of eroded bone surface was not significantly different.

Overall, we showed that hiPSC-derived osteoclasts displayed a characteristic morphology and gene expression as seen in primary osteoclasts and were able to perform bone resorption *in vitro*.

5.2 Investigation of ARO hiPSCs and differentiated osteoclasts

In the second part of my PhD project, the newly established osteoclast differentiation procedure described above was applied to patient-derived hiPSCs for disease modelling and development of novel therapeutic approaches. In 2019, an osteopetrotic hiPSC line (BIHi002-A or ARO hiPSCs) and its detailed characterisation was published by my colleagues and me (Hennig et al., 2019). These hiPSCs were generated from blood cells obtained from a male infant, who was diagnosed with autosomal recessive osteopetrosis (ARO). Neurological symptoms were unusually severe and brain imaging revealed

impaired cortical development and a neuronal migration defect. First symptoms were detected at the age of 8 to 10 weeks and resulted in a progressive developmental delay. A chest x-ray showed generalised bone sclerosis and together with the diagnosed progressive brain atrophy, hydrocephalus and mild anaemia, a neuronopathic form of osteopetrosis was assumed. Sanger sequencing revealed compound heterozygous mutations c.875G>A, p.(G292E) and c.1208G>A, p.(R403Q) in the *CLCN7* gene. The second mutation has already been described as disease-causing (Pangrazio et al., 2010). The novel mutation c.875G>A affects an evolutionary conserved glycine residue that is surrounded by known variants causing autosomal recessive osteopetrosis. Furthermore, mutations in the *CLCN7* gene are often associated with neurodegeneration which was also observed here. At the age of 14 months, the child deceased and, in order to further study the exceptionally severe phenotype of this ARO case, hiPSCs were generated for further functional investigations.

First, the consequences of the identified sequence variants on protein function were investigated. ClC-7 is primarily localised in lysosomes and forms a stable complex with OSTM1 (Kornak et al., 2001; Lange et al., 2006). Mutant *CLCN7* was overexpressed in HeLa cells, and the localisation was investigated. Here, physiological localisation in lysosomes and even co-localisation of mutated ClC-7 proteins with OSTM1 were visualised in immunostainings. RNA levels of *OSTM1* were increased in ARO hiPSCs, but protein levels were not investigated. Hence, the complex formation between OSTM1 and the mutated ClC-7 was still possible and mutated ClC-7 was able to deliver OSTM1 from the endoplasmatic reticulum to the lysosomes. These findings were important, because the stability of ClC-7 is dependent on the complex formation with OSTM1 as it protects ClC-7 from protein degradation in lysosomes (Lange et al., 2006). Both proteins together form a $2Cl^-/H^+$ antiporter, which is responsible for pH maintenance in lysosomes. Therefore, the lysosomal pH was determined using dual-excitation ratio fluorescence imaging and showed to be unchanged in ARO hiPSCs compared to control hiPSCs.

RNA expression levels of mutated *CLCN7* in patient hiPSCs were not different from wildtype *CLCN7* in hiPSCs from healthy donors, which was shown in quantitative RT-PCR. However, western blot analysis revealed a reduction of mutated ClC-7 protein by 70% in ARO hiPSCs compared to control hiPSCs. In addition, the electrophysiological features of mutant ClC-7 were investigated in patch clamp experiments by overexpressing mutated ClC-7 with plasma membrane expression in HEK-293 cells. This

demonstrated a reduced ion current density of 13% in cells expressing the mutated ClC-7 p.(R409Q), whereas in cells expressing mutated ClC-7 p.(G292E) no ion conductance was detectable at all.

Further western blot analysis of proteins representative for the autophagic flux demonstrated that LC3-II levels in ARO hiPSCs were elevated. Under normal culture conditions, ARO hiPSCs showed an increased autophagic flux. After autophagy induction by starvation, the level was as high as in control hiPSCs showing that ARO hiPSCs were already at the limit of their autophagy capacity, even without autophagy induction. Accumulation of the autophagic protein LC3-II was already reported for *Clcn7*-deficient murine tissues (Wartosch et al., 2009; Weinert et al., 2014) and confirmed here in ARO hiPSCs.

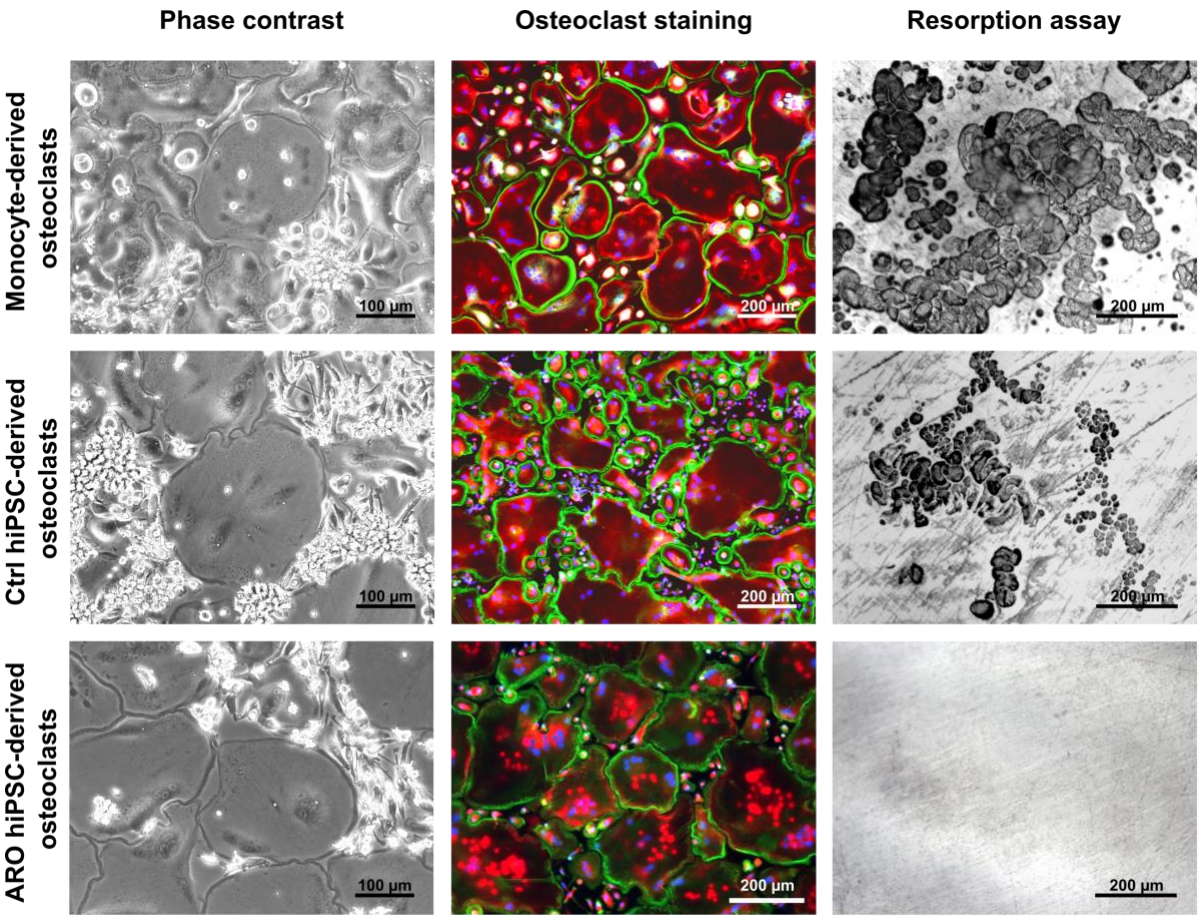

Figure 3: hiPSC-derived osteoclasts in phase contrast and staining images and resorption on dentine. A comparison of osteoclasts differentiated from primary monocytes, control hiPSCs and ARO hiPSCs. Representative images of the in vitro culture (phase contrast images, left), stained osteoclasts (Phalloidin in green, TRAcP in red, DAPI in blue, middle) and black stained

cavities on dentine representing osteoclast-mediated resorption (right). (in accordance to Figure 3, Rössler et al., 2021)

Finally, ARO hiPSCs were differentiated into osteoclasts and characterised in detail at each step of the differentiation protocol. Quantitative RT-PCR showed characteristic gene expression proving the pluripotency of ARO hiPSCs, the successful mesodermal induction into embryoid bodies, and successful activation of osteoclast marker genes at the end of differentiation. The surface marker expression of monocyte-like cells was investigated by flow cytometry showing a $CD45^+$, $CD11b^+$ and $CD14^+$ cell population as shown in control hiPSC differentiation. Terminally differentiated osteoclasts appeared as giant, multinucleated cells able to form a podosome belt and with high TRAcP-activity. For comparison, patient-derived PBMCs were differentiated into osteoclasts and no significant differences between primary and hiPSC-derived osteopetrotic osteoclasts were detected in morphology or staining (see figure 3). Most importantly, neither ARO hiPSC-derived osteoclasts nor ARO PBMC-derived osteoclasts showed any bone resorption activity on dentine (see figure 3) or bovine cortical bone slices, which is typical for osteoclasts harbouring mutations in the *CLCN7* gene (Kornak et al., 2001). Our osteoclast differentiation method had thus proven to be a useful disease model reflecting the osteopetrotic phenotype *in vitro*. Quantification analysis identified that ARO osteoclasts were slightly larger and accordingly revealed a higher number of nuclei, in direct comparison to osteoclasts differentiated from control hiPSCs.

Overall, only minor differences between primary ARO osteoclasts and hiPSC-derived ARO osteoclasts were detected and the expected cellular phenotype was reproduced. Thus, our newly developed osteoclast differentiation protocol represents a very beneficial *in vitro* disease model system for this rare bone disorder.

6 Discussion

An *in vitro* disease model for autosomal recessive osteopetrosis is needed because the usage of primary osteoclasts for research on ARO as well as for diagnostic purposes has multiple limitations. For instance, in most cases fresh blood samples need to be transported over long distances, patients suffering from ARO are rare and usually very young, and primary blood cells are unable to proliferate *in vitro*. Hence, the utilization of hiPSCs as infinite source of cells was considered the best option and in the first part of my PhD project, I developed an osteoclast differentiation technique of hiPSCs, which is characterised by being particularly efficient. The average osteoclast density of 41% was very high and sometimes reached even maximal levels of 73%. Cui et al. presented a differentiation efficiency of hiPSC osteoclasts of only 1.5% (Cui et al., 2019) and other publications did not reveal any information regarding efficiencies. Compared to other previously published hiPSC osteoclast differentiation protocols (Chen et al., 2017; Choi et al., 2009; Cui et al., 2019; Grigoriadis et al., 2010; Jeon et al., 2016), the here described technique is faster, uses less expensive components and, most importantly, it is highly efficient allowing for multiple experiments and investigations. Due to the step of continuous production of hiPSC-derived monocytic suspension cells, one single hiPS cell can generate more than 4,000 osteoclasts (nine nuclei on average).

The followed characterisation of the hiPSC-derived osteoclasts in comparison to primary osteoclasts demonstrated high similarities. No significant differences were detected in osteoclast morphology, gene expression, transcriptome analysis and the resorption activity, except for a slightly higher number of nuclei, the tendency to grow bigger and a minor variation in the resorption pattern in hiPSC osteoclasts. Our observations led us to the assumption that a correlation might exist between the slightly enlarged hiPSC-derived osteoclasts harbouring higher numbers of nuclei and their tendency to form more trenches in comparison to primary osteoclasts. Further investigations would be needed to prove this. However, it is known that the expression of specific proteins and the release of resorption products influences the mode of resorption. For instance, the level of active cathepsin K switches the resorption mode from pits to trenches (Borggaard et al., 2020). During osteoclast differentiation, we analysed the RNA level of *CTSK* in hiPSC osteoclasts and primary osteoclasts. No significant differences were found, but it would be of interest to additionally analyse the protein level of cathepsin K, especially during the

resorption process itself. Furthermore, former studies showed that osteoclast size and multinucleation is donor-dependent (Møller et al., 2020). The evaluation and quantification of hiPSC osteoclasts from several additional hiPSC lines and thus also from various donors seems necessary to draw further conclusions. In addition, we proposed that the increased production of pseudoresorption could be a secondary effect due to enlarged hiPSC osteoclasts, which might have problems to polarise and form a proper sealing zone above a certain size (Howaldt et al., 2020). Hence, there is more superficial resorption with undefined edges and no deep caviation. Time-lapse recordings of resorbing osteoclasts (Søe and Delaissé, 2017) and fluorescence stainings of the podosome belt together with a detailed analysis of the resorption type could provide some insights into this proposition.

Overall, we showed numerous similarities between osteoclasts differentiated from primary blood cells and hiPSCs, but it is widely known that cells differentiated from hiPSCs are less mature than their primary counterpart, e.g. hiPSC-derived cardiomyocytes (Bellin et al., 2012). Thus, we suggest that the minor differences detected, could be a variance in the maturation status of hiPSC-derived osteoclasts. This is also mirrored by the expression of the hematopoietic stem cell marker CD34 at the beginning of the culture, which later vanished when monocytic markers started to be more strongly expressed. Furthermore, transcriptome analysis revealed a few genes, which were only elevated in hiPSC osteoclasts and typical for macrophages (*MAF*) and early osteoclast differentiation (*FOS* and *NFATC1*). Once again, this underlines the theory of slightly immature osteoclasts derived from hiPSCs and demonstrates the limit of this model system. Maturation protocols were developed for hiPSC-derived cardiomyocytes (Yang et al., 2014). Further research regarding the maturation of hiPSC-derived osteoclasts could give novel insights and improve the similarity to primary osteoclasts.

In the second part of my PhD project, patient-specific ARO hiPSCs and the disease-causing mutations were examined in more detail, in order to draw conclusions on the underlying defects and the pathomechanism leading to the patient's death. Here we found not only that the mutated ClC-7 proteins was still located in the lysosomes, we also showed the formation of complexes with OSTM1. Thereby the ClC-7 protein is protected from protein degradation in lysosomes (Lange et al., 2006). Both proteins form a $2Cl^-/H^+$ antiporter, which is responsible for pH maintenance in lysosomes. We detected that the lysosomal pH remained unchanged in ARO hiPSCs, which was shown already in murine

ClC-7-deficient cells (Kasper et al., 2005; Steinberg et al., 2010). The exact mechainsm is still unclear, but it is assumed that an unknown compensatory effect regulates the lysosomal pH if ClC-7 is not functional. Further investigations are needed to analyse which other lysosomal transporters might be involved and how they compensate ClC-7 deficiency.

We further showed that RNA levels of mutated *CLCN7* in ARO hiPSCs were identical with wildtype *CLCN7* in control hiPSCs, but protein levels were reduced although the complex formation with OSTM1 was still possible and hampered the lysosomal degradation. Patch clamp experiment demonstrated that the ion conductance was severly decreased or even undectable. Even though the mutated ClC-7 was still present in lysosomes together with OSTM1 and the lysosomal pH in ARO hiPSCs was unchanged, the reduced protein levels and the fact that the mutated ion channels were not able to fulfil their normal function led to the conclusion that a loss-of-function pathomechanism was disease-causing. Former transgenic experiments showed that 25 to 30% residual ClC-7 expression is needed to rescue cellular function and prevent the osteopetrotic phenotype (Supanchart et al., 2014). Here, it is claimed that the 30% reduced protein level with a reduction of transport function to 13% (probably less) contributed to the exceptional and severe phenotype of the described ARO patient and finally led to the death.

When we looked at autophagy in osteopetrotic hiPSCs, we detected an enhanced level of the autophagy marker LC3-II in not induced ARO hiPSCs and this resulted in an increased autophagic flux. It was proposed that the reduced turnover of autophagosomes and also the slowed protein degradation might be responsible for it. This was shown in ClC-7 deficient cells before (Wartosch and Stauber, 2010). A dysregulation of autophagy is reported to provoke several neurodevelopmental disorders (Teinert et al., 2020). Therefore, accumulation of cell constituents or lack of energy might be responsible for the severe neurological phenotype of the neuronal involvement in *CLCN7*-related ARO. These alternative mechanisms could be investigated in 3D brain models generated from hiPSCs (Bagley et al., 2017; Lancaster et al., 2013).

In the final part, osteopetrotic hiPSCs were differentiated into osteoclasts and displayed characteristic morphology as well as typical gene expression. According to the osteopetrotic cellular phenotype, osteoclasts differentiated from ARO hiPSCs were unable to resorb bone or dentine. Furthermore, ARO osteoclasts were larger in size and harbour more nuclei compared to osteoclasts from control hiPSCs. The reasons remain

unclear, but it has already been published that *Clcn7* and *Ostm1* deficiency in mice resulted in enlarged osteoclasts and enhanced multinucleation as a typical sign of osteopetrosis (Neutzsky-Wulff et al., 2010; Pata and Vacher, 2018). There are two theories for this phenomenon: firstly, an indirect compensation mechanism becomes activated due to the lack of resorption (Pata and Vacher, 2018) and secondly, the absence of apoptotic factors normally released during resorption leads to an increased preosteoclast fusion and prolonged osteoclast lifespan (Neutzsky-Wulff et al., 2010). Recently, McDonalds and colleagues proposed that instead of spontaneous apoptosis, osteoclasts undergo fission events and form osteomorphs before fusing again into osteoclasts. This osteoclast recycling process is regulated by RANKL signaling (McDonald et al., 2021). Enlarged ARO hiPSC osteoclasts might lack those fission events and might show an increased number of fusion processes. Additional investigations using our ARO disease model system could shed more light on these findings. For instance, the investigation of apoptotic or other secreted factors comparing resorbing and non-resorbing osteoclasts would be interesting. The fusion and fission of ARO osteoclasts could be examined in life cell imaging experiments and the apoptosis rate of osteoclasts during resorption could be studied in ARO osteoclasts and healthy control osteoclasts.

Finally, we showed that our newly developed osteoclast differentiation technique provides a good model system to characterise osteoclasts and their resorption behaviour and to study the pathomechanism of osteopetrosis. Due to the long-lasting monocyte-like cell production and the efficient differentiation of osteoclasts, multiple experiments can be performed from only one differentiation approach. Furthermore, other osteoclast-related diseases namely osteoporosis, rheumatoid arthritis, or Paget’s disease, could be investigated by studying osteoclasts differentiated with this procedure from a particular patient-derived hiPSC line. Hence, it is a valuable tool for medical research regarding osteoclast-related diseases and may give inspirations for scientific studies and shed some more light on the jungle of inextricable interactions.

7 Further scientific questions and outlook

With the help of ARO hiPSCs and the developed osteoclast differentiation protocol, it was possible to shed some light on hiPSC-derived osteoclasts and the cellular dysfunctions resulting from compound heterozygous missense mutations in the *CLCN7* gene. On the other hand, this has led to new scientific questions requiring further experiments and investigations. Some ideas for future studies are discussed in the following paragraphs.

When comparing the resorption behaviour of primary osteoclasts and hiPSC-derived osteoclasts, slight differences in the type of resorption and the frequency of pseudoresorption were detected. Its was shown that not only the levels of active cathepsin K, but also the release of resorption products influences the resorption mode (Borggaard et al., 2020). Therefore, a more detailed analysis regarding the released bone degradation products during bone resorption and cathepsin K levels using western blot might be worthwhile. As the preferred type of resorption is also donor-dependent (Merrild et al., 2015), it is recommended to analyse the resorption pattern of osteoclasts differentiated from several blood donors and additional hiPSC lines.

Osteopetrotic osteoclasts differentiated from ARO hiPSCs were extremely large. One theory to explain this was the absence of apoptotic factors released during resorption (Neutzsky-Wulff et al., 2010), which has recently become controversial as McDonalds et al. (2021) could not detect spontaneous apoptosis of osteoclasts and instead described an osteoclast recycling process. Hence, another reason for enlarged osteoclasts could be elevated fusion of monocytic precursors or the lack of osteoclast fission into osteomorphs (McDonald et al., 2021). We also speculated that enlarged osteoclasts are unable to build up a proper sealing zone, which might explain the increased pseudoresorption in hiPSC-derived osteoclasts (Howaldt et al., 2020). All these aspects might be investigated through time-lapse recordings of resorbing osteoclasts using life-cell-imaging (Søe and Delaissé, 2017). Additional fluorescent markers could be engineered into the ARO hiPSCs allowing for the monitoring of nuclei during fusion or fission events, the formation and duration of a sealing zone, and of apoptosis.

We determined an unchanged lysosomal pH in *CLCN7*-deficient hiPSCs, which confirms previous data obtained in mice (Kasper et al., 2005; Steinberg et al., 2010). Possible explanations for this counter-intuitive finding are: i) the main responsibility of ClC-7 is to

regulate lysosomal chloride, not pH; ii) other channels of transporters compensate for the lack of ClC-7. Both hypotheses might be investigated in ARO hiPSCs, for example through CRISPR- or RNAi-screenings in combination with appropriate readout systems.

Moreover, we detected an enhanced autophagic flux in ARO hiPSCs, but reasons or consequences were not investigated. Protein degradation kinetics and autophagosome turnover in ARO hiPSCs and differentiated osteoclasts could be evaluated in future studies. Altered autophagy is involved in several neurodevelopmental disorders (Teinert et al., 2020). As *CLCN7*-related ARO is often associated with neurodegeneration (Kornak et al., 2001; Lange et al., 2006) and the presented patient showed an exceptional severe neuronopathic ARO, further investigations about the role of autophagy in osteopetrosis in particular with regards to the neurodegeneration are recommended.

The brain abnormalities of the presented ARO patient appeared unusually severe and a malfunction during postnatal brain development was presumed. Mutations in the *CLCN7* gene are often associated with lysosomal storage disease, neuronal cell loss and inflammatory processes in the brain (Kasper et al., 2005). Hence, the ARO hiPSCs could be additionally investigated during neuronal lineage differentiation. Differentiation techniques for neurons or other major brain cells from hiPSCs have been already published (Penney et al., 2020) and are being continuously improved. Even the generation of 3D cerebral organoids of patient-specific hiPSCs have been developed over the last years to mimic the neurological development and diseases (Lancaster et al., 2013). Here, it is possible to study cell organisation and interaction, brain structure and composition. Time-lapse experiments of human interneuron migration in 3D cerebral organoids has been shown for modelling complex interactions between different regions during brain development (Bagley et al., 2017).

The only successful therapy for autosomal recessive osteopetrosis is an allogenic hematopoietic stem cell transplantation which still habours significant risks (Penna et al., 2019). Patients need to take life-long medications and the probability of finding a perfectly matched stem cell donor, in time, is rather low. Novel therapeutic strategies are urgently needed, and the described ARO disease model provides a good test system for it. As mutations in osteoclast-related genes are responsible for the resorption defect in osteopetrosis, it is obvious to develop a gene therapeutic approach. The use of the CRISPR/Cas9 technology for genome editing is one approach proposed here (Doudna and Charpentier, 2014; Jinek et al., 2012). Its precise targeting could make it possible to

directly correct one of or even both of the disease-causing mutations. As a more general approach, not specific for individual mutations, the *CLCN7* cDNA could be integrated together with a whole expression cassette into a safe habour region in the cell`s genome (Papapetrou and Schambach, 2016). Moreover, DNA-transposons could be used to integrate *CLCN7* cDNA and the expression cassette into ARO hiPSCs (Belay et al., 2011). Transposon-based gene therapy has the advantage of the efficient delivery of large cargo sizes and high transfection efficiencies (Robbins et al., 2021), but the random integration profile always raises safety concerns. All the described gene therapy approaches bear the potential to rescue the disease phenotype which could be evaluated by the differentiation of genetically modified ARO hiPSCs into osteoclasts and resorption assays together with other characterisation methods. Off-target effects need to be predicted and minimised (Doench et al., 2016) in order to ensure safety of the therapeutic approach. Additional genetic alterations due to the gene therapy could have devastating effects. Also, the site of integration or genome editing needs to be thoroughly examined to ensure safety. Different gene therapy techniques using CRISPR/Cas9 in hiPSCs were already published for other genetic disease such as beta-thalassemia, recessive dystrophic epidermolysis bullosa or Duchenne muscular dystrophy (De Masi et al., 2020). Not only gene correction, but also knock-in strategies showed promising results (Banan, 2020; Eyquem et al., 2017) and laid the foundation for innovative autologous stem cell-based therapies. Besides, transposon-mediated gene therapy proof-of-concept studies were successfully tested for rare genetic diseases and even a clinical use was shown for T-cell based immunotherapy (Tipanee et al., 2017).

8 References

Arai, F., Miyamoto, T., Ohneda, O., Inada, T., Sudo, T., Brasel, K., Miyata, T., Anderson, D.M., Suda, T., 1999. Commitment and differentiation of osteoclast precursor cells by the sequential expression of c-Fms and receptor activator of nuclear factor kappaB (RANK) receptors. J. Exp. Med. 190, 1741–1754. https://doi.org/10.1084/jem.190.12.1741

Bagley, J.A., Reumann, D., Bian, S., Lévi-Strauss, J., Knoblich, J.A., 2017. Fused cerebral organoids model interactions between brain regions. Nat. Methods 14, 743–751. https://doi.org/10.1038/nmeth.4304

Banan, M., 2020. Recent advances in CRISPR/Cas9-mediated knock-ins in mammalian cells. J. Biotechnol. 308, 1–9. https://doi.org/10.1016/j.jbiotec.2019.11.010

Baron, R., Neff, L., Brown, W., Courtoy, P.J., Louvard, D., Farquhar, M.G., 1988. Polarized secretion of lysosomal enzymes: co-distribution of cation-independent mannose-6-phosphate receptors and lysosomal enzymes along the osteoclast exocytic pathway. J. Cell Biol. 106, 1863–1872. https://doi.org/10.1083/jcb.106.6.1863

Belay, E., Dastidar, S., VandenDriessche, T., Chuah, M.K.L., 2011. Transposon-mediated gene transfer into adult and induced pluripotent stem cells. Curr. Gene Ther. 11, 406–413. https://doi.org/10.2174/156652311797415836

Bellin, M., Marchetto, M.C., Gage, F.H., Mummery, C.L., 2012. Induced pluripotent stem cells: the new patient? Nat. Rev. Mol. Cell Biol. 13, 713–726. https://doi.org/10.1038/nrm3448

Bénichou, O.D., Laredo, J.D., de Vernejoul, M.C., 2000. Type II autosomal dominant osteopetrosis (Albers-Schönberg disease): clinical and radiological manifestations in 42 patients. Bone 26, 87–93. https://doi.org/10.1016/s8756-3282(99)00244-6

Bonewald, L.F., 2007. Osteocytes as dynamic multifunctional cells. Ann. N. Y. Acad. Sci. 1116, 281–290. https://doi.org/10.1196/annals.1402.018

Borggaard, X.G., Pirapaharan, D.C., Delaissé, J.-M., Søe, K., 2020. Osteoclasts' Ability to Generate Trenches Rather Than Pits Depends on High Levels of Active Cathepsin K and Efficient Clearance of Resorption Products. Int. J. Mol. Sci. 21, E5924. https://doi.org/10.3390/ijms21165924

Boyle, W.J., Simonet, W.S., Lacey, D.L., 2003. Osteoclast differentiation and activation. Nature 423, 337–342. https://doi.org/10.1038/nature01658

Brandt, S., Jentsch, T.J., 1995. ClC-6 and ClC-7 are two novel broadly expressed members of the CLC chloride channel family. FEBS Lett. 377, 15–20. https://doi.org/10.1016/0014-5793(95)01298-2

Buchrieser, J., James, W., Moore, M.D., 2017. Human Induced Pluripotent Stem Cell-Derived Macrophages Share Ontogeny with MYB-Independent Tissue-Resident Macrophages. Stem Cell Rep. 8, 334–345. https://doi.org/10.1016/j.stemcr.2016.12.020

Canton, J., Grinstein, S., 2015. Measuring lysosomal pH by fluorescence microscopy. Methods Cell Biol. 126, 85–99. https://doi.org/10.1016/bs.mcb.2014.10.021

Cappariello, A., Maurizi, A., Veeriah, V., Teti, A., 2014. The Great Beauty of the osteoclast. Arch. Biochem. Biophys. 558, 70–78. https://doi.org/10.1016/j.abb.2014.06.017

Chatterjee, D., Chakraborty, M., Leit, M., Neff, L., Jamsa-Kellokumpu, S., Fuchs, R., Baron, R., 1992. Sensitivity to vanadate and isoforms of subunits A and B distinguish the osteoclast proton pump from other vacuolar H+ ATPases. Proc. Natl. Acad. Sci. U. S. A. 89, 6257–6261. https://doi.org/10.1073/pnas.89.14.6257

Chen, I.-P., Luxmi, R., Kanaujiya, J., Hao, Z., Reichenberger, E.J., 2017. Craniometaphyseal Dysplasia Mutations in ANKH Negatively Affect Human Induced Pluripotent Stem Cell Differentiation into Osteoclasts. Stem Cell Rep. 9, 1369–1376. https://doi.org/10.1016/j.stemcr.2017.09.016

Choi, K.-D., Vodyanik, M.A., Slukvin, I.I., 2009. Generation of mature human myelomonocytic cells through expansion and differentiation of pluripotent stem cell–derived lin–CD34+CD43+CD45+ progenitors. J. Clin. Invest. 119, 2818–2829. https://doi.org/10.1172/JCI38591

Coudert, A.E., de Vernejoul, M.-C., Muraca, M., Del Fattore, A., 2015. Osteopetrosis and its relevance for the discovery of new functions associated with the skeleton. Int. J. Endocrinol. 2015, 372156. https://doi.org/10.1155/2015/372156

Cui, X., Cui, Y., Shi, L., Luan, J., Zhou, X., Han, J., 2019. A preliminary study on the mechanism of skeletal abnormalities in Turner syndrome using inducing pluripotent stem cells (iPS)- based disease models. Intractable Rare Dis. Res. 8, 113–119.

https://doi.org/10.5582/irdr.2019.01025

De Masi, C., Spitalieri, P., Murdocca, M., Novelli, G., Sangiuolo, F., 2020. Application of CRISPR/Cas9 to human-induced pluripotent stem cells: from gene editing to drug discovery. Hum. Genomics 14, 25. https://doi.org/10.1186/s40246-020-00276-2

Doench, J.G., Fusi, N., Sullender, M., Hegde, M., Vaimberg, E.W., Donovan, K.F., Smith, I., Tothova, Z., Wilen, C., Orchard, R., Virgin, H.W., Listgarten, J., Root, D.E., 2016. Optimized sgRNA design to maximize activity and minimize off-target effects of CRISPR-Cas9. Nat. Biotechnol. 34, 184–191. https://doi.org/10.1038/nbt.3437

Doudna, J.A., Charpentier, E., 2014. Genome editing. The new frontier of genome engineering with CRISPR-Cas9. Science 346, 1258096. https://doi.org/10.1126/science.1258096

Eyquem, J., Mansilla-Soto, J., Giavridis, T., van der Stegen, S.J.C., Hamieh, M., Cunanan, K.M., Odak, A., Gönen, M., Sadelain, M., 2017. Targeting a CAR to the TRAC locus with CRISPR/Cas9 enhances tumour rejection. Nature 543, 113–117. https://doi.org/10.1038/nature21405

Forgac, M., 1999. Structure and properties of the vacuolar (H+)-ATPases. J. Biol. Chem. 274, 12951–12954. https://doi.org/10.1074/jbc.274.19.12951

Frattini, A., Orchard, P.J., Sobacchi, C., Giliani, S., Abinun, M., Mattsson, J.P., Keeling, D.J., Andersson, A.K., Wallbrandt, P., Zecca, L., Notarangelo, L.D., Vezzoni, P., Villa, A., 2000. Defects in TCIRG1 subunit of the vacuolar proton pump are responsible for a subset of human autosomal recessive osteopetrosis. Nat. Genet. 25, 343–346. https://doi.org/10.1038/77131

Freemont, A.J., 1993. Basic bone cell biology. Int. J. Exp. Pathol. 74, 411–416.

Georgess, D., Machuca-Gayet, I., Blangy, A., Jurdic, P., 2014. Podosome organization drives osteoclast-mediated bone resorption. Cell Adhes. Migr. 8, 192–204. https://doi.org/10.4161/cam.27840

Graves, A.R., Curran, P.K., Smith, C.L., Mindell, J.A., 2008. The Cl-/H+ antiporter ClC-7 is the primary chloride permeation pathway in lysosomes. Nature 453, 788–792. https://doi.org/10.1038/nature06907

Grigoriadis, A.E., Kennedy, M., Bozec, A., Brunton, F., Stenbeck, G., Park, I.-H., Wagner, E.F., Keller, G.M., 2010. Directed differentiation of hematopoietic precursors and

functional osteoclasts from human ES and iPS cells. Blood 115, 2769–2776. https://doi.org/10.1182/blood-2009-07-234690

Hennig, A.F., Rössler, U., Boiti, F., von der Hagen, M., Gossen, M., Kornak, U., Stachelscheid, H., 2019. Generation of a human induced pluripotent stem cell line (BIHi002-A) from a patient with CLCN7-related infantile malignant autosomal recessive osteopetrosis. Stem Cell Res. 35, 101367. https://doi.org/10.1016/j.scr.2018.101367

Howaldt, A., Hennig, A.F., Rolvien, T., Rössler, U., Stelzer, N., Knaus, A., Böttger, S., Zustin, J., Geißler, S., Oheim, R., Amling, M., Howaldt, H.-P., Kornak, U., 2020. Adult Osteosclerotic Metaphyseal Dysplasia With Progressive Osteonecrosis of the Jaws and Abnormal Bone Resorption Pattern Due to a LRRK1 Splice Site Mutation. J. Bone Miner. Res. Off. J. Am. Soc. Bone Miner. Res. 35, 1322–1332. https://doi.org/10.1002/jbmr.3995

Jentsch, T.J., Pusch, M., 2018. CLC Chloride Channels and Transporters: Structure, Function, Physiology, and Disease. Physiol. Rev. 98, 1493–1590. https://doi.org/10.1152/physrev.00047.2017

Jeon, O.H., Panicker, L.M., Lu, Q., Chae, J.J., Feldman, R.A., Elisseeff, J.H., 2016. Human iPSC-derived osteoblasts and osteoclasts together promote bone regeneration in 3D biomaterials. Sci. Rep. 6, 26761. https://doi.org/10.1038/srep26761

Jinek, M., Chylinski, K., Fonfara, I., Hauer, M., Doudna, J.A., Charpentier, E., 2012. A programmable dual-RNA-guided DNA endonuclease in adaptive bacterial immunity. Science 337, 816–821. https://doi.org/10.1126/science.1225829

Kasper, D., Planells-Cases, R., Fuhrmann, J.C., Scheel, O., Zeitz, O., Ruether, K., Schmitt, A., Poët, M., Steinfeld, R., Schweizer, M., Kornak, U., Jentsch, T.J., 2005. Loss of the chloride channel ClC-7 leads to lysosomal storage disease and neurodegeneration. EMBO J. 24, 1079–1091. https://doi.org/10.1038/sj.emboj.7600576

Katsimbri, P., 2017. The biology of normal bone remodelling. Eur. J. Cancer Care (Engl.) 26. https://doi.org/10.1111/ecc.12740

Klionsky, D.J., Abdelmohsen, K., Abe, A., Abedin, M.J., Abeliovich, H., Acevedo Arozena, A., Adachi, H., Adams, C.M., Adams, P.D., Adeli, K., Adhihetty, P.J., Adler, S.G., Agam, G., Agarwal, R., Aghi, M.K., Agnello, M., Agostinis, P., Aguilar, P.V., Aguirre-Ghiso, J., Airoldi, E.M., Ait-Si-Ali, S., Akematsu, T., Akporiaye, E.T., Al-Rubeai, M., Albaiceta, G.M., Albanese, C., Albani, D., Albert, M.L., Aldudo, J., Algül, H., Alirezaei, M., Alloza, I.,

Almasan, A., Almonte-Beceril, M., Alnemri, E.S., Alonso, C., Altan-Bonnet, N., Altieri, D.C., Alvarez, S., Alvarez-Erviti, L., Alves, S., Amadoro, G., Amano, A., Amantini, C., Ambrosio, S., Amelio, I., Amer, A.O., Amessou, M., Amon, A., An, Z., Anania, F.A., Andersen, S.U., Andley, U.P., Andreadi, C.K., Andrieu-Abadie, N., Anel, A., Ann, D.K., Anoopkumar-Dukie, S., Antonioli, M., Aoki, H., Apostolova, N., Aquila, S., Aquilano, K., Araki, K., Arama, E., Aranda, A., Araya, J., Arcaro, A., Arias, E., Arimoto, H., Ariosa, A.R., Armstrong, J.L., Arnould, T., Arsov, I., Asanuma, K., Askanas, V., Asselin, E., Atarashi, R., Atherton, S.S., Atkin, J.D., Attardi, L.D., Auberger, P., Auburger, G., Aurelian, L., Autelli, R., Avagliano, L., Avantaggiati, M.L., Avrahami, L., Awale, S., Azad, N., Bachetti, T., Backer, J.M., Bae, D.-H., Bae, J.-S., Bae, O.-N., Bae, S.H., Baehrecke, E.H., Baek, S.-H., Baghdiguian, S., Bagniewska-Zadworna, A., Bai, H., Bai, J., Bai, X.-Y., Bailly, Y., Balaji, K.N., Balduini, W., Ballabio, A., Balzan, R., Banerjee, R., Bánhegyi, G., Bao, H., Barbeau, B., Barrachina, M.D., Barreiro, E., Bartel, B., Bartolomé, A., Bassham, D.C., Bassi, M.T., Bast, R.C., Basu, A., Batista, M.T., Batoko, H., Battino, M., Bauckman, K., Baumgarner, B.L., Bayer, K.U., Beale, R., Beaulieu, J.-F., Beck, G.R., Becker, C., Beckham, J.D., Bédard, P.-A., Bednarski, P.J., Begley, T.J., Behl, C., Behrends, C., Behrens, G.M., Behrns, K.E., Bejarano, E., Belaid, A., Belleudi, F., Bénard, G., Berchem, G., Bergamaschi, D., Bergami, M., Berkhout, B., Berliocchi, L., Bernard, A., Bernard, M., Bernassola, F., Bertolotti, A., Bess, A.S., Besteiro, S., Bettuzzi, S., Bhalla, S., Bhattacharyya, S., Bhutia, S.K., Biagosch, C., Bianchi, M.W., Biard-Piechaczyk, M., Billes, V., Bincoletto, C., Bingol, B., Bird, S.W., Bitoun, M., Bjedov, I., Blackstone, C., Blanc, L., Blanco, G.A., Blomhoff, H.K., Boada-Romero, E., Böckler, S., Boes, M., Boesze-Battaglia, K., Boise, L.H., Bolino, A., Boman, A., Bonaldo, P., Bordi, M., Bosch, J., Botana, L.M., Botti, J., Bou, G., Bouché, M., Bouchecareilh, M., Boucher, M.-J., Boulton, M.E., Bouret, S.G., Boya, P., Boyer-Guittaut, M., Bozhkov, P.V., Brady, N., Braga, V.M., Brancolini, C., Braus, G.H., Bravo-San Pedro, J.M., Brennan, L.A., Bresnick, E.H., Brest, P., Bridges, D., Bringer, M.-A., Brini, M., Brito, G.C., Brodin, B., Brookes, P.S., Brown, E.J., Brown, K., Broxmeyer, H.E., Bruhat, A., Brum, P.C., Brumell, J.H., Brunetti-Pierri, N., Bryson-Richardson, R.J., Buch, S., Buchan, A.M., Budak, H., Bulavin, D.V., Bultman, S.J., Bultynck, G., Bumbasirevic, V., Burelle, Y., Burke, R.E., Burmeister, M., Bütikofer, P., Caberlotto, L., Cadwell, K., Cahova, M., Cai, D., Cai, J., Cai, Q., Calatayud, S., Camougrand, N., Campanella, M., Campbell, G.R., Campbell, M., Campello, S., Candau, R., Caniggia, I., Cantoni, L., Cao, L., Caplan, A.B., Caraglia, M., Cardinali, C., Cardoso, S.M., Carew, J.S., Carleton, L.A., Carlin, C.R., Carloni, S.,

Carlsson, S.R., Carmona-Gutierrez, D., Carneiro, L.A., Carnevali, O., Carra, S., Carrier, A., Carroll, B., Casas, C., Casas, J., Cassinelli, G., Castets, P., Castro-Obregon, S., Cavallini, G., Ceccherini, I., Cecconi, F., Cederbaum, A.I., Ceña, V., Cenci, S., Cerella, C., Cervia, D., Cetrullo, S., Chaachouay, H., Chae, H.-J., Chagin, A.S., Chai, C.-Y., Chakrabarti, G., Chamilos, G., Chan, E.Y., Chan, M.T., Chandra, D., Chandra, P., Chang, C.-P., Chang, R.C.-C., Chang, T.Y., Chatham, J.C., Chatterjee, S., Chauhan, S., Che, Y., Cheetham, M.E., Cheluvappa, R., Chen, C.-J., Chen, Gang, Chen, G.-C., Chen, Guoqiang, Chen, H., Chen, J.W., Chen, J.-K., Chen, Min, Chen, Mingzhou, Chen, P., Chen, Qi, Chen, Quan, Chen, S.-D., Chen, S., Chen, S.S.-L., Chen, Wei, Chen, W.-J., Chen, W.Q., Chen, Wenli, Chen, X., Chen, Y.-H., Chen, Y.-G., Chen, Yin, Chen, Yingyu, Chen, Yongshun, Chen, Y.-J., Chen, Y.-Q., Chen, Yujie, Chen, Zhen, Chen, Zhong, Cheng, A., Cheng, C.H., Cheng, H., Cheong, H., Cherry, S., Chesney, J., Cheung, C.H.A., Chevet, E., Chi, H.C., Chi, S.-G., Chiacchiera, F., Chiang, H.-L., Chiarelli, R., Chiariello, M., Chieppa, M., Chin, L.-S., Chiong, M., Chiu, G.N., Cho, D.-H., Cho, S.-G., Cho, W.C., Cho, Y.-Y., Cho, Y.-S., Choi, A.M., Choi, E.-J., Choi, E.-K., Choi, J., Choi, M.E., Choi, S.-I., Chou, T.-F., Chouaib, S., Choubey, D., Choubey, V., Chow, K.-C., Chowdhury, K., Chu, C.T., Chuang, T.-H., Chun, T., Chung, H., Chung, T., Chung, Y.-L., Chwae, Y.-J., Cianfanelli, V., Ciarcia, R., Ciechomska, I.A., Ciriolo, M.R., Cirone, M., Claerhout, S., Clague, M.J., Clària, J., Clarke, P.G., Clarke, R., Clementi, E., Cleyrat, C., Cnop, M., Coccia, E.M., Cocco, T., Codogno, P., Coers, J., Cohen, E.E., Colecchia, D., Coletto, L., Coll, N.S., Colucci-Guyon, E., Comincini, S., Condello, M., Cook, K.L., Coombs, G.H., Cooper, C.D., Cooper, J.M., Coppens, I., Corasaniti, M.T., Corazzari, M., Corbalan, R., Corcelle-Termeau, E., Cordero, M.D., Corral-Ramos, C., Corti, O., Cossarizza, A., Costelli, P., Costes, S., Cotman, S.L., Coto-Montes, A., Cottet, S., Couve, E., Covey, L.R., Cowart, L.A., Cox, J.S., Coxon, F.P., Coyne, C.B., Cragg, M.S., Craven, R.J., Crepaldi, T., Crespo, J.L., Criollo, A., Crippa, V., Cruz, M.T., Cuervo, A.M., Cuezva, J.M., Cui, T., Cutillas, P.R., Czaja, M.J., Czyzyk-Krzeska, M.F., Dagda, R.K., Dahmen, U., Dai, C., Dai, W., Dai, Y., Dalby, K.N., Dalla Valle, L., Dalmasso, G., D'Amelio, M., Damme, M., Darfeuille-Michaud, A., Dargemont, C., Darley-Usmar, V.M., Dasarathy, S., Dasgupta, B., Dash, S., Dass, C.R., Davey, H.M., Davids, L.M., Dávila, D., Davis, R.J., Dawson, T.M., Dawson, V.L., Daza, P., de Belleroche, J., de Figueiredo, P., de Figueiredo, R.C.B.Q., de la Fuente, J., De Martino, L., De Matteis, A., De Meyer, G.R., De Milito, A., De Santi, M., de Souza, W., De Tata, V., De Zio, D., Debnath, J., Dechant, R., Decuypere, J.-P., Deegan, S., Dehay, B., Del Bello, B., Del Re, D.P., Delage-

Mourroux, R., Delbridge, L.M., Deldicque, L., Delorme-Axford, E., Deng, Y., Dengjel, J., Denizot, M., Dent, P., Der, C.J., Deretic, V., Derrien, B., Deutsch, E., Devarenne, T.P., Devenish, R.J., Di Bartolomeo, S., Di Daniele, N., Di Domenico, F., Di Nardo, A., Di Paola, S., Di Pietro, A., Di Renzo, L., DiAntonio, A., Díaz-Araya, G., Díaz-Laviada, I., Diaz-Meco, M.T., Diaz-Nido, J., Dickey, C.A., Dickson, R.C., Diederich, M., Digard, P., Dikic, I., Dinesh-Kumar, S.P., Ding, C., Ding, W.-X., Ding, Z., Dini, L., Distler, J.H., Diwan, A., Djavaheri-Mergny, M., Dmytruk, K., Dobson, R.C., Doetsch, V., Dokladny, K., Dokudovskaya, S., Donadelli, M., Dong, X.C., Dong, X., Dong, Z., Donohue, T.M., Doran, K.S., D'Orazi, G., Dorn, G.W., Dosenko, V., Dridi, S., Drucker, L., Du, J., Du, L.-L., Du, L., du Toit, A., Dua, P., Duan, L., Duann, P., Dubey, V.K., Duchen, M.R., Duchosal, M.A., Duez, H., Dugail, I., Dumit, V.I., Duncan, M.C., Dunlop, E.A., Dunn, W.A., Dupont, N., Dupuis, L., Durán, R.V., Durcan, T.M., Duvezin-Caubet, S., Duvvuri, U., Eapen, V., Ebrahimi-Fakhari, D., Echard, A., Eckhart, L., Edelstein, C.L., Edinger, A.L., Eichinger, L., Eisenberg, T., Eisenberg-Lerner, A., Eissa, N.T., El-Deiry, W.S., El-Khoury, V., Elazar, Z., Eldar-Finkelman, H., Elliott, C.J., Emanuele, E., Emmenegger, U., Engedal, N., Engelbrecht, A.-M., Engelender, S., Enserink, J.M., Erdmann, R., Erenpreisa, J., Eri, R., Eriksen, J.L., Erman, A., Escalante, R., Eskelinen, E.-L., Espert, L., Esteban-Martínez, L., Evans, T.J., Fabri, M., Fabrias, G., Fabrizi, C., Facchiano, A., Færgeman, N.J., Faggioni, A., Fairlie, W.D., Fan, C., Fan, D., Fan, J., Fang, S., Fanto, M., Fanzani, A., Farkas, T., Faure, M., Favier, F.B., Fearnhead, H., Federici, M., Fei, E., Felizardo, T.C., Feng, H., Feng, Yibin, Feng, Yuchen, Ferguson, T.A., Fernández, Á.F., Fernandez-Barrena, M.G., Fernandez-Checa, J.C., Fernández-López, A., Fernandez-Zapico, M.E., Feron, O., Ferraro, E., Ferreira-Halder, C.V., Fesus, L., Feuer, R., Fiesel, F.C., Filippi-Chiela, E.C., Filomeni, G., Fimia, G.M., Fingert, J.H., Finkbeiner, S., Finkel, T., Fiorito, F., Fisher, P.B., Flajolet, M., Flamigni, F., Florey, O., Florio, S., Floto, R.A., Folini, M., Follo, C., Fon, E.A., Fornai, F., Fortunato, F., Fraldi, A., Franco, R., Francois, A., François, A., Frankel, L.B., Fraser, I.D., Frey, N., Freyssenet, D.G., Frezza, C., Friedman, S.L., Frigo, D.E., Fu, D., Fuentes, J.M., Fueyo, J., Fujitani, Y., Fujiwara, Y., Fujiya, M., Fukuda, M., Fulda, S., Fusco, C., Gabryel, B., Gaestel, M., Gailly, P., Gajewska, M., Galadari, S., Galili, G., Galindo, I., Galindo, M.F., Galliciotti, G., Galluzzi, Lorenzo, Galluzzi, Luca, Galy, V., Gammoh, N., Gandy, S., Ganesan, A.K., Ganesan, S., Ganley, I.G., Gannagé, M., Gao, F.-B., Gao, F., Gao, J.-X., García Nannig, L., García Véscovi, E., Garcia-Macía, M., Garcia-Ruiz, C., Garg, A.D., Garg, P.K., Gargini, R., Gassen, N.C., Gatica, D., Gatti, E., Gavard, J., Gavathiotis, E., Ge, L., Ge, P., Ge, S., Gean, P.-W., Gelmetti, V., Genazzani,

A.A., Geng, J., Genschik, P., Gerner, L., Gestwicki, J.E., Gewirtz, D.A., Ghavami, S., Ghigo, E., Ghosh, D., Giammarioli, A.M., Giampieri, F., Giampietri, C., Giatromanolaki, A., Gibbings, D.J., Gibellini, L., Gibson, S.B., Ginet, V., Giordano, A., Giorgini, F., Giovannetti, E., Girardin, S.E., Gispert, S., Giuliano, S., Gladson, C.L., Glavic, A., Gleave, M., Godefroy, N., Gogal, R.M., Gokulan, K., Goldman, G.H., Goletti, D., Goligorsky, M.S., Gomes, A.V., Gomes, L.C., Gomez, H., Gomez-Manzano, C., Gómez-Sánchez, R., Gonçalves, D.A., Goncu, E., Gong, Q., Gongora, C., Gonzalez, C.B., Gonzalez-Alegre, P., Gonzalez-Cabo, P., González-Polo, R.A., Goping, I.S., Gorbea, C., Gorbunov, N.V., Goring, D.R., Gorman, A.M., Gorski, S.M., Goruppi, S., Goto-Yamada, S., Gotor, C., Gottlieb, R.A., Gozes, I., Gozuacik, D., Graba, Y., Graef, M., Granato, G.E., Grant, G.D., Grant, S., Gravina, G.L., Green, D.R., Greenhough, A., Greenwood, M.T., Grimaldi, B., Gros, F., Grose, C., Groulx, J.-F., Gruber, F., Grumati, P., Grune, T., Guan, J.-L., Guan, K.-L., Guerra, B., Guillen, C., Gulshan, K., Gunst, J., Guo, C., Guo, L., Guo, M., Guo, W., Guo, X.-G., Gust, A.A., Gustafsson, Å.B., Gutierrez, E., Gutierrez, M.G., Gwak, H.-S., Haas, A., Haber, J.E., Hadano, S., Hagedorn, M., Hahn, D.R., Halayko, A.J., Hamacher-Brady, A., Hamada, K., Hamai, A., Hamann, A., Hamasaki, M., Hamer, I., Hamid, Q., Hammond, E.M., Han, F., Han, W., Handa, J.T., Hanover, J.A., Hansen, M., Harada, M., Harhaji-Trajkovic, L., Harper, J.W., Harrath, A.H., Harris, A.L., Harris, J., Hasler, U., Hasselblatt, P., Hasui, K., Hawley, R.G., Hawley, T.S., He, C., He, C.Y., He, F., He, G., He, R.-R., He, X.-H., He, Y.-W., He, Y.-Y., Heath, J.K., Hébert, M.-J., Heinzen, R.A., Helgason, G.V., Hensel, M., Henske, E.P., Her, C., Herman, P.K., Hernández, A., Hernandez, C., Hernández-Tiedra, S., Hetz, C., Hiesinger, P.R., Higaki, K., Hilfiker, S., Hill, B.G., Hill, J.A., Hill, W.D., Hino, K., Hofius, D., Hofman, P., Höglinger, G.U., Höhfeld, J., Holz, M.K., Hong, Y., Hood, D.A., Hoozemans, J.J., Hoppe, T., Hsu, C., Hsu, C.-Y., Hsu, L.-C., Hu, D., Hu, G., Hu, H.-M., Hu, H., Hu, M.C., Hu, Y.-C., Hu, Z.-W., Hua, F., Hua, Y., Huang, C., Huang, H.-L., Huang, K.-H., Huang, K.-Y., Huang, Shile, Huang, Shiqian, Huang, W.-P., Huang, Y.-R., Huang, Yong, Huang, Yunfei, Huber, T.B., Huebbe, P., Huh, W.-K., Hulmi, J.J., Hur, G.M., Hurley, J.H., Husak, Z., Hussain, S.N., Hussain, S., Hwang, J.J., Hwang, S., Hwang, T.I., Ichihara, A., Imai, Y., Imbriano, C., Inomata, M., Into, T., Iovane, V., Iovanna, J.L., Iozzo, R.V., Ip, N.Y., Irazoqui, J.E., Iribarren, P., Isaka, Y., Isakovic, A.J., Ischiropoulos, H., Isenberg, J.S., Ishaq, M., Ishida, H., Ishii, I., Ishmael, J.E., Isidoro, C., Isobe, K.-I., Isono, E., Issazadeh-Navikas, S., Itahana, K., Itakura, E., Ivanov, A.I., Iyer, A.K.V., Izquierdo, J.M., Izumi, Y., Izzo, V., Jäättelä, M., Jaber, N., Jackson, D.J., Jackson, W.T., Jacob, T.G., Jacques, T.S., Jagannath, C., Jain, A., Jana,

N.R., Jang, B.K., Jani, A., Janji, B., Jannig, P.R., Jansson, P.J., Jean, S., Jendrach, M., Jeon, J.-H., Jessen, N., Jeung, E.-B., Jia, K., Jia, L., Jiang, Hong, Jiang, Hongchi, Jiang, L., Jiang, T., Jiang, Xiaoyan, Jiang, Xuejun, Jiang, Xuejun, Jiang, Ying, Jiang, Yongjun, Jiménez, A., Jin, C., Jin, H., Jin, L., Jin, M., Jin, S., Jinwal, U.K., Jo, E.-K., Johansen, T., Johnson, D.E., Johnson, G.V., Johnson, J.D., Jonasch, E., Jones, C., Joosten, L.A., Jordan, J., Joseph, A.-M., Joseph, B., Joubert, A.M., Ju, D., Ju, J., Juan, H.-F., Juenemann, K., Juhász, G., Jung, H.S., Jung, J.U., Jung, Y.-K., Jungbluth, H., Justice, M.J., Jutten, B., Kaakoush, N.O., Kaarniranta, K., Kaasik, A., Kabuta, T., Kaeffer, B., Kågedal, K., Kahana, A., Kajimura, S., Kakhlon, O., Kalia, M., Kalvakolanu, D.V., Kamada, Y., Kambas, K., Kaminskyy, V.O., Kampinga, H.H., Kandouz, M., Kang, C., Kang, R., Kang, T.-C., Kanki, T., Kanneganti, T.-D., Kanno, H., Kanthasamy, A.G., Kantorow, M., Kaparakis-Liaskos, M., Kapuy, O., Karantza, V., Karim, M.R., Karmakar, P., Kaser, A., Kaushik, S., Kawula, T., Kaynar, A.M., Ke, P.-Y., Ke, Z.-J., Kehrl, J.H., Keller, K.E., Kemper, J.K., Kenworthy, A.K., Kepp, O., Kern, A., Kesari, S., Kessel, D., Ketteler, R., Kettelhut, I. do C., Khambu, B., Khan, M.M., Khandelwal, V.K., Khare, S., Kiang, J.G., Kiger, A.A., Kihara, A., Kim, A.L., Kim, C.H., Kim, D.R., Kim, D.-H., Kim, E.K., Kim, H.Y., Kim, H.-R., Kim, J.-S., Kim, Jeong Hun, Kim, J.C., Kim, Jin Hyoung, Kim, K.W., Kim, M.D., Kim, M.-M., Kim, P.K., Kim, S.W., Kim, S.-Y., Kim, Y.-S., Kim, Y., Kimchi, A., Kimmelman, A.C., Kimura, T., King, J.S., Kirkegaard, K., Kirkin, V., Kirshenbaum, L.A., Kishi, S., Kitajima, Y., Kitamoto, K., Kitaoka, Y., Kitazato, K., Kley, R.A., Klimecki, W.T., Klinkenberg, M., Klucken, J., Knævelsrud, H., Knecht, E., Knuppertz, L., Ko, J.-L., Kobayashi, S., Koch, J.C., Koechlin-Ramonatxo, C., Koenig, U., Koh, Y.H., Köhler, K., Kohlwein, S.D., Koike, M., Komatsu, M., Kominami, E., Kong, D., Kong, H.J., Konstantakou, E.G., Kopp, B.T., Korcsmaros, T., Korhonen, L., Korolchuk, V.I., Koshkina, N.V., Kou, Y., Koukourakis, M.I., Koumenis, C., Kovács, A.L., Kovács, T., Kovacs, W.J., Koya, D., Kraft, C., Krainc, D., Kramer, H., Kravic-Stevovic, T., Krek, W., Kretz-Remy, C., Krick, R., Krishnamurthy, M., Kriston-Vizi, J., Kroemer, G., Kruer, M.C., Kruger, R., Ktistakis, N.T., Kuchitsu, K., Kuhn, C., Kumar, A.P., Kumar, Anuj, Kumar, Ashok, Kumar, Deepak, Kumar, Dhiraj, Kumar, R., Kumar, S., Kundu, M., Kung, H.-J., Kuno, A., Kuo, S.-H., Kuret, J., Kurz, T., Kwok, T., Kwon, T.K., Kwon, Y.T., Kyrmizi, I., La Spada, A.R., Lafont, F., Lahm, T., Lakkaraju, A., Lam, T., Lamark, T., Lancel, S., Landowski, T.H., Lane, D.J.R., Lane, J.D., Lanzi, C., Lapaquette, P., Lapierre, L.R., Laporte, J., Laukkarinen, J., Laurie, G.W., Lavandero, S., Lavie, L., LaVoie, M.J., Law, B.Y.K., Law, H.K.-W., Law, K.B., Layfield, R., Lazo, P.A., Le Cam, L., Le Roch, K.G., Le Stunff, H.,

Leardkamolkarn, V., Lecuit, M., Lee, B.-H., Lee, C.-H., Lee, E.F., Lee, G.M., Lee, H.-J., Lee, H., Lee, J.K., Lee, J., Lee, J.-H., Lee, J.H., Lee, M., Lee, M.-S., Lee, P.J., Lee, S.W., Lee, Seung-Jae, Lee, Shiow-Ju, Lee, S.Y., Lee, S.H., Lee, S.S., Lee, Sung-Joon, Lee, S., Lee, Y.-R., Lee, Y.J., Lee, Y.H., Leeuwenburgh, C., Lefort, S., Legouis, R., Lei, J., Lei, Q.-Y., Leib, D.A., Leibowitz, G., Lekli, I., Lemaire, S.D., Lemasters, J.J., Lemberg, M.K., Lemoine, A., Leng, S., Lenz, G., Lenzi, P., Lerman, L.O., Lettieri Barbato, D., Leu, J.I.-J., Leung, H.Y., Levine, B., Lewis, P.A., Lezoualc'h, F., Li, C., Li, F., Li, F.-J., Li, J., Li, K., Li, L., Li, M., Li, M., Li, Q., Li, R., Li, S., Li, W., Li, W., Li, X., Li, Y., Lian, J., Liang, C., Liang, Q., Liao, Y., Liberal, J., Liberski, P.P., Lie, P., Lieberman, A.P., Lim, H.J., Lim, K.-L., Lim, K., Lima, R.T., Lin, C.-S., Lin, C.-F., Lin, Fang, Lin, Fangming, Lin, F.-C., Lin, K., Lin, K.-H., Lin, P.-H., Lin, T., Lin, W.-W., Lin, Y.-S., Lin, Y., Linden, R., Lindholm, D., Lindqvist, L.M., Lingor, P., Linkermann, A., Liotta, L.A., Lipinski, M.M., Lira, V.A., Lisanti, M.P., Liton, P.B., Liu, B., Liu, C., Liu, C.-F., Liu, F., Liu, H.-J., Liu, J., Liu, J.-J., Liu, J.-L., Liu, K., Liu, Leyuan, Liu, Liang, Liu, Q., Liu, R.-Y., Liu, Shiming, Liu, Shuwen, Liu, W., Liu, X.-D., Liu, Xiangguo, Liu, X.-H., Liu, Xinfeng, Liu, Xu, Liu, Xueqin, Liu, Yang, Liu, Yule, Liu, Zexian, Liu, Zhe, Liuzzi, J.P., Lizard, G., Ljujic, M., Lodhi, I.J., Logue, S.E., Lokeshwar, B.L., Long, Y.C., Lonial, S., Loos, B., López-Otín, C., López-Vicario, C., Lorente, M., Lorenzi, P.L., Lõrincz, P., Los, M., Lotze, M.T., Lovat, P.E., Lu, Binfeng, Lu, Bo, Lu, J., Lu, Q., Lu, S.-M., Lu, S., Lu, Y., Luciano, F., Luckhart, S., Lucocq, J.M., Ludovico, P., Lugea, A., Lukacs, N.W., Lum, J.J., Lund, A.H., Luo, H., Luo, J., Luo, S., Luparello, C., Lyons, T., Ma, J., Ma, Yi, Ma, Yong, Ma, Z., Machado, J., Machado-Santelli, G.M., Macian, F., MacIntosh, G.C., MacKeigan, J.P., Macleod, K.F., MacMicking, J.D., MacMillan-Crow, L.A., Madeo, F., Madesh, M., Madrigal-Matute, J., Maeda, A., Maeda, T., Maegawa, G., Maellaro, E., Maes, H., Magariños, M., Maiese, K., Maiti, T.K., Maiuri, L., Maiuri, M.C., Maki, C.G., Malli, R., Malorni, W., Maloyan, A., Mami-Chouaib, F., Man, N., Mancias, J.D., Mandelkow, E.-M., Mandell, M.A., Manfredi, A.A., Manié, S.N., Manzoni, C., Mao, K., Mao, Z., Mao, Z.-W., Marambaud, P., Marconi, A.M., Marelja, Z., Marfe, G., Margeta, M., Margittai, E., Mari, M., Mariani, F.V., Marin, C., Marinelli, S., Mariño, G., Markovic, I., Marquez, R., Martelli, A.M., Martens, S., Martin, K.R., Martin, S.J., Martin, S., Martin-Acebes, M.A., Martín-Sanz, P., Martinand-Mari, C., Martinet, W., Martinez, J., Martinez-Lopez, N., Martinez-Outschoorn, U., Martínez-Velázquez, M., Martinez-Vicente, M., Martins, W.K., Mashima, H., Mastrianni, J.A., Matarese, G., Matarrese, P., Mateo, R., Matoba, S., Matsumoto, N., Matsushita, T., Matsuura, A., Matsuzawa, T., Mattson, M.P., Matus, S., Maugeri, N., Mauvezin, C., Mayer, A., Maysinger, D., Mazzolini, G.D.,

McBrayer, M.K., McCall, K., McCormick, C., McInerney, G.M., McIver, S.C., McKenna, S., McMahon, J.J., McNeish, I.A., Mechta-Grigoriou, F., Medema, J.P., Medina, D.L., Megyeri, K., Mehrpour, M., Mehta, J.L., Mei, Y., Meier, U.-C., Meijer, A.J., Meléndez, A., Melino, G., Melino, S., de Melo, E.J.T., Mena, M.A., Meneghini, M.D., Menendez, J.A., Menezes, R., Meng, L., Meng, L.-H., Meng, S., Menghini, R., Menko, A.S., Menna-Barreto, R.F., Menon, M.B., Meraz-Ríos, M.A., Merla, G., Merlini, L., Merlot, A.M., Meryk, A., Meschini, S., Meyer, J.N., Mi, M.-T., Miao, C.-Y., Micale, L., Michaeli, S., Michiels, C., Migliaccio, A.R., Mihailidou, A.S., Mijaljica, D., Mikoshiba, K., Milan, E., Miller-Fleming, L., Mills, G.B., Mills, I.G., Minakaki, G., Minassian, B.A., Ming, X.-F., Minibayeva, F., Minina, E.A., Mintern, J.D., Minucci, S., Miranda-Vizuete, A., Mitchell, C.H., Miyamoto, S., Miyazawa, K., Mizushima, N., Mnich, K., Mograbi, B., Mohseni, S., Moita, L.F., Molinari, Marco, Molinari, Maurizio, Møller, A.B., Mollereau, B., Mollinedo, F., Mongillo, M., Monick, M.M., Montagnaro, S., Montell, C., Moore, D.J., Moore, M.N., Mora-Rodriguez, R., Moreira, P.I., Morel, E., Morelli, M.B., Moreno, S., Morgan, M.J., Moris, A., Moriyasu, Y., Morrison, J.L., Morrison, L.A., Morselli, E., Moscat, J., Moseley, P.L., Mostowy, S., Motori, E., Mottet, D., Mottram, J.C., Moussa, C.E.-H., Mpakou, V.E., Mukhtar, H., Mulcahy Levy, J.M., Muller, S., Muñoz-Moreno, R., Muñoz-Pinedo, C., Münz, C., Murphy, M.E., Murray, J.T., Murthy, A., Mysorekar, I.U., Nabi, I.R., Nabissi, M., Nader, G.A., Nagahara, Y., Nagai, Y., Nagata, K., Nagelkerke, A., Nagy, P., Naidu, S.R., Nair, S., Nakano, H., Nakatogawa, H., Nanjundan, M., Napolitano, G., Naqvi, N.I., Nardacci, R., Narendra, D.P., Narita, M., Nascimbeni, A.C., Natarajan, R., Navegantes, L.C., Nawrocki, S.T., Nazarko, T.Y., Nazarko, V.Y., Neill, T., Neri, L.M., Netea, M.G., Netea-Maier, R.T., Neves, B.M., Ney, P.A., Nezis, I.P., Nguyen, H.T., Nguyen, H.P., Nicot, A.-S., Nilsen, H., Nilsson, P., Nishimura, M., Nishino, I., Niso-Santano, M., Niu, H., Nixon, R.A., Njar, V.C., Noda, T., Noegel, A.A., Nolte, E.M., Norberg, E., Norga, K.K., Noureini, S.K., Notomi, S., Notterpek, L., Nowikovsky, K., Nukina, N., Nürnberger, T., O'Donnell, V.B., O'Donovan, T., O'Dwyer, P.J., Oehme, I., Oeste, C.L., Ogawa, M., Ogretmen, B., Ogura, Y., Oh, Y.J., Ohmuraya, M., Ohshima, T., Ojha, R., Okamoto, K., Okazaki, T., Oliver, F.J., Ollinger, K., Olsson, S., Orban, D.P., Ordonez, P., Orhon, I., Orosz, L., O'Rourke, E.J., Orozco, H., Ortega, A.L., Ortona, E., Osellame, L.D., Oshima, J., Oshima, S., Osiewacz, H.D., Otomo, T., Otsu, K., Ou, J.-H.J., Outeiro, T.F., Ouyang, D.-Y., Ouyang, H., Overholtzer, M., Ozbun, M.A., Ozdinler, P.H., Ozpolat, B., Pacelli, C., Paganetti, P., Page, G., Pages, G., Pagnini, U., Pajak, B., Pak, S.C., Pakos-Zebrucka, K., Pakpour, N., Palková, Z., Palladino, F., Pallauf, K., Pallet, N., Palmieri, M., Paludan,

S.R., Palumbo, C., Palumbo, S., Pampliega, O., Pan, H., Pan, W., Panaretakis, T., Pandey, A., Pantazopoulou, A., Papackova, Z., Papademetrio, D.L., Papassideri, I., Papini, A., Parajuli, N., Pardo, J., Parekh, V.V., Parenti, G., Park, J.-I., Park, J., Park, O.K., Parker, R., Parlato, R., Parys, J.B., Parzych, K.R., Pasquet, J.-M., Pasquier, B., Pasumarthi, K.B., Patschan, D., Patterson, C., Pattingre, S., Pattison, S., Pause, A., Pavenstädt, H., Pavone, F., Pedrozo, Z., Peña, F.J., Peñalva, M.A., Pende, M., Peng, J., Penna, F., Penninger, J.M., Pensalfini, A., Pepe, S., Pereira, G.J., Pereira, P.C., Pérez-de la Cruz, V., Pérez-Pérez, M.E., Pérez-Rodríguez, D., Pérez-Sala, D., Perier, C., Perl, A., Perlmutter, D.H., Perrotta, I., Pervaiz, S., Pesonen, M., Pessin, J.E., Peters, G.J., Petersen, M., Petrache, I., Petrof, B.J., Petrovski, G., Phang, J.M., Piacentini, M., Pierdominici, M., Pierre, P., Pierrefite-Carle, V., Pietrocola, F., Pimentel-Muiños, F.X., Pinar, M., Pineda, B., Pinkas-Kramarski, R., Pinti, M., Pinton, P., Piperdi, B., Piret, J.M., Platanias, L.C., Platta, H.W., Plowey, E.D., Pöggeler, S., Poirot, M., Polčic, P., Poletti, A., Poon, A.H., Popelka, H., Popova, B., Poprawa, I., Poulose, S.M., Poulton, J., Powers, S.K., Powers, T., Pozuelo-Rubio, M., Prak, K., Prange, R., Prescott, M., Priault, M., Prince, S., Proia, R.L., Proikas-Cezanne, T., Prokisch, H., Promponas, V.J., Przyklenk, K., Puertollano, R., Pugazhenthi, S., Puglielli, L., Pujol, A., Puyal, J., Pyeon, D., Qi, X., Qian, W.-B., Qin, Z.-H., Qiu, Y., Qu, Z., Quadrilatero, J., Quinn, F., Raben, N., Rabinowich, H., Radogna, F., Ragusa, M.J., Rahmani, M., Raina, K., Ramanadham, S., Ramesh, R., Rami, A., Randall-Demllo, S., Randow, F., Rao, H., Rao, V.A., Rasmussen, B.B., Rasse, T.M., Ratovitski, E.A., Rautou, P.-E., Ray, S.K., Razani, B., Reed, B.H., Reggiori, F., Rehm, M., Reichert, A.S., Rein, T., Reiner, D.J., Reits, E., Ren, J., Ren, X., Renna, M., Reusch, J.E., Revuelta, J.L., Reyes, L., Rezaie, A.R., Richards, R.I., Richardson, D.R., Richetta, C., Riehle, M.A., Rihn, B.H., Rikihisa, Y., Riley, B.E., Rimbach, G., Rippo, M.R., Ritis, K., Rizzi, F., Rizzo, E., Roach, P.J., Robbins, J., Roberge, M., Roca, G., Roccheri, M.C., Rocha, S., Rodrigues, C.M., Rodríguez, C.I., de Cordoba, S.R., Rodriguez-Muela, N., Roelofs, J., Rogov, V.V., Rohn, T.T., Rohrer, B., Romanelli, D., Romani, L., Romano, P.S., Roncero, M.I.G., Rosa, J.L., Rosello, A., Rosen, K.V., Rosenstiel, P., Rost-Roszkowska, M., Roth, K.A., Roué, G., Rouis, M., Rouschop, K.M., Ruan, D.T., Ruano, D., Rubinsztein, D.C., Rucker, E.B., Rudich, A., Rudolf, E., Rudolf, R., Ruegg, M.A., Ruiz-Roldan, C., Ruparelia, A.A., Rusmini, P., Russ, D.W., Russo, G.L., Russo, G., Russo, R., Rusten, T.E., Ryabovol, V., Ryan, K.M., Ryter, S.W., Sabatini, D.M., Sacher, M., Sachse, C., Sack, M.N., Sadoshima, J., Saftig, P., Sagi-Eisenberg, R., Sahni, S., Saikumar, P., Saito, T., Saitoh, T., Sakakura, K., Sakoh-

Nakatogawa, M., Sakuraba, Y., Salazar-Roa, M., Salomoni, P., Saluja, A.K., Salvaterra, P.M., Salvioli, R., Samali, A., Sanchez, A.M., Sánchez-Alcázar, J.A., Sanchez-Prieto, R., Sandri, M., Sanjuan, M.A., Santaguida, S., Santambrogio, L., Santoni, G., Dos Santos, C.N., Saran, S., Sardiello, M., Sargent, G., Sarkar, P., Sarkar, S., Sarrias, M.R., Sarwal, M.M., Sasakawa, C., Sasaki, M., Sass, M., Sato, K., Sato, M., Satriano, J., Savaraj, N., Saveljeva, S., Schaefer, L., Schaible, U.E., Scharl, M., Schatzl, H.M., Schekman, R., Scheper, W., Schiavi, A., Schipper, H.M., Schmeisser, H., Schmidt, J., Schmitz, I., Schneider, B.E., Schneider, E.M., Schneider, J.L., Schon, E.A., Schönenberger, M.J., Schönthal, A.H., Schorderet, D.F., Schröder, B., Schuck, S., Schulze, R.J., Schwarten, M., Schwarz, T.L., Sciarretta, S., Scotto, K., Scovassi, A.I., Screaton, R.A., Screen, M., Seca, H., Sedej, S., Segatori, L., Segev, N., Seglen, P.O., Seguí-Simarro, J.M., Segura-Aguilar, J., Seki, E., Sell, C., Seiliez, I., Semenkovich, C.F., Semenza, G.L., Sen, U., Serra, A.L., Serrano-Puebla, A., Sesaki, H., Setoguchi, T., Settembre, C., Shacka, J.J., Shajahan-Haq, A.N., Shapiro, I.M., Sharma, S., She, H., Shen, C.-K.J., Shen, C.-C., Shen, H.-M., Shen, S., Shen, W., Sheng, R., Sheng, X., Sheng, Z.-H., Shepherd, T.G., Shi, J., Shi, Qiang, Shi, Qinghua, Shi, Y., Shibutani, S., Shibuya, K., Shidoji, Y., Shieh, J.-J., Shih, C.-M., Shimada, Y., Shimizu, S., Shin, D.W., Shinohara, M.L., Shintani, M., Shintani, T., Shioi, T., Shirabe, K., Shiri-Sverdlov, R., Shirihai, O., Shore, G.C., Shu, C.-W., Shukla, D., Sibirny, A.A., Sica, V., Sigurdson, C.J., Sigurdsson, E.M., Sijwali, P.S., Sikorska, B., Silveira, W.A., Silvente-Poirot, S., Silverman, G.A., Simak, J., Simmet, T., Simon, A.K., Simon, H.-U., Simone, C., Simons, M., Simonsen, A., Singh, R., Singh, S.V., Singh, S.K., Sinha, D., Sinha, S., Sinicrope, F.A., Sirko, A., Sirohi, K., Sishi, B.J., Sittler, A., Siu, P.M., Sivridis, E., Skwarska, A., Slack, R., Slaninová, I., Slavov, N., Smaili, S.S., Smalley, K.S., Smith, D.R., Soenen, S.J., Soleimanpour, S.A., Solhaug, A., Somasundaram, K., Son, J.H., Sonawane, A., Song, C., Song, F., Song, H.K., Song, J.-X., Song, W., Soo, K.Y., Sood, A.K., Soong, T.W., Soontornniyomkij, V., Sorice, M., Sotgia, F., Soto-Pantoja, D.R., Sotthibundhu, A., Sousa, M.J., Spaink, H.P., Span, P.N., Spang, A., Sparks, J.D., Speck, P.G., Spector, S.A., Spies, C.D., Springer, W., Clair, D.S., Stacchiotti, A., Staels, B., Stang, M.T., Starczynowski, D.T., Starokadomskyy, P., Steegborn, C., Steele, J.W., Stefanis, L., Steffan, J., Stellrecht, C.M., Stenmark, H., Stepkowski, T.M., Stern, S.T., Stevens, C., Stockwell, B.R., Stoka, V., Storchova, Z., Stork, B., Stratoulias, V., Stravopodis, D.J., Strnad, P., Strohecker, A.M., Ström, A.-L., Stromhaug, P., Stulik, J., Su, Y.-X., Su, Z., Subauste, C.S., Subramaniam, S., Sue, C.M., Suh, S.W., Sui, X., Sukseree, S., Sulzer, D., Sun, F.-L., Sun, Jiaren, Sun, Jun, Sun, S.-

Y., Sun, Yang, Sun, Yi, Sun, Yingjie, Sundaramoorthy, V., Sung, J., Suzuki, H., Suzuki, K., Suzuki, N., Suzuki, T., Suzuki, Y.J., Swanson, M.S., Swanton, C., Swärd, K., Swarup, G., Sweeney, S.T., Sylvester, P.W., Szatmari, Z., Szegezdi, E., Szlosarek, P.W., Taegtmeyer, H., Tafani, M., Taillebourg, E., Tait, S.W., Takacs-Vellai, K., Takahashi, Y., Takáts, S., Takemura, G., Takigawa, N., Talbot, N.J., Tamagno, E., Tamburini, J., Tan, C.-P., Tan, L., Tan, M.L., Tan, M., Tan, Y.-J., Tanaka, K., Tanaka, M., Tang, Daolin, Tang, Dingzhong, Tang, G., Tanida, I., Tanji, K., Tannous, B.A., Tapia, J.A., Tasset-Cuevas, I., Tatar, M., Tavassoly, I., Tavernarakis, N., Taylor, A., Taylor, G.S., Taylor, G.A., Taylor, J.P., Taylor, M.J., Tchetina, E.V., Tee, A.R., Teixeira-Clerc, F., Telang, S., Tencomnao, T., Teng, B.-B., Teng, R.-J., Terro, F., Tettamanti, G., Theiss, A.L., Theron, A.E., Thomas, K.J., Thomé, M.P., Thomes, P.G., Thorburn, A., Thorner, J., Thum, T., Thumm, M., Thurston, T.L., Tian, L., Till, A., Ting, J.P.-Y., Titorenko, V.I., Toker, L., Toldo, S., Tooze, S.A., Topisirovic, I., Torgersen, M.L., Torosantucci, L., Torriglia, A., Torrisi, M.R., Tournier, C., Towns, R., Trajkovic, V., Travassos, L.H., Triola, G., Tripathi, D.N., Trisciuoglio, D., Troncoso, R., Trougakos, I.P., Truttmann, A.C., Tsai, K.-J., Tschan, M.P., Tseng, Y.-H., Tsukuba, T., Tsung, A., Tsvetkov, A.S., Tu, S., Tuan, H.-Y., Tucci, M., Tumbarello, D.A., Turk, B., Turk, V., Turner, R.F., Tveita, A.A., Tyagi, S.C., Ubukata, M., Uchiyama, Y., Udelnow, A., Ueno, T., Umekawa, M., Umemiya-Shirafuji, R., Underwood, B.R., Ungermann, C., Ureshino, R.P., Ushioda, R., Uversky, V.N., Uzcátegui, N.L., Vaccari, T., Vaccaro, M.I., Váchová, L., Vakifahmetoglu-Norberg, H., Valdor, R., Valente, E.M., Vallette, F., Valverde, A.M., Van den Berghe, G., Van Den Bosch, L., van den Brink, G.R., van der Goot, F.G., van der Klei, I.J., van der Laan, L.J., van Doorn, W.G., van Egmond, M., van Golen, K.L., Van Kaer, L., van Lookeren Campagne, M., Vandenabeele, P., Vandenberghe, W., Vanhorebeek, I., Varela-Nieto, I., Vasconcelos, M.H., Vasko, R., Vavvas, D.G., Vega-Naredo, I., Velasco, G., Velentzas, A.D., Velentzas, P.D., Vellai, T., Vellenga, E., Vendelbo, M.H., Venkatachalam, K., Ventura, N., Ventura, S., Veras, P.S., Verdier, M., Vertessy, B.G., Viale, A., Vidal, M., Vieira, H.L.A., Vierstra, R.D., Vigneswaran, N., Vij, N., Vila, M., Villar, M., Villar, V.H., Villarroya, J., Vindis, C., Viola, G., Viscomi, M.T., Vitale, G., Vogl, D.T., Voitsekhovskaja, O.V., von Haefen, C., von Schwarzenberg, K., Voth, D.E., Vouret-Craviari, V., Vuori, K., Vyas, J.M., Waeber, C., Walker, C.L., Walker, M.J., Walter, J., Wan, L., Wan, X., Wang, B., Wang, Caihong, Wang, C.-Y., Wang, Chengshu, Wang, Chenran, Wang, Chuangui, Wang, D., Wang, Fen, Wang, Fuxin, Wang, G., Wang, H.-J., Wang, Haichao, Wang, H.-G., Wang, Hongmin, Wang, H.-D., Wang, Jing, Wang, Junjun, Wang, M., Wang, M.-Q., Wang, P.-Y., Wang,

P., Wang, R.C., Wang, S., Wang, T.-F., Wang, Xian, Wang, X.-J., Wang, X.-W., Wang, Xin, Wang, Xuejun, Wang, Yan, Wang, Yanming, Wang, Ying, Wang, Y.-J., Wang, Yipeng, Wang, Yu, Wang, Y.T., Wang, Yuqing, Wang, Z.-N., Wappner, P., Ward, C., Ward, D.M., Warnes, G., Watada, H., Watanabe, Y., Watase, K., Weaver, T.E., Weekes, C.D., Wei, J., Weide, T., Weihl, C.C., Weindl, G., Weis, S.N., Wen, L., Wen, X., Wen, Y., Westermann, B., Weyand, C.M., White, A.R., White, E., Whitton, J.L., Whitworth, A.J., Wiels, J., Wild, F., Wildenberg, M.E., Wileman, T., Wilkinson, D.S., Wilkinson, S., Willbold, D., Williams, C., Williams, K., Williamson, P.R., Winklhofer, K.F., Witkin, S.S., Wohlgemuth, S.E., Wollert, T., Wolvetang, E.J., Wong, E., Wong, G.W., Wong, R.W., Wong, V.K.W., Woodcock, E.A., Wright, K.L., Wu, C., Wu, D., Wu, G.S., Wu, Jian, Wu, Junfang, Wu, Mian, Wu, Min, Wu, S., Wu, W.K., Wu, Y., Wu, Z., Xavier, C.P., Xavier, R.J., Xia, G.-X., Xia, T., Xia, W., Xia, Y., Xiao, H., Xiao, J., Xiao, S., Xiao, W., Xie, C.-M., Xie, Zhiping, Xie, Zhonglin, Xilouri, M., Xiong, Y., Xu, Chuanshan, Xu, Congfeng, Xu, F., Xu, Haoxing, Xu, Hongwei, Xu, Jian, Xu, Jianzhen, Xu, Jinxian, Xu, L., Xu, X., Xu, Yangqing, Xu, Ye, Xu, Z.-X., Xu, Z., Xue, Y., Yamada, T., Yamamoto, A., Yamanaka, K., Yamashina, S., Yamashiro, S., Yan, Bing, Yan, Bo, Yan, X., Yan, Z., Yanagi, Y., Yang, D.-S., Yang, J.-M., Yang, L., Yang, M., Yang, P.-M., Yang, P., Yang, Q., Yang, W., Yang, W.Y., Yang, X., Yang, Yi, Yang, Ying, Yang, Zhifen, Yang, Zhihong, Yao, M.-C., Yao, P.J., Yao, X., Yao, Zhenyu, Yao, Zhiyuan, Yasui, L.S., Ye, M., Yedvobnick, B., Yeganeh, B., Yeh, E.S., Yeyati, P.L., Yi, F., Yi, L., Yin, X.-M., Yip, C.K., Yoo, Y.-M., Yoo, Y.H., Yoon, S.-Y., Yoshida, K.-I., Yoshimori, T., Young, K.H., Yu, H., Yu, J.J., Yu, J.-T., Yu, J., Yu, L., Yu, W.H., Yu, X.-F., Yu, Z., Yuan, J., Yuan, Z.-M., Yue, B.Y., Yue, J., Yue, Z., Zacks, D.N., Zacksenhaus, E., Zaffaroni, N., Zaglia, T., Zakeri, Z., Zecchini, V., Zeng, J., Zeng, M., Zeng, Q., Zervos, A.S., Zhang, D.D., Zhang, F., Zhang, G., Zhang, G.-C., Zhang, Hao, Zhang, Hong, Zhang, Hong, Zhang, Hongbing, Zhang, Jian, Zhang, Jian, Zhang, Jiangwei, Zhang, Jianhua, Zhang, J.-P., Zhang, Li, Zhang, Lin, Zhang, Lin, Zhang, Long, Zhang, M.-Y., Zhang, X., Zhang, X.D., Zhang, Yan, Zhang, Yang, Zhang, Yanjin, Zhang, Yingmei, Zhang, Yunjiao, Zhao, M., Zhao, W.-L., Zhao, X., Zhao, Y.G., Zhao, Ying, Zhao, Yongchao, Zhao, Y.-X., Zhao, Z., Zhao, Z.J., Zheng, D., Zheng, X.-L., Zheng, X., Zhivotovsky, B., Zhong, Q., Zhou, G.-Z., Zhou, G., Zhou, H., Zhou, S.-F., Zhou, X.-J., Zhu, Hongxin, Zhu, Hua, Zhu, W.-G., Zhu, W., Zhu, X.-F., Zhu, Y., Zhuang, S.-M., Zhuang, X., Ziparo, E., Zois, C.E., Zoladek, T., Zong, W.-X., Zorzano, A., Zughaier, S.M., 2016. Guidelines for the use and interpretation of assays for monitoring autophagy (3rd edition). Autophagy 12, 1–222. https://doi.org/10.1080/15548627.2015.1100356

Kornak, U., Kasper, D., Bösl, M.R., Kaiser, E., Schweizer, M., Schulz, A., Friedrich, W., Delling, G., Jentsch, T.J., 2001. Loss of the ClC-7 chloride channel leads to osteopetrosis in mice and man. Cell 104, 205–215. https://doi.org/10.1016/s0092-8674(01)00206-9

Lachmann, N., Ackermann, M., Frenzel, E., Liebhaber, S., Brennig, S., Happle, C., Hoffmann, D., Klimenkova, O., Lüttge, D., Buchegger, T., Kühnel, M.P., Schambach, A., Janciauskiene, S., Figueiredo, C., Hansen, G., Skokowa, J., Moritz, T., 2015. Large-scale hematopoietic differentiation of human induced pluripotent stem cells provides granulocytes or macrophages for cell replacement therapies. Stem Cell Rep. 4, 282–296. https://doi.org/10.1016/j.stemcr.2015.01.005

Lakkakorpi, P.T., Väänänen, K.H., 1991. Kinetics of the osteoclast cytoskeleton during the resorption cycle in vitro. J. Bone Miner. Res. 6, 817–826. https://doi.org/10.1002/jbmr.5650060806

Lancaster, M.A., Renner, M., Martin, C.-A., Wenzel, D., Bicknell, L.S., Hurles, M.E., Homfray, T., Penninger, J.M., Jackson, A.P., Knoblich, J.A., 2013. Cerebral organoids model human brain development and microcephaly. Nature 501, 10.1038/nature12517. https://doi.org/10.1038/nature12517

Lange, P.F., Wartosch, L., Jentsch, T.J., Fuhrmann, J.C., 2006. ClC-7 requires Ostm1 as a beta-subunit to support bone resorption and lysosomal function. Nature 440, 220–223. https://doi.org/10.1038/nature04535

Leisle, L., Ludwig, C.F., Wagner, F.A., Jentsch, T.J., Stauber, T., 2011. ClC-7 is a slowly voltage-gated 2Cl−/1H+-exchanger and requires Ostm1 for transport activity. EMBO J. 30, 2140–2152. https://doi.org/10.1038/emboj.2011.137

McDonald, M.M., Khoo, W.H., Ng, P.Y., Xiao, Y., Zamerli, J., Thatcher, P., Kyaw, W., Pathmanandavel, K., Grootveld, A.K., Moran, I., Butt, D., Nguyen, A., Warren, S., Biro, M., Butterfield, N.C., Guilfoyle, S.E., Komla-Ebri, D., Dack, M.R.G., Dewhurst, H.F., Logan, J.G., Li, Y., Mohanty, S.T., Byrne, N., Terry, R.L., Simic, M.K., Chai, R., Quinn, J.M.W., Youlten, S.E., Pettitt, J.A., Abi-Hanna, D., Jain, R., Weninger, W., Lundberg, M., Sun, S., Ebetino, F.H., Timpson, P., Lee, W.M., Baldock, P.A., Rogers, M.J., Brink, R., Williams, G.R., Bassett, J.H.D., Kemp, J.P., Pavlos, N.J., Croucher, P.I., Phan, T.G., 2021. Osteoclasts recycle via osteomorphs during RANKL-stimulated bone resorption. Cell 184, 1330-1347.e13. https://doi.org/10.1016/j.cell.2021.02.002

Mellis, D.J., Itzstein, C., Helfrich, M.H., Crockett, J.C., 2011. The skeleton: a multi-

functional complex organ: the role of key signalling pathways in osteoclast differentiation and in bone resorption. J. Endocrinol. 211, 131–143. https://doi.org/10.1530/JOE-11-0212

Merrild, D.M., Pirapaharan, D.C., Andreasen, C.M., Kjærsgaard-Andersen, P., Møller, A.M., Ding, M., Delaissé, J.-M., Søe, K., 2015. Pit- and trench-forming osteoclasts: a distinction that matters. Bone Res. 3, 15032. https://doi.org/10.1038/boneres.2015.32

Møller, A.M.J., Delaissé, J.-M., Olesen, J.B., Canto, L.M., Rogatto, S.R., Madsen, J.S., Søe, K., 2020. Fusion Potential of Human Osteoclasts In Vitro Reflects Age, Menopause, and In Vivo Bone Resorption Levels of Their Donors—A Possible Involvement of DC-STAMP. Int. J. Mol. Sci. 21, 6368. https://doi.org/10.3390/ijms21176368

Mulari, M.T.K., Zhao, H., Lakkakorpi, P.T., Väänänen, H.K., 2003. Osteoclast ruffled border has distinct subdomains for secretion and degraded matrix uptake. Traffic Cph. Den. 4, 113–125. https://doi.org/10.1034/j.1600-0854.2003.40206.x

Neutzsky-Wulff, A.V., Sims, N.A., Supanchart, C., Kornak, U., Felsenberg, D., Poulton, I.J., Martin, T.J., Karsdal, M.A., Henriksen, K., 2010. Severe developmental bone phenotype in ClC-7 deficient mice. Dev. Biol. 344, 1001–1010. https://doi.org/10.1016/j.ydbio.2010.06.018

Pangrazio, A., Pusch, M., Caldana, E., Frattini, A., Lanino, E., Tamhankar, P.M., Phadke, S., Lopez, A.G.M., Orchard, P., Mihci, E., Abinun, M., Wright, M., Vettenranta, K., Bariae, I., Melis, D., Tezcan, I., Baumann, C., Locatelli, F., Zecca, M., Horwitz, E., Mansour, L.S.B., Van Roij, M., Vezzoni, P., Villa, A., Sobacchi, C., 2010. Molecular and clinical heterogeneity in CLCN7-dependent osteopetrosis: report of 20 novel mutations. Hum. Mutat. 31, E1071-1080. https://doi.org/10.1002/humu.21167

Papapetrou, E.P., Schambach, A., 2016. Gene Insertion Into Genomic Safe Harbors for Human Gene Therapy. Mol. Ther. J. Am. Soc. Gene Ther. 24, 678–684. https://doi.org/10.1038/mt.2016.38

Pata, M., Vacher, J., 2018. Ostm1 Bifunctional Roles in Osteoclast Maturation: Insights From a Mouse Model Mimicking a Human OSTM1 Mutation. J. Bone Miner. Res. Off. J. Am. Soc. Bone Miner. Res. 33, 888–898. https://doi.org/10.1002/jbmr.3378

Penna, S., Capo, V., Palagano, E., Sobacchi, C., Villa, A., 2019. One Disease, Many Genes: Implications for the Treatment of Osteopetroses. Front. Endocrinol. 10, 85.

https://doi.org/10.3389/fendo.2019.00085

Penney, J., Ralvenius, W.T., Tsai, L.-H., 2020. Modeling Alzheimer's disease with iPSC-derived brain cells. Mol. Psychiatry 25, 148–167. https://doi.org/10.1038/s41380-019-0468-3

Robbins, G.M., Wang, M., Pomeroy, E.J., Moriarity, B.S., 2021. Nonviral genome engineering of natural killer cells. Stem Cell Res. Ther. 12, 350. https://doi.org/10.1186/s13287-021-02406-6

Röntgenbilder einer seltenen Knochenerkrankungen (p.365). von Albers-Schönberg, Heinrich Ernst: (1904) | Antiq. F.-D. Söhn - Medicusbooks.Com [WWW Document], n.d. URL https://www.zvab.com/R%C3%B6ntgenbilder-seltenen-Knochenerkrankungen-p.365-Albers-Sch%C3%B6nberg-Heinrich/988612533/bd (accessed 7.9.23).

Rössler, U., Hennig, A.F., Stelzer, N., Bose, S., Kopp, J., Søe, K., Cyganek, L., Zifarelli, G., Ali, S., von der Hagen, M., Strässler, E., Hahn, G., Pusch, M., Stauber, T., Izsvák, Z., Gossen, M., Stachelscheid, H., Kornak, U., 2021. Efficient generation of osteoclasts from human induced pluripotent stem cells and functional investigations of lethal CLCN7-related osteopetrosis. J. Bone Miner. Res. Off. J. Am. Soc. Bone Miner. Res. https://doi.org/10.1002/jbmr.4322

Saltel, F., Chabadel, A., Bonnelye, E., Jurdic, P., 2008. Actin cytoskeletal organisation in osteoclasts: a model to decipher transmigration and matrix degradation. Eur. J. Cell Biol. 87, 459–468. https://doi.org/10.1016/j.ejcb.2008.01.001

Seeman, E., Delmas, P.D., 2006. Bone quality--the material and structural basis of bone strength and fragility. N. Engl. J. Med. 354, 2250–2261. https://doi.org/10.1056/NEJMra053077

Sobacchi, C., Schulz, A., Coxon, F.P., Villa, A., Helfrich, M.H., 2013. Osteopetrosis: genetics, treatment and new insights into osteoclast function. Nat. Rev. Endocrinol. 9, 522–536. https://doi.org/10.1038/nrendo.2013.137

Søe, K., Delaissé, J.-M., 2017. Time-lapse reveals that osteoclasts can move across the bone surface while resorbing. J. Cell Sci. 130, 2026–2035. https://doi.org/10.1242/jcs.202036

Søe, K., Merrild, D.M.H., Delaissé, J.-M., 2013. Steering the osteoclast through the demineralization-collagenolysis balance. Bone 56, 191–198.

https://doi.org/10.1016/j.bone.2013.06.007

Stauber, T., Jentsch, T.J., 2010. Sorting motifs of the endosomal/lysosomal CLC chloride transporters. J. Biol. Chem. 285, 34537–34548. https://doi.org/10.1074/jbc.M110.162545

Steinberg, B.E., Huynh, K.K., Brodovitch, A., Jabs, S., Stauber, T., Jentsch, T.J., Grinstein, S., 2010. A cation counterflux supports lysosomal acidification. J. Cell Biol. 189, 1171–1186. https://doi.org/10.1083/jcb.200911083

Stenbeck, G., Horton, M.A., 2004. Endocytic trafficking in actively resorbing osteoclasts. J. Cell Sci. 117, 827–836. https://doi.org/10.1242/jcs.00935

Supanchart, C., Wartosch, L., Schlack, C., Kühnisch, J., Felsenberg, D., Fuhrmann, J.C., de Vernejoul, M.-C., Jentsch, T.J., Kornak, U., 2014. ClC-7 expression levels critically regulate bone turnover, but not gastric acid secretion. Bone 58, 92–102. https://doi.org/10.1016/j.bone.2013.09.022

Takahashi, K., Yamanaka, S., 2006. Induction of pluripotent stem cells from mouse embryonic and adult fibroblast cultures by defined factors. Cell 126, 663–676. https://doi.org/10.1016/j.cell.2006.07.024

Teinert, J., Behne, R., Wimmer, M., Ebrahimi-Fakhari, D., 2020. Novel insights into the clinical and molecular spectrum of congenital disorders of autophagy. J. Inherit. Metab. Dis. 43, 51–62. https://doi.org/10.1002/jimd.12084

Tipanee, J., Chai, Y.C., VandenDriessche, T., Chuah, M.K., 2017. Preclinical and clinical advances in transposon-based gene therapy. Biosci. Rep. 37, BSR20160614. https://doi.org/10.1042/BSR20160614

Walker, D.G., 1975. Control of bone resorption by hematopoietic tissue. The induction and reversal of congenital osteopetrosis in mice through use of bone marrow and splenic transplants. J. Exp. Med. 142, 651–663. https://doi.org/10.1084/jem.142.3.651

Wartosch, L., Fuhrmann, J.C., Schweizer, M., Stauber, T., Jentsch, T.J., 2009. Lysosomal degradation of endocytosed proteins depends on the chloride transport protein ClC-7. FASEB J. Off. Publ. Fed. Am. Soc. Exp. Biol. 23, 4056–4068. https://doi.org/10.1096/fj.09-130880

Wartosch, L., Stauber, T., 2010. A role for chloride transport in lysosomal protein degradation. Autophagy 6, 158–159. https://doi.org/10.4161/auto.6.1.10590

Weinert, S., Jabs, S., Hohensee, S., Chan, W.L., Kornak, U., Jentsch, T.J., 2014. Transport activity and presence of ClC-7/Ostm1 complex account for different cellular functions. EMBO Rep. 15, 784–791. https://doi.org/10.15252/embr.201438553

Weinert, S., Jabs, S., Supanchart, C., Schweizer, M., Gimber, N., Richter, M., Rademann, J., Stauber, T., Kornak, U., Jentsch, T.J., 2010. Lysosomal pathology and osteopetrosis upon loss of H+-driven lysosomal Cl- accumulation. Science 328, 1401–1403. https://doi.org/10.1126/science.1188072

Yang, X., Pabon, L., Murry, C.E., 2014. Engineering adolescence: maturation of human pluripotent stem cell-derived cardiomyocytes. Circ. Res. 114, 511–523. https://doi.org/10.1161/CIRCRESAHA.114.300558

Statutory declaration

“I, Uta Rössler, by personally signing this document in lieu of an oath, hereby affirm that I prepared the submitted dissertation on the topic “*In vitro* differentiated osteoclasts from human induced pluripotent stem cells as a disease model for *CLCN7*-related autosomal recessive osteopetrosis / *In vitro*-Differenzierung von Osteoklasten aus humanen induziert pluripotenten Stammzellen als ein Krankheitsmodell für *CLCN7*-Autosomal Rezessive Osteopetrose” independently and without the support of third parties, and that I used no other sources and aids than those stated.

All parts which are based on the publications or presentations of other authors, either in letter or in spirit, are specified as such in accordance with the citing guidelines. The sections on methodology (in particular regarding practical work, laboratory regulations, statistical processing) and results (in particular regarding figures, charts and tables) are exclusively my responsibility.

Furthermore, I declare that I have correctly marked all of the data, the analyses, and the conclusions generated from data obtained in collaboration with other persons, and that I have correctly marked my own contribution and the contributions of other persons (cf. declaration of contribution). I have correctly marked all texts or parts of texts that were generated in collaboration with other persons.

My contributions to any publications to this dissertation correspond to those stated in the below joint declaration made together with the supervisor. All publications created within the scope of the dissertation comply with the guidelines of the ICMJE (International Committee of Medical Journal Editors; http://www.icmje.org) on authorship. In addition, I declare that I shall comply with the regulations of Charité – Universitätsmedizin Berlin on ensuring good scientific practice.

I declare that I have not yet submitted this dissertation in identical or similar form to another Faculty.

The significance of this statutory declaration and the consequences of a false statutory declaration under criminal law (Sections 156, 161 of the German Criminal Code) are known to me.”

Date Signature

Author's contribution

Title: Efficient generation of osteoclasts from human induced pluripotent stem cells and functional investigations of lethal *CLCN7*-related osteopetrosis.

Authors: Uta Rössler, Anna Floriane Hennig, Nina Stelzer, Shroddha Bose, Johannes Kopp, Kent Søe, Lukas Cyganek, Giovanni Zifarelli, Salaheddine Ali, Maja von der Hagen, Elisabeth Tamara Strässler, Gabriele Hahn, Michael Pusch, Tobias Stauber, Zsuzsanna Izsvák, Manfred Gossen, Harald Stachelscheid, Uwe Kornak

Journal: Journal of Bone and Mineral Research.
Submission date: September 2020
Publication date: August 2021 (Epub: 18th May 2021)

Author contribution in details:

My contribution to the publication included the design of the study together with Anna Floriane Hennig, Uwe Kornak and Zsuzsanna Izsvák. I was responsible to conduct the study and to collect the data, to analyse as well as to interprete them. I put the data together, presented them in figures and wrote the manuscript, which was mainly revised by Uwe Kornak and Anna Floriane Hennig. The final version of the publication was approved by all authors.

I performed extensive literature research and multiple test experiments in order to develop the final osteoclast differentiation protocol (figure 1A) building the basis of all following characterisation steps and application experiments. For technical support, I worked in close contact with Harald Stachelscheid and his team of the BIH iPS core facility and got scientific support by Uwe Kornak, Manfred Gossen and Zsuzsanna Izsvák. I personally characterised each step of osteoclast differentiation via quantitative RT-PCR (figure 1B, 2C, 3B, 6A, S3 and S20A). For this purpose, I designed particular primers (table S2), established the optimal PCR program and collected sufficient cells of every differentiation step. Generated data were put into diagrams and statistically analysed by myself (table S3 and S10). Furthermore, I analysed primary PBMC-monocytes and hiPSC-derived monocyte-like cells of BIHi004-A and ARO hiPSCs using flow cytometry. For this purpose,

I developed the monocyte-specific antibody panel for flow cytometry by literature research, the support of Angelika Rose from Miltenyi Biotec and the help of Anna Floriane Hennig and the iPS core facility. Data acquisition, analysis, interpretation, and the presentation in figures was done by me (figure 2A, 2B, 2D, S1, S4, S20B and S20C, table S4). I conducted multiple osteoclast differentiation experiments using several hiPSC lines in order to get phase contrast pictures, osteoclast stainings and the proof of bone resorption ability (figure 1A, 3A, 6B, S2, S13 cell line 10211.EURCC and S21 cell line BIHi002-B). For the quantitative analysis of the osteoclasts, Anna Floriane Hennig and Nina Stelzer performed multiple osteoclast differentiations in accordance with my protocol and my technical support using different hiPS cell lines and analysed the pictures regarding the number of nuclei, the size of the cells and number of cells. I processed data generated by Anna Floriane Hennig and Nina Stelzer and I performed statistical evaluation with the advice of Asanka Gunawardana and prepared diagrams accordingly (figure 3C, 3D and 6C, table S6). In addition, I established a protocol how to transfer differentiated osteoclasts onto bone chips and stain the resorption pits and trenches. For the quantitative analysis of the resorption behaviour, resorption assays were performed by Anna Floriane Hennig and Nina Stelzer and bone chips were analysed by Kent Søe and his team. I processed the generated data and evaluated them statistically with the advice of Asanka Gunawardana and prepared the figure (figure 3E, table S8). In order to conduct additional characterisation experiments, I cultivated hiPSCs and prepared lysates for western blot analysis of LC3I and II levels carried out by Johannes Kopp (figure 5D, 5E and S19) and I prepared fixed hiPSCs on slides for determination of the lysosomal pH of several hiPSC lines, ultimately performed by Shroddha Bose (figure S18). Electrophysiological experiments were done by Giovanni Zifarelli, Michael Pusch and their colleagues (figure 5C and S17).

Signature

_____

Publication

ORIGINAL ARTICLE

JBMR®

Efficient generation of osteoclasts from human induced pluripotent stem cells and functional investigations of lethal CLCN7-related osteopetrosis

Uta Rössler,[1,2,3] Anna Floriane Hennig,[1,2,4,5] Nina Stelzer,[1,2] Shroddha Bose,[6] Johannes Kopp,[1,2,4,7] Kent Søe,[8,9,10] Lukas Cyganek,[11,12] Giovanni Zifarelli,[13] Salaheddine Ali,[1,2,7] Maja von der Hagen,[14] Elisabeth Tamara Strässler,[15,16] Gabriele Hahn,[17] Michael Pusch,[13] Tobias Stauber,[6,18] Zsuzsanna Izsvák,[19] Manfred Gossen,[20,21] Harald Stachelscheid,[22,23] and Uwe Kornak[1,2,5,7]

[1]BIH Center for Regenerative Therapies (BCRT), Charité - Universitätsmedizin Berlin, corporate member of Freie Universität Berlin, Humboldt-Universität zu Berlin, and Berlin Institute of Health, Berlin, Germany
[2]Institute for Medical Genetics and Human Genetics, Charité - Universitätsmedizin Berlin, corporate member of Freie Universität Berlin, Humboldt-Universität zu Berlin, and Berlin Institute of Health, Berlin, Germany
[3]Berlin Institute of Health (BIH), Berlin, Germany
[4]Freie Universität Berlin, Berlin, Germany
[5]Institute of Human Genetics, University Medical Center Göttingen, Göttingen, Germany
[6]Institute of Chemistry and Biochemistry, Freie Universität Berlin, Berlin, Germany
[7]Max Planck Institute for Molecular Genetics, Berlin, Germany
[8]Clinical Cell Biology, Department of Pathology, Odense University Hospital, Odense C, Denmark
[9]Department of Clinical Research, University of Southern Denmark, Odense M, Denmark
[10]Department of Molecular Medicine, University of Southern Denmark, Odense M, Denmark
[11]Stem Cell Unit, Clinic for Cardiology and Pneumology, University Medical Center Göttingen, Göttingen, Germany
[12]German Center for Cardiovascular Research (DZHK), Partner Site Göttingen, Göttingen, Germany
[13]Istituto di Biofisica, CNR, Genoa, Italy
[14]Abteilung Neuropädiatrie, Medizinische Fakultät Carl Gustav Carus, Technische Universität Dresden, Dresden, Germany
[15]Department of Cardiology, Charité - Universitätsmedizin Berlin, Campus Benjamin Franklin, Berlin, Germany
[16]German Centre for Cardiovascular Research (DZHK), Partner Site Berlin, Berlin, Germany
[17]Institut und Poliklinik für Radiologische Diagnostik, Medizinische Fakultät Carl Gustav Carus Technische Universität Dresden, Dresden, Germany
[18]Department of Human Medicine, and Institute for Molecular Medicine, MSH Medical School Hamburg, Hamburg, Germany
[19]Max-Delbrück-Center for Molecular Medicine (MDC), Helmholtz Association, Berlin, Germany
[20]Berlin-Brandenburg Center for Regenerative Therapies, Charité Virchow Campus, Berlin, Germany
[21]Institute of Active Polymers, Helmholtz-Zentrum Hereon, Teltow, Germany
[22]Charité - Universitätsmedizin Berlin, corporate member of Freie Universität Berlin, Humboldt-Universität zu Berlin, and Berlin Institute of Health, Berlin, Germany
[23]Berlin Institute of Health (BIH), BIH Stem Cell Core Facility, Berlin, Germany

ABSTRACT

Human induced pluripotent stem cells (hiPSCs) hold great potential for modeling human diseases and the development of innovative therapeutic approaches. Here, we report on a novel, simplified differentiation method for forming functional osteoclasts from hiPSCs. The three-step protocol starts with embryoid body formation, followed by hematopoietic specification, and finally osteoclast differentiation. We observed continuous production of monocyte-like cells over a period of up to 9 weeks, generating sufficient material for several osteoclast differentiations. The analysis of stage-specific gene and surface marker expression proved mesodermal priming, the presence of monocyte-like cells, and of terminally differentiated multinucleated osteoclasts, able to form resorption pits and trenches on bone and dentine in vitro. In comparison to peripheral blood mononuclear cell (PBMC)-derived osteoclasts hiPSC-derived osteoclasts

Received in original form September 9, 2020; revised form March 26, 2021; accepted April 21, 2021.
Address correspondence to: Uwe Kornak, MD PhD, and Anna Floriane Hennig, PhD, Institut für Humangenetik, University Medical Center Göttingen, Heinrich-Düker-Weg 12, 37073 Göttingen, Germany. Email: floriane.hennig@med.uni-goettingen.de
Additional Supporting Information may be found in the online version of this article.
Journal of Bone and Mineral Research, Vol. 00, No. 00, Month 2021, pp 1–15.
DOI: 10.1002/jbmr.4322

were larger and contained a higher number of nuclei. Detailed functional studies on the resorption behavior of hiPSC-osteoclasts indicated a trend towards forming more trenches than pits and an increase in pseudoresorption. We used hiPSCs from an autosomal recessive osteopetrosis (ARO) patient (BIHi002-A, ARO hiPSCs) with compound heterozygous missense mutations p.(G292E) and p.(R403Q) in *CLCN7*, coding for the Cl^-/H^+-exchanger ClC-7, for functional investigations. The patient's leading clinical feature was a brain malformation due to defective neuronal migration. Mutant ClC-7 displayed residual expression and retained lysosomal co-localization with OSTM1, the gene coding for the osteopetrosis-associated transmembrane protein 1, but only ClC-7 harboring the mutation p.(R403Q) gave strongly reduced ion currents. An increased autophagic flux in spite of unchanged lysosomal pH was evident in undifferentiated ARO hiPSCs. ARO hiPSC-derived osteoclasts showed an increased size compared to hiPSCs of healthy donors. They were not able to resorb bone, underlining a loss-of-function effect of the mutations. In summary, we developed a highly reproducible, straightforward hiPSC-osteoclast differentiation protocol. We demonstrated that osteoclasts differentiated from ARO hiPSCs can be used as a disease model for ARO and potentially also other osteoclast-related diseases. © 2021 The Authors. *Journal of Bone and Mineral Research* published by Wiley Periodicals LLC on behalf of American Society for Bone and Mineral Research (ASBMR).

KEY WORDS: *CLCN7*; hiPSCs; OSTEOCLASTS; OSTEOPETROSIS

INTRODUCTION

Osteoclasts (OCs) are giant multinucleated cells formed by fusion of mononuclear precursors that differentiate from monocytes.[1] Although closely related to tissue macrophages, osteoclasts have a special capacity to resorb mineralized cartilage and bone, distinguishing them from all other phagocytosing cells. This resorption process crucially depends on extracellular acidification, which is required for dissolving the basic hydroxyapatite crystals deposited in the mineralized extracellular matrix.[2]

Genetic defects resulting in dysfunction of the components of this acid secretion mechanism partially or entirely block the resorption capacity, and lead to the accumulation of mineralized cartilage and bone with multiple consequences: (i) increased fracture rates; (ii) bone marrow insufficiency with anemia and immune deficiency; (iii) osteomyelitis; and (iv) blindness due to optic nerve damage.[1] Autosomal recessive osteopetrosis (ARO) is the most dramatic type of such defects, it is usually lethal during childhood. About 50% of the ARO cases are due to mutations in the T cell immune regulator gene 1 (*TCIRG1*, MIM #604592) encoding a subunit of the vacuolar proton pump. In 10% to 15% of ARO cases, biallelic mutations in the chloride channel 7 gene (*CLCN7*, MIM #602727) are responsible and in 2% to 5% mutations in the gene coding osteopetrosis-associated transmembrane protein 1 (*OSTM1*, MIM #607649). ARO is a rare disease, the incidence of all forms of ARO together is around 1:100,000. Mice deficient in *Ostm1* or *Clcn7* show a neuronal lysosomal storage disease and a progressive deterioration of neurological function.[3–5] This is in line with the function of ClC-7 residing in lysosomes, where it regulates intraluminal ion homeostasis together with its β-subunit Ostm1.[6,7] A subset of patients with biallelic *CLCN7* loss-of-function mutations develops neurodegeneration, the so-called neuronopathic form of ARO. However, patients with *OSTM1*-ARO not only show neurodegeneration, but also cortical brain malformations, implying disturbed developmental processes.[8] Interestingly, also activating mutations in *CLCN7* can lead to abnormal brain development, albinism, and lysosomal storage without any bone phenotype.[9]

Human induced pluripotent stem cells (hiPSCs) with their capacity for unlimited self-renewal and differentiation into almost all cell types hold great potential for modeling human diseases and developing novel therapeutic approaches. Several protocols for differentiation of hiPSCs into macrophages and osteoclasts have been published, all of which rely on the formation of embryoid bodies for mesodermal specification and the induction of hematopoiesis.[10–15] However, the combination of cytokines, their concentrations, and the media used vary between the existing protocols, which can have a strong impact on the outcome and costs of the experiments. Furthermore, the exact yield of hiPSC-osteoclasts and their characteristics have not been described in detail.

Here we report on a novel, robust osteoclast differentiation protocol with optimized media composition resulting in high osteoclast yield. We demonstrate comparable morphology and function of hiPSC-derived and primary peripheral blood mononuclear cell (PBMC)-derived osteoclasts. In addition, we successfully use our protocol to establish a disease model for ARO, using hiPSCs from a pediatric patient with biallelic *CLCN7* mutations and a lethal phenotype.

MATERIALS AND METHODS

Maintenance of hiPSCs

Osteoclast-related experiments were performed using hiPSC lines BIHi001-A and BIHi004-A (https://hpscreg.eu/cell-line/BIHi001-A, https://hpscreg.eu/cell-line/BIHi004-A, kindly provided by the BIH Core Facility Stem Cells), 10211.EURCC, UMGi014-C clone 14, and UMGi020-B clone 21 (isWT1.14 and isWT7.21 respectively, https://hpscreg.eu/cell-line/UMGi014-C, https://hpscreg.eu/cell-line/UMGi020-B, kindly provided by the UMG Stem Cell Unit) from control donors as well as osteopetrosis patient-derived cell lines BIHi002-A,[16] BIHi002-B, and BIHi002-C. Origins and reprogramming methods of the hiPSC lines are listed in Table S1. Methods and materials used for hiPSC reprogramming and characterization are further described in Supplementary Methods and shown in Table S11, Table S12 and Table S13. The hiPSCs were maintained in Essential 8 medium (Life Technologies, Bleiswijk, Netherlands) in Geltrex-coated (Life Technologies, Bleiswijk, Netherlands) 6-well dishes in a humidified normoxic incubator (37°C, 5% CO_2) and routinely passaged in colonies at a ratio of ~1:20 every 4 to 5 days by using 0.5mM ethylenediamine tetraacetic acid (EDTA) (Life Technologies, Bleiswijk, Netherlands).

Osteoclast differentiation of hiPSCs

At least 3 days before starting the differentiation, hiPSCs cultured in Essential 8 medium were adapted to mTeSR™1 (Stemcell Technologies, Vancouver, Canada) medium. For embryoid body (EB) formation and mesodermal induction, single cells were harvested by TrypLE Select Enzyme (Life Technologies, Bleiswijk, Netherlands) treatment. Subsequently, 1.25×10^4 cells were seeded per well in a round bottom ultra-low attachment 96-well plate (Corning, Kennebunk, ME, USA) in 100 µl mTeSR™1

medium supplemented with 50 ng/ml human bone morphogenetic protein 4 (hBMP4), 50 ng/ml human vascular endothelial growth factor-165 ($hVEGF_{165}$), 20 ng/ml human stem cell factor (hSCF), and 10μM Rock-inhibitor Y-27632 (Wako Chemicals, Neuss, Germany). The plate was centrifuged for 3 min at 100*g*. Half of the medium was changed on day 1 and day 2. Four days after initiation of EB formation, EBs with a diameter of ~500 μm were transferred to 6-well culture dishes coated with 0.1% gelatin (eight EBs per well) and containing 3 ml/well differentiation medium (X-VIVO 15 medium [Lonza, Verviers, Belgium], 2mM Ultraglutamine, 55μM 2-mercaptoethanol, 1% Penicillin/Streptomycin [Pen/Strep], 25 ng/ml human interleukin 3 [hIL-3], 100 ng/ml human macrophage colony-stimulating factor [hM-CSF] [R&D Systems, Minneapolis, MN, USA]). Once per week, produced monocyte-like suspension cells were harvested and myeloid-cell-forming complexes (MCFCs) were supplied with 2 ml/well fresh medium. For terminal osteoclast differentiation, harvested monocyte-like cells were seeded at a density of 1×10^5 cells/cm^2 in cell culture vessels supplied with α minimum essential medium (α-MEM) Eagle medium (Lonza, Verviers, Belgium) containing 10% fetal bovine serum (FBS) Superior (Sigma-Aldrich, St. Louis, MO, USA), 1% Pen/Strep, and 50 ng/ml hM-CSF. Three days after seeding, half of the culture medium was replaced with fresh osteoclast medium (α-MEM Eagle, 10% FBS Superior, 1% Pen/Strep, 100 ng/ml hM-CSF, 100 ng/ml human soluble receptor activator of nuclear factor-κ B ligand [hsRANKL]). Due to one half remaining old culture medium, the final cytokine concentration of freshly added hM-CSF and hsRANKL in the culture was 50 ng/ml. The cells were cultured for additional 3 to 7 days. Every 2 to 3 days, half of the medium was replaced with fresh osteoclast medium. All cytokines were purchased from Peprotech (Rocky Hill, NJ, USA) if not indicated differently. The procedure was adapted from a hiPSC-based macrophage differentiation protocol.[17]

Isolation and differentiation of primary blood monocytes

PBMCs were isolated from whole blood of two healthy donors (female donor P1 and male donor P2) by density centrifugation (Biocoll, 1.077 g/ml; Merck Millipore, Molsheim, France), followed by MACS cell separation for monocyte enrichment (Monocyte Isolation Kit II; Miltenyi Biotec, Bergisch Gladbach, Germany). Freshly isolated primary monocytes underwent terminal osteoclast differentiation as described for hiPSCs in the previous paragraph.

Flow cytometry

Surface marker staining of 5×10^5 freshly isolated monocytes or harvested hiPSC-derived monocyte-like cells was performed in 50 μl staining solution for 10 min at 4°C. The staining solution contained Miltenyi Biotec (Bergisch Gladbach, Germany) antibodies and reagents diluted as indicated in fluorescence-activated cell sorting (FACS) buffer (2mM EDTA and 0.5% bovine serum albumin [BSA] in Dulbecco's phosphate-buffered saline [DPBS]): human Tandem Signal Enhancer 1:17, human Fc receptor [FcR]-Blocking Reagent 1:5, and Isotype controls 1:10 or human surface marker antibodies (CD34-fluorescein isothiocyanate [FITC] 1:10, CD45-VioBlue 1:20, CD66b-phycoerythrin [PE]-Vio770 1:20, CD11b-PE 1:50, CD14-allophycocyanin [APC] 1:50). Cells were washed with FACS buffer once before and three times after staining. Directly before sample acquisition by MACSQuant® VYB Analyzer (Miltenyi Biotec), cells were stained with propidium iodide (1 μg/ml, Molecular Probes, Eugene, OR, USA) in 200 μl sample volume. Acquired data were analyzed with FlowJo 10.5.3 (FlowJo, LLC, Ashland, OR, USA). Debris, dead cells and cell doublets were excluded from the analysis as shown in the representative gating strategy in Figure S1.

Osteoclast staining

Osteoclasts were fixed with 4% paraformaldehyde (PFA) 4 days after detection of the first osteoclasts in the culture. Staining of tartrate resistant acid phosphatase (TRAcP) activity was performed using Naphthol AS-MX phosphate disodium salt (Sigma-Aldrich, Taufkirchen, Germany) and Fast Red Violet LB Salt (Sigma-Aldrich, Taufkirchen, Germany). Actin was stained with fluorescently labeled phalloidin (Alexa Fluor™ 488; Molecular Probes, Eugene, OR, USA) and 4′,6-diamidino-2-phenylindole (DAPI; Life Technologies, Bleiswijk, Netherlands) detected the cell nuclei. Staining was performed as described .[18]

Resorption assay

Two days after the first osteoclasts were detected in the culture, small mature osteoclasts were detached by Accutase treatment (Sigma-Aldrich, Taufkirchen, Germany) for 10 to 15 min at 37°C and seeded at a density of 6.6×10^4 osteoclasts per 96-well either on dentine slices or cortical bovine bone slices (BoneSlices.com, Jelling, Denmark) in α-MEM Eagle medium containing 10% FBS Superior, 1% Pen/Strep, and 50 ng/ml hM-CSF and hsRANKL. Osteoclast cultures were maintained for 5 days. After 2 days, half of the medium was replaced with fresh one. At culture termination, bone slices were washed in purified water and cells were removed with a paper towel. Resorption pits were stained with either 0.25% toluidine solution (Sigma-Aldrich, Taufkirchen, Germany) or black ink (Pelikan, Feusisberg, Switzerland) for 15 s. The identification of pits, trenches, pseudoresorption, and the quantification was done as shown in Figure S2 and as described.[19] All quantification experiments were performed blinded.

Quantitative reverse transcription polymerase chain reaction

RNA was extracted from the cells and purified by using the Direct-zol™ RNA MiniPrep Kit (Zymo Research, Freiburg, Germany). Total complementary DNA (cDNA) was transcribed by RevertAid™ H Minus First Strand cDNA Synthesis Kit (Life Technologies, Bleiswijk, Netherlands) using random hexamer primers. Quantitative polymerase chain reaction (qPCR) was performed with 5× HOT FIREPol® EvaGreen® qPCR Mix Plus (Solis BioDyne, Tartu, Estonia) on Quant Studio 3 Real-Time PCR System (Life Technologies, Singapore). Data were analyzed according to the delta-delta threshold cycle (ΔΔCt) method, whereby glyceraldehyde-3-phosphate dehydrogenase (*GAPDH*) levels served as internal controls. Primer sequences are listed in Table S2.

Quantitative analysis of osteoclasts

Images of stained osteoclasts of three independent differentiation experiments of each cell line were taken using the Opera Phenix high content screener (Perkin Elmer, Waltham, MA, USA) and quantified. Three technical replicates of each differentiation and two pictures (one with high and one with low osteoclast density, each covering 6.5 mm^2) of each replicate were

analyzed. By using image analysis software (CellProfiler; https://cellprofiler.org/) nuclei were identified, osteoclast cells were selected manually, and osteoclast number and size were quantified. On average, 812 osteoclasts per cell line and experiment were analyzed. All quantification experiments were performed blinded.

Lysosomal pH measurement

Lysosomal pH was measured essentially as described.[7] Human iPSCs were dissociated to single cells using TrypLE Select Enzyme and seeded onto glass-bottom live-cell dishes (MatTek, Ashland, MA, USA) in Essential 8 medium supplemented with 10μM Rock-inhibitor Y-27632. Twenty-four hours (24 h) after plating, lysosomes were loaded with 0.5 mg/ml Oregon Green 488-dextran (Life Technologies, Bleiswijk, Netherlands) in growth medium overnight, followed by a 2 h chase. For imaging, the medium was changed to imaging buffer containing 135mM NaCl, 5mM KCl, 1mM $MgCl_2$, 1mM $CaCl_2$, and 10mM glucose, 10mM *N*-2-hydroxyethylpiperazine-*N*′-2-ethanesulfonic acid (HEPES), pH 7.4. Images were acquired using a Leica DMi8 microscope (Leica Microsystems, Wetzlar, Germany) equipped with a 63 × 1.40 numerical aperture (NA) oil-immersion lens and an Oregon Green filter cube (AHF analysentechnik AG, Tübingen-Pfrondorf, Germany) with excitation at 440 or 480 nm, respectively, delivered by an OptoScan monochromator (Cairn Research, Faversham, UK) controlled by the microscopy software WinFluor (John Dempster, University of Strathclyde, Glasgow, Scotland), and emission at 516 to 556 nm. At the end of each experiment, in situ pH calibration curves were obtained in isotonic K-based solutions (5mM NaCl, 115mM KCl, 1.2mM $MgSO_4$, 10mM glucose, 25mM of either HEPES, 2-(N-morpholino)ethanesulfonic acid [MES], or acetate, ranging in pH from 3.9 through 6.5) supplemented with 10μM of both nigericin and monensin after equilibration for at least 2 min for each pH. Images were analyzed using ImageJ software (NIH, Bethesda, MD, USA; https://imagej.nih.gov/ij/), where regions of interest (ROIs) were defined as areas above a defined fluorescence threshold in the acquired images at 440 nm excitation (pH-insensitive). The mean intensity ratio between 480 and 440 nm excitation was calculated after background subtraction for each ROI. The fluorescence intensity ratios (488/440) as a function of pH was fit to a sigmoid and used to interpolate the pH values from the cells prior to the calibration.

Immunostaining

Plasmid DNA encoding the respective constructs (hClC-7 wild-type [WT] or mutant, and human OSTM1 (hOSTM1)–monomeric red fluorescent protein (mRFP) was transfected into HeLa cells at 40% confluency, using Fugene 6 reagent (Promega, Madison, WI, USA), 48 h before fixation with 4% PFA in PBS for 15 min. For immunolabeling, cells were incubated with 30mM glycine in PBS for 5 min, permeabilized with antibody buffer (0.05% saponin and 3% BSA in PBS) for 15 min and then subsequently incubated with primary and AlexaFluor-coupled secondary antibodies diluted in antibody buffer for 90 and 60 min, respectively, with washing steps in antibody buffer. Primary antibodies were rabbit anti-ClC-7 (7N4B; kind gift from Thomas Jentsch[5]) and mouse anti-lysosomal-associated membrane protein 1 (anti-LAMP-1) (H4A3 was deposited to the DSHB by August, J.T. / Hildreth, J.E.K. [DSHB Hybridoma Product H4A3]). Images were acquired with a Leica DMi8 light microscope (Leica Microsystems, Wetzlar, Germany) equipped with a 63× 1.40 NA oil-immersion lens and respective filter cubes (FITC for Alexa488; tetramethylrhodamine isothiocyanate [TRITC] for mRFP; and Y5.5 [filter cube] for Alexa633).

Electrophysiology

hClC-7 and h-OSTM1-mRFP expressing plasmids were co-transfected in HEK-293 cells by using Effectene Transfection Reagent (Qiagen, Hilden, Germany). Patch-clamp experiments were performed in whole-cell configuration 24 to 72 h posttransfection. Pipettes were pulled from borosilicate capillaries (Hilgenberg, Malsfeld, Germany) and had a resistance of 1.5 to 2.5 MOhm in measuring solutions. The standard intracellular (pipette) solution contained (in mM) 130 NaCl, 10 HEPES, 2 $MgSO_4$, and 2 EGTA (pH 7.3). The extracellular (bath) solution contained (in mM) 147 NaCl, 10 HEPES, and 4 $MgSO_4$ (pH 7.3). Voltage steps of 1 s duration from 120 to 60 mV in decrements of 20 mV with 1 s interval between pulses were conducted, holding potential was 0 mV. Data were acquired at 20 to 50 kHz after filtering at 10 kHz with an eight-pole Bessel filter using an Axopatch 200 amplifier (Molecular Devices, San Jose, CA, USA) with GePulse software. Data analysis was performed with Ana software (GePulse and Ana available at: http://users.ge.ibf.cnr.it/pusch/).

Plasmids

The expression plasmid for hClC-7 was described.[20] The mutations p.(G292E) and p.(R403Q) were introduced by recombinant PCR. For patch-clamp experiments, four additional mutations deleting lysosomal targeting di-leucine motifs (leucine 23, 24, 68, and 69 changed to alanines) were introduced into *CLCN7*.[21] For expression of hOSTM1-mRFP, the open reading frame (ORF) was cloned into pmRFP-N1. The complete ORFs were confirmed by Sanger sequencing.

LC3 and ClC-7 Western blot

For the analysis of the autophagic markers like microtubule-associated protein light chain 3 (LC3)-I and II and the determination of the autophagic flux, hiPSCs were seeded at about 70% confluency. The next day, cells were starved for 2 h in Krebs-Ringer solution (Alfa Aesar; Thermo Fisher, Kandel, Germany) and incubated with or without 50μM chloroquine (autophagy inhibitor). Cells were lysed with radioimmunoprecipitation assay (RIPA) buffer containing cOmplete™ protease inhibitors (Roche, Mannheim, Germany) and the proteins LC3 (Cell Signaling Technology, Beverly, MA, USA; #4108, 1:1000) and GAPDH (Thermo Fisher Scientific; #AM4300, 1:20,000) were analyzed by immunoblotting after 12% sodium dodecyl sulfate–polyacrylamide gel electrophoresis (SDS-PAGE) and transferred to a polyvinylidene fluoride (PVDF) membrane. GAPDH and LC3-II levels were determined by densitometric quantification and LC3-II was normalized to GAPDH. For each culture condition (standard and starvation), the autophagic flux was calculated by subtracting densitometrically quantified relative LC3-II levels obtained without chloroquine treatment from LC3-II levels acquired with chloroquine.[22] For ClC-7 immunoblotting hiPSCs were lysed, separated, blotted, and quantified as described earlier in this paragraph for LC3 Western blot analysis. A total of 20 μg of protein per lane was separated by 10% SDS-PAGE and blotted proteins were probed with following antibodies: guinea-pig anti ClC-7

(7N4B[5]; gift from Thomas Jentsch) and rabbit anti GAPDH (14C10; Cell Signaling Technology; #2118, 1:1,000).

Statistical analysis

Data were plotted and statistically evaluated using GraphPad Prism Version 8 (GraphPad Software, Inc., La Jolla, CA, USA).

RESULTS

Efficient generation of monocyte-like cells from hiPSC-derived myeloid-cell-forming complexes

To establish an efficient osteoclast differentiation protocol, we used two hiPSC lines (BIHi001-A and BIHi004-A), derived from skin fibroblasts of healthy control individuals. The first differentiation step was induced via the formation of embryoid bodies (EBs) in ultra-low attachment plates (Figure 1*A*). Next, a combination of hBMP4, hVEGF, and hSCF initiated mesodermal priming of EBs. In order to monitor the differentiation process, we analyzed marker gene expression by quantitative reverse transcription polymerase chain reaction (qRT-PCR). Comparing undifferentiated hiPSCs and EBs, we observed successful mesodermal induction by decreased expression of pluripotency markers *OCT4*, *SOX2*, and *NANOG*, and increased expression of mesodermal markers *CD34*, *HAND1*, *TBXT*, and *CDX2* (Figure 1*B*, Figure S3).

As a second step, EBs were differentiated into myeloid-cell-forming complexes (MCFCs). Depending on the hiPSC line, over a time period of 9 to 13 weeks, MCFCs were exposed to hIL-3 and hM-CSF, which triggered the release of suspension cells into the medium (Figure 1*A*). Between weeks 2 and 3, our tested hiPSC lines showed the highest suspension cell release (up to 7.5×10^5 cells per well containing eight MCFCs). After this production peak, the number of suspension cells slowly decreased (Figure 2*A*). On average, every MCFC released 3.2×10^5

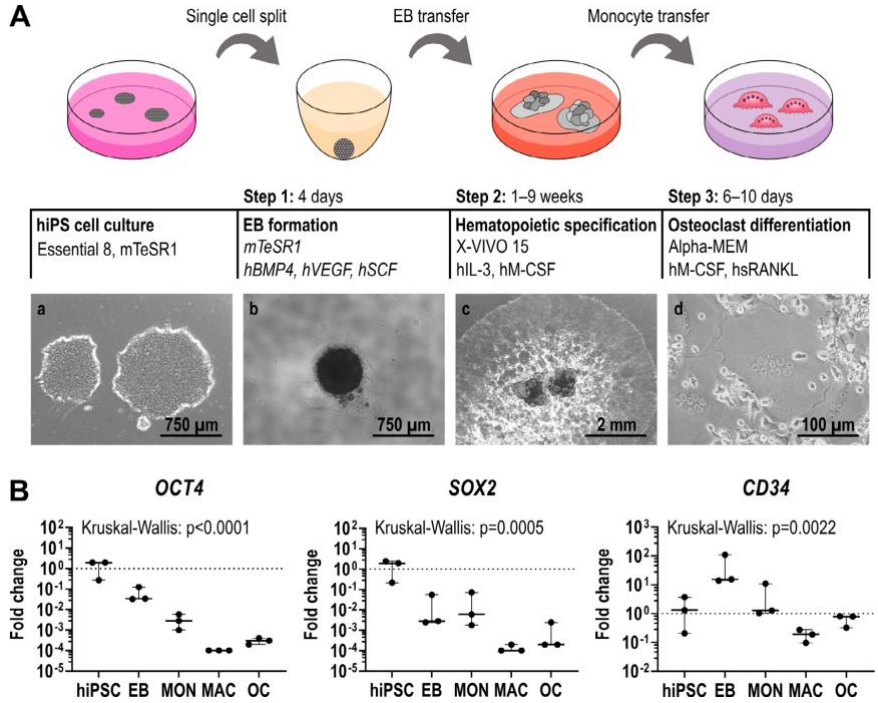

FIGURE 1. Differentiation of hiPSCs into osteoclasts. (*A*) Schematic illustration of the osteoclast differentiation procedure. Step 1: EB formation. Step 2: Differentiation of EBs into MCFCs, which produce monocyte-like suspension cells. Step 3: Final osteoclast differentiation of monocyte-like cells. Phase contrast images of hiPSC colonies (a), a single EB (b), MCFCs (c), and osteoclasts (d). (*B*) Expression of pluripotency markers *OCT4* and *SOX2* and mesodermal marker *CD34* determined by qRT-PCR analysis in BIHi004-A hiPSC-derived cells in undifferentiated hiPSCs, 4-day-old EBs, MONs, MACs, and OCs. Expression is normalized to hiPSCs, *GAPDH* expression was used as housekeeping control. Data show box-plots with median, interquartile range, maximum, and minimum values, and all data points of three independent experiments. For statistical analysis, Kruskal-Wallis test and Dunn's multiple comparisons were used (Table S3). Abbreviations: EB, embryoid body; *GAPDH*, glyceraldehyde-3-phosphate dehydrogenase; hiPSC, human induced pluripotent stem cell; MAC, macrophage, MCFC, myeloid-cell-forming complex; MON, monocyte-like cell; OC, osteoclast; qRT-PCR, quantitative reverse transcription polymerase chain reaction.

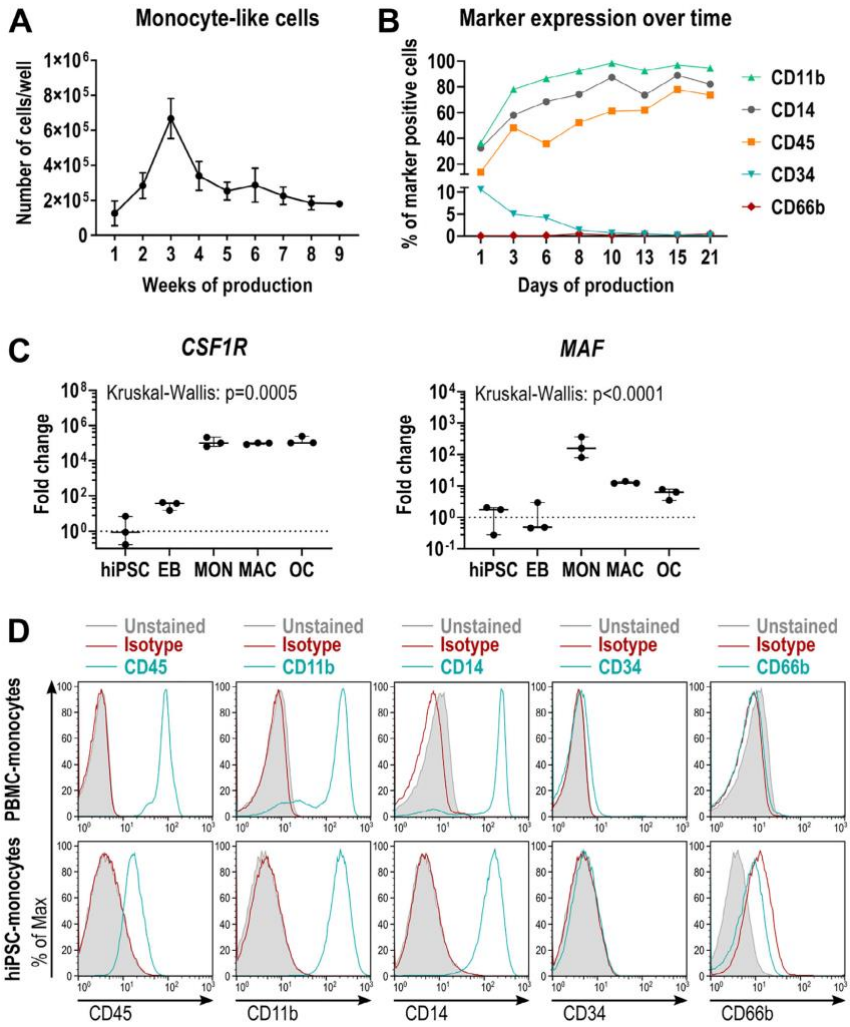

FIGURE 2. Characterization of hiPSC-derived monocyte-like cells. (*A*) Kinetics of monocyte-like cell production in BIHi004-A hiPSCs. Data are absolute numbers of harvested suspension cells per 6-well containing eight MCFCs (means and SD of three independent experiments, each with twelve 6-wells. (*B*) Frequency of surface marker-expressing monocyte-like cells determined by flow cytometry, harvested at different time points. (*C*) Expression of monocytic markers *CSF1R* and *MAF* determined by qRT-PCR analysis in BIHi004-A hiPSC-derived cells in undifferentiated hiPSCs, 4-day-old EBs, MONs, MACs, and OCs. Expression is normalized to hiPSCs, *GAPDH* expression was used as housekeeping control. Data show box-plots with median, interquartile range, maximum, and minimum values and all data points of three independent experiments. For statistical analysis, Kruskal-Wallis test and Dunn's multiple comparisons were used (Table S3). (*D*) Representative flow cytometry analysis of human primary monocytes (donor P2) and hiPSC-derived monocyte-like cells (BIHi004-A, harvested in week 5 after EB transfer). Histograms show unstained cells (gray-filled), cells stained with isotype controls (red), and cells stained with the respective surface markers (blue). Abbreviations: EB, embryoid body; *GAPDH*, glyceraldehyde-3-phosphate dehydrogenase; hiPSC, human induced pluripotent stem cell; MAC, macrophage, MCFC, myeloid-cell-forming complex; MON, monocyte-like cell; OC, osteoclast; qRT-PCR, quantitative reverse transcription polymerase chain reaction; SD, standard deviation.

suspension cells within 9 weeks. During the first days of production, flow cytometry showed a considerable fraction of $CD34^+$ cells, indicating an immature phenotype (Figure 2*B*, Figure S4). We also detected many dead cells during this early phase of the differentiation protocol (Table S4). The released cells gradually matured over the next 2 weeks. Around the time of maximal production, the suspension cells were positive for monocyte markers like CD11b, CD14, CD45, but negative for CD34 (marker for hematopoietic stem cells [HSCs]) and CD66b (marker for eosinophils and neutrophils). qRT-PCR also revealed an increased expression of the hM-CSF receptor *CSF1R* and *MAF* (involved in macrophage proliferation) when compared to undifferentiated hiPSCs and EBs (Figure 2*C*). Hence, the released cells closely resembled monocyte-like cells. Indeed, primary monocytes freshly isolated from peripheral blood displayed the same surface marker profile as hiPSC-derived monocyte-like cells (Figure 2*D*). In the final step of the protocol, the harvested monocyte-like cells were differentiated into osteoclasts by exposing them to hM-CSF and hsRANKL (Figure 1*A*).

Physiological gene expression and an increased size of hiPSC-derived osteoclasts

Next, we analyzed the hiPSC-derived osteoclasts for typical osteoclast features and functionality and compared them to osteoclasts differentiated from monocytes from PBMCs of healthy donors. First, TRAcP-Phalloidin-DAPI staining of PBMC-derived and hiPSC-derived osteoclasts differentiated by our protocol, revealed multinucleated TRAcP-positive cells and the formation of a podosome belt (Figure 3*A*, middle). Furthermore, both osteoclast types were able to form resorption pits and trenches on dentine (Figure 3*A*, right). Finally, osteoclast markers like cathepsin K (*CTSK*) and matrix metalloproteinase 9 (*MMP9)* were similarly upregulated in primary and hiPSC-osteoclasts, as demonstrated by transcriptome and qRT-PCR analysis (Figure S6, Figure 3*B*, Figure S5, Table S3, Table S5). A comparison of global expression signatures revealed close similarity between PBMC-derived and hiPSC-derived osteoclasts in comparison to monocytes (Figure S6). Among the genes with elevated expression in hiPSC-derived osteoclasts were *FOS*, *MAF*, and *NFATC1*. *MAF* is a macrophage marker gene and *FOS* is important for early differentiation of macrophages and osteoclasts.[23] We thus conclude that our differentiation protocol generated slightly immature osteoclasts that are fully functional.

To evaluate the efficiency of our osteoclast differentiation protocol and to investigate osteoclast morphology, we quantified the osteoclast yield in more detail. Interestingly, the time between seeding of monocytes and the formation of the first visible osteoclasts was highly dependent on the donor, but not on the origin (primary or hiPSC) of the cells (Figure S7, Table S7). Thus, in order to compare osteoclast differentiation and morphology between different donors, cells for quantitative analysis from all donors were fixed 4 days after the appearance of the first osteoclasts. Osteoclasts differentiated from hiPSCs covered a larger area of the culture dish surface than PBMC-derived osteoclasts (Figure 3*C*). In contrast, we determined that numbers of hiPSC-derived osteoclasts per area were lower compared to PBMC-derived osteoclasts (Figure 3*D*, right). The slightly bigger area covered by hiPSC-derived osteoclasts and the reduced number of osteoclasts/mm^2 was in line with an increased size of the osteoclasts and higher number of nuclei per osteoclast, when compared to PBMC-derived osteoclasts (Figure 3*D*, Figure S8). Hence, hiPSC-derived osteoclasts seem to grow bigger in a shorter time period. Nevertheless, we observed no major difference in cell morphology between hiPSC-derived osteoclasts and osteoclasts differentiated from PBMCs. We estimate that, using our differentiation protocol, we are able to generate 4640 osteoclasts (nine nuclei on average) out of one hiPSC within 3 months.

Subtle differences in resorption behavior of hiPSC-derived osteoclasts

For further characterization of the resorption ability of hiPSC-derived osteoclasts, we cultured osteoclasts this time on cortical bone slices instead of dentine, because bovine bone is a more physiological substrate. We showed that there are no significant differences in the total amount of eroded bone surface (Figure 3*E* left, Table S8). However, there was an insignificant trend toward more bone resorption made by hiPSC-derived osteoclasts (around 5% of the bone surface) compared to PBMC-derived osteoclasts (around 3% of the bone surface). Interestingly, we detected that hiPSC-osteoclasts only superficially eroded 2% of the bone surface (pseudoresorption; Figure S2), whereas for primary osteoclasts this was at a comparable level around 1% (Figure 3*E*, right). Furthermore, we found that the morphology of the resorption cavities formed by hiPSC-osteoclasts from different healthy donors were variable: although BIHi004-A formed around 60% trenches and 40% pits, BIHi001-A only generated 20% trenches and 80% pits (Figure 3*E*, middle). The resorption pattern of primary osteoclasts showed an even lower proportion of trenches (10%) and up to 90% pits.

To test our established protocol with additional hiPSC lines, we generated the hiPSC lines isWT1 and isWT7 from dermal fibroblasts of healthy donors. The detailed characterization of the isWT1 and isWT7 hiPSCs proved their pluripotency (Figure S9), differentiation potential (Figure S10), and chromosomal stability (Figure S11 and S12). Applying our differentiation protocol to isWT1 and isWT7 cells and one additional hiPSC line led to terminally differentiated and bone-resorbing osteoclasts (Figure S13), demonstrating the robustness of our method.

A case of lethal neuronopathic ARO with brain malformation due to compound heterozygous missense mutations in the *CLCN7* gene

The male infant was the second child of healthy nonconsanguineous white parents. Beyond the neonatal period from the age of 8 to 10 weeks he exhibited failure to thrive, reduced weight gain, muscular hypotonia, and nystagmus. At the age of 4 months, he developed refractory infantile spasms and progressive developmental delay. Electroencephalogram (EEG) revealed hypsarrhythmia and amplitude depression. The cranial magnetic resonance imaging (MRI) showed a mild reduction of brain volume and subependymal heterotopic bands indicating a neuronal migration disorder (Figure 4*A*,*B*). At the age of 7 months, the cerebral ultrasound revealed progressive brain atrophy and a hydrocephalus ex vacuo. Retinal pigmentary changes were diagnosed in fundoscopy. A chest x-ray showing generalized bone sclerosis hinted toward a neuronopathic form of osteopetrosis (Figure 4*C*). In the further course of the disease, the infant developed a spastic tetraparesis, dysphagia, and chronic respiratory failure. From the age of 8 months, he had a mild hypochromic anemia. Candidate gene analysis by Sanger sequencing

detected the mutations c.875G>A, p.(G292E) and c.1208G>A, p.(R403Q) in the *CLCN7* gene in a compound heterozygous state (Figure 4*D*). Although the latter mutation has already been described in an ARO patient,[24] the c.875G>A mutation was novel. The affected glycine residue is evolutionarily conserved and flanking missense mutations have been previously identified in ARO patients.[25] The child deceased at the age of 14 months as a consequence of progressive respiratory failure. Given the exceptional phenotype of ARO, with predominant neurological symptoms and impaired cortical development, we

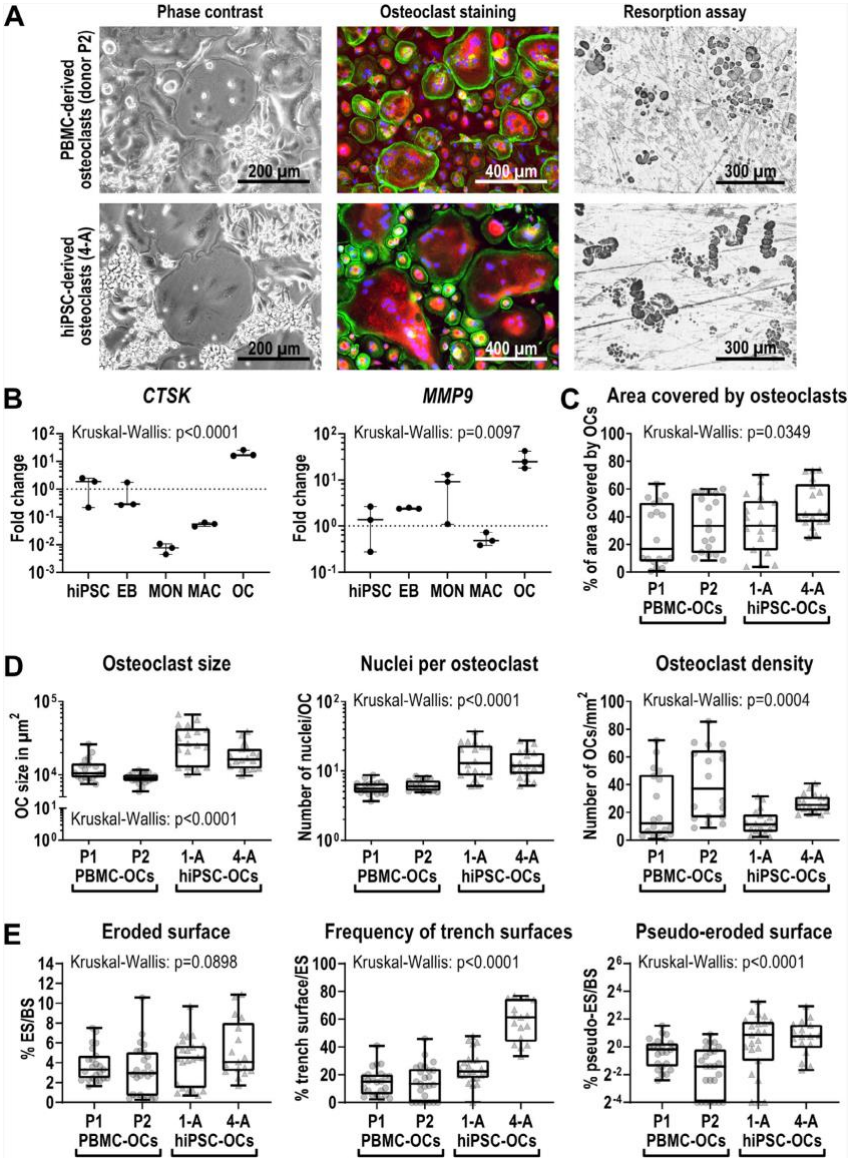

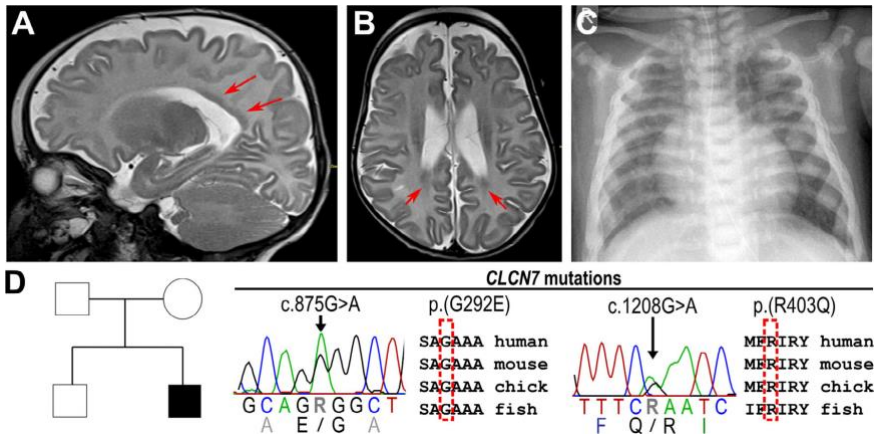

FIGURE 4. Radiologic images of an ARO patient with compound heterozygous mutations in the *CLCN7* gene. (*A*) T2W sagittal MRI and (*B*) axial MRI of the head of 4-month-old patient with reduced brain volume and periventricular laminar subependymal heterotopias (red arrows). (*C*) Chest x-ray of 7-month-old patient showing sclerosis and plump configuration of the ribs. (*D*) Pedigree of the affected family carrying the heterozygous missense mutations c.875G>A p.(G292E) and c.1208G>A p.(R403Q) in conserved regions of the *CLCN7* gene. Abbreviations: ARO, autosomal recessive osteopetrosis; MRI, magnetic resonance imaging; T2W, T2-weighted.

decided to generate ARO hiPSCs from blood cells for follow-up investigations (cell line BIHi002-A[16]).

Reduced stability and residual lysosomal localization of the mutated ClC-7 protein showing reduced ion currents

The pronounced neurological phenotype was reminiscent of patients with an activating ClC-7 mutation, impairing lysosomal function and reportedly enhancing lysosomal acidification.[9] To decipher the functional consequences of the identified mutations, we first overexpressed both p.(G292E) and p.(R403Q) ClC-7 in HeLa cells. This approach revealed normal lysosomal localization and co-localization with OSTM1 of the mutated proteins (Figure 5*A*, Figure S14). We next analyzed *CLCN7* expression levels in undifferentiated ARO hiPSCs in comparison to control hiPSCs. We could not detect any differences in *CLCN7* expression at the RNA level (Figure S15, Table S9), whereas immunoblot analysis showed a reduction of ClC-7 protein levels by 70% in ARO hiPSCs (Figure 5*B*, Figure S16). However, because residual expression and physiological localization of the ClC-7 protein were still detectable, we wondered about the electrophysiological features of the mutated Cl^-/H^+-exchanger. In comparison to WT ClC-7 protein, overexpression of the mutants in HEK-293 cells revealed an ion current density reduced to 13% in cells expressing the ClC-7 p.(R403Q) protein, whereas ion conductance was completely abolished in ClC-7 p.(G292E)-expressing cells (Figure 5*C*, Figure S17). In aggregation, the mutations lead to lower ClC-7 protein levels and strongly reduced ion currents hinting primarily at a loss-of-function pathomechanism.

FIGURE 3. Characterization of differentiated hiPSC-derived osteoclasts. Osteoclasts were differentiated from PBMCs (donors P1 and P2) and the two hiPSC lines BIHi001-A (1-A) and BIHi004-A (4-A). (*A*) Representative images of osteoclasts in culture (phase contrast), stained osteoclasts (Phalloidin in green, TRAcP in red, DAPI in blue) and osteoclast-mediated resorption shown as black-stained cavities on dentine. (*B*) Expression of osteoclast markers *CTSK* and *MMP9* determined by qRT-PCR analysis in BIHi004-A hiPSC-derived cells in undifferentiated hiPSCs, 4-day-old EBs, MONs, MACs, and OCs. Expression is normalized to hiPSCs, *GAPDH* expression was used as housekeeping control. Shown are data of three independent experiments. For statistical analysis, Kruskal-Wallis test and Dunn's multiple comparisons were used (Table S3). (*C*,*D*) Quantitative analysis of osteoclast morphology parameters. Shown are pooled data from three independent experiments. For statistical analysis, Kruskal-Wallis test and Dunn's multiple comparisons were used (Table S6). (*C*) Percentage of area covered by osteoclasts of total well area. (*D*) Osteoclast size in μm^2 (left), number of nuclei per osteoclast (middle) and osteoclast density (right). (*E*) Analysis of the resorption pattern on cortical bone slices. Percentage of the ES to the BS (left), percentage of the trench surface to the total eroded surface (middle), and percentage of the pseudo-eroded surface to the total bone surface (right). Shown are pooled data of individual bone slices used in three independent differentiation experiments of each cell line (donor P1 and 1-A $n = 23$, donor P2 $n = 25$, 4-A $n = 17$). Significance was calculated using Kruskal-Wallis and Dunn's multiple comparisons test (Table S8). Box-plots shown in *B*–*E* are plotted with median, interquartile range, maximum, and minimum values and all data points. Abbreviations: BS, total bone surface; DAPI, 4′,6-diamidino-2-phenylindole; EB, embryoid body; ES, eroded bone surface; GAPDH, glyceraldehyde-3-phosphate dehydrogenase; hiPSC, human induced pluripotent stem cell; MAC, macrophage, MCFC, myeloid-cell-forming complex; MON, monocyte-like cell; OC, osteoclast; PBMC, peripheral blood mononuclear cell; qRT-PCR, quantitative reverse transcription polymerase chain reaction; TRAcP, tartrate resistant acid phosphatase.

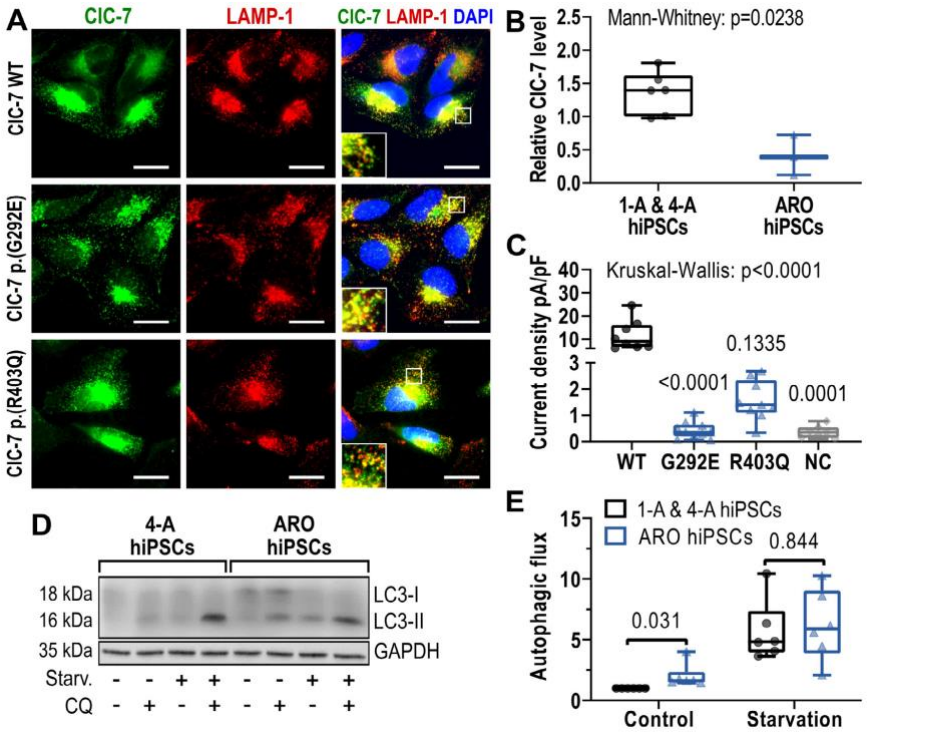

FIGURE 5. Characterization of the degradative pathway in *CLCN7* mutant cells. (*A*) Subcellular localization of ClC-7 in HeLa cells transfected with WT or mutated hClC-7 shown by immunostaining: Anti-ClC-7 (green), late endosomal/lysosomal marker anti-LAMP-1 (red), DAPI (blue). Scale bar = 25 µm. (*B*) Densitometric quantification of relative ClC-7 protein levels in undifferentiated control hiPSCs BIHi001-A (1-A) and BIHi004-A (4-A) and ARO (representative immunoblot shown in Figure S16). Shown are data of three independent experiments (pooled data points of control hiPSCs). ClC-7 levels were quantified against the loading control GAPDH. Significance was calculated by Mann-Whitney test (control hiPSCs 1-A and 4-A $n = 6$, ARO hiPSCs $n = 3$). (*C*) Electrophysiological analysis in HEK-293 cells co-transfected with OSTM1 and either WT or mutated (G292E or R403Q) hClC-7. Untransfected cells served as NC. Values of *p* shown were calculated with Dunn's multiple comparisons (compared to WT). (*D*) Representative LC3 immunoblot of BIHi004-A and ARO hiPSCs under control culture conditions or starvation with or without autophagy inhibitor CQ. (*E*) Autophagic flux in BIHi001-A, BIHi004-A, and ARO hiPSCs under normal culture conditions and starvation determined by relative LC3-II protein levels. Shown are pooled data of three independent experiments ($n = 6$), which were normalized to BIHi001-A and BIHi004-A in control culture conditions. Significance was calculated by Wilcoxon matched-pairs signed rank test. Box-plots shown in *B*, *C*, and *E* are plotted with median, interquartile range, maximum, and minimum values and all data points. Abbreviations: ARO, autosomal recessive osteopetrosis; CQ, chloroquine; DAPI, 4′,6-diamidino-2-phenylindole; GAPDH, glyceraldehyde-3-phosphate dehydrogenase; hiPSC, human induced pluripotent stem cell; LAMP-1, lysosomal-associated membrane protein 1; LC3, microtubule-associated protein light chain 3; NC, negative control; OSTM1, osteopetrosis-associated transmembrane protein 1; WT, wild-type.

Lysosomes play a fundamental role in autophagy by fusing with autophagosomes to form autolysosomes. Our analysis of the lysosomal pH in ARO hiPSCs revealed no significant differences compared to control hiPSCs (Figure S18). Nevertheless, we detected an increased level of the autophagy marker LC3-II in undifferentiated ARO hiPSCs under standard culture conditions (Figure 5*D*, Figure S18, Figure S19). To determine the autophagic flux, we both induced autophagy by starvation and inhibited the further processing of LC3-II by chloroquine treatment.[22] Although ARO hiPSCs displayed a higher autophagic flux at control conditions, there was no difference to control hiPSCs under starvation (Figure 5*E*). Because elevated LC3-II levels have been described also for murine *Clcn7*-deficient tissues,[6] this further corroborates a loss-of-function effect.

ARO hiPSCs form enlarged osteoclasts with normal marker gene expression, but without resorptive activity

As a test case for our in vitro model system, we applied the established osteoclast differentiation protocol to the patient-derived ARO hiPSCs. During all steps of differentiation ARO hiPSCs showed expression of the typical markers like hiPSCs of healthy

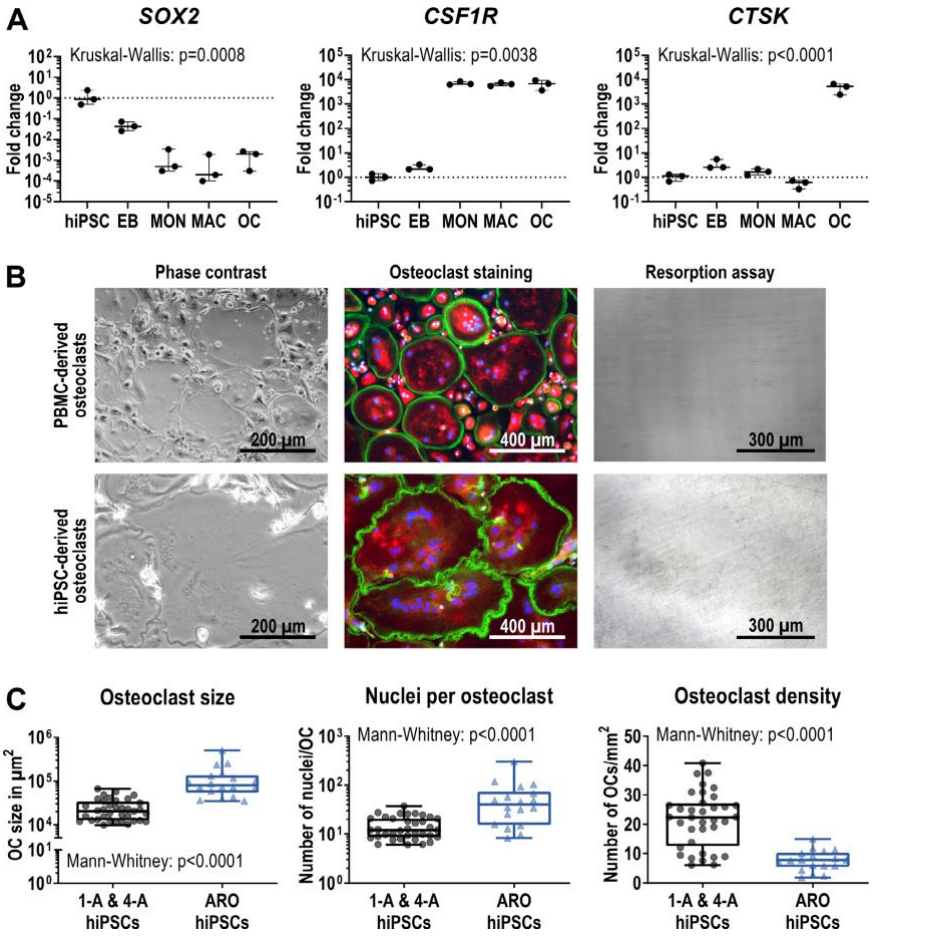

FIGURE 6. Characterization of osteoclasts differentiated from ARO hiPSCs. (*A*) Expression of pluripotency marker *SOX2*, monocytic marker *CSF1R* and osteoclast marker *CTSK* determined by qRT-PCR analysis in ARO hiPSC-derived cells in undifferentiated hiPSCs, 4-day-old EBs, MONs, MACs, and OCs. Expression is normalized to hiPSCs, *GAPDH* expression was used as housekeeping control. Shown are data of three independent experiments. For statistical analysis, Kruskal-Wallis test and Dunn's multiple comparisons were used (Table S10). (*B*) Representative images showing osteoclasts in culture (phase contrast), stained osteoclasts (Phalloidin in green, TRAcP in red, DAPI in blue) and lack of osteoclast-mediated resorption (resorption assay shows no black stained resorption cavities on dentine, see Figure 3*A* for comparison). Osteoclasts were differentiated from ARO patient-derived PBMCs and BIHi002-A ARO hiPSCs. (*C*) Osteoclasts differentiated from BIHi001-A (1-A), BIHi004-A (4-A), and ARO hiPSCs quantified according to their size in μm^2 (left), the number of nuclei per osteoclast (middle), and the osteoclast density (right). Shown are pooled data of three independent differentiation experiments of each cell line (control hiPSCs 1-A and 4-A $n = 36$, ARO hiPSCs $n = 18$). Significance was calculated using Mann-Whitney test. Box-plots shown in *A* and *C* are plotted with median, interquartile range, maximum, and minimum values and all data points. Abbreviations: ARO, autosomal recessive osteopetrosis; DAPI, 4′,6-diamidino-2-phenylindole; EB, embryoid body; hiPSC, human induced pluripotent stem cell; MAC, macrophage; MON, monocyte-like cell; PBMC, peripheral blood mononuclear cell; OC, osteoclast; qRT-PCR, quantitative reverse transcription polymerase chain reaction; TRAcP, tartrate resistant acid phosphatase.

controls (Figure 6*A*, Figure S20*A*). The production of $CD45^+$, $CD11b^+$, $CD14^+$ monocyte-like cells was even better than in BIHi004-A hiPSCs and peaked at 1×10^6 cells/well in week three (Figure 2*A*, Figure S20*B*,*C*). ARO osteoclasts were large, multinucleated TRAcP-positive cells forming a podosome belt and exhibited high expression of *CTSK* and *MMP9* (Figure 6*A*,*B*,

Figures S20*A* and S21). In addition, we also differentiated osteoclasts from PBMCs derived from the same patient. No significant differences in morphology or characteristics in the TRAcP-Phalloidin-DAPI staining were detectable between both osteoclasts (Figure 6*B*). Our quantification analysis revealed that osteoclasts differentiated from ARO hiPSCs had a larger diameter and displayed higher numbers of nuclei compared to hiPSC-osteoclasts from healthy controls (BIHi001-A and BIHi004-A), resulting in a lower number of osteoclasts per surface unit (Figure 6*C*). Notably, compared to the healthy control (Figure 3*A*), neither PBMC-derived nor hiPSC-derived ARO osteoclasts showed any sign of bone resorption activity (Figure 6*B*), suggesting that ARO hiPSC-derived osteoclasts reproduced the expected cellular phenotype.

DISCUSSION

CLCN7-related ARO is a rare genetic bone disorder due to defects in bone resorption by osteoclasts. Investigations of the pathomechanisms of ARO are important for determining the molecular effects of individual mutations as well as for providing guidance for therapeutic strategies. Although these experiments are mostly performed in mouse models, the results from these animal model experiments can often not be extrapolated to humans. Besides, the use of animal models is increasingly criticized for ethical reasons. As an alternative approach, primary patient-derived cells can be used; however, the access to biopsy material is usually limited. For osteopetrosis, PBMC-derived osteoclasts provide a good model, but the quality of blood samples is often compromised due to prolonged transport and storage. In addition, only a limited number of experiments can be performed as in vitro expansion of these primary cells is not feasible.

Several osteoclast differentiation protocols from hiPSCs have been published. In 2009, Choi et al.[26] differentiated human ESCs and iPSCs using time-consuming techniques as Percoll gradient centrifugation and cell selection by surface marker expression for progenitor enrichment. Grigoriadis et al.[15] described a protocol utilizing five different differentiation media including up to seven cytokines and supplements. More recently, Jeon et al.[13] developed a more simplified osteoclast differentiation method based on only three media and in total three different cytokines. However, the efficiency of the osteoclast differentiation or the number of produced monocytes were not specified, but appeared rather low. In 2017, Chen et al.[12] presented their osteoclast differentiation protocol, which includes only one single monocyte harvesting step and required up to six cytokines and supplement additives in four differentiation media. Finally, Cui et al.[11] published a differentiation approach in 2019 using three different differentiation media based on expensive STEMdiff APEL 2 medium supplemented with up to eight cytokines and small molecules. Furthermore, the protocol does not include a monocyte production step, lasts up to 5 weeks, and the differentiation efficiency of 1.5% is low. By contrast, the osteoclast differentiation technique described here allows the continuous harvesting of monocyte-like cells over at least 9 weeks. We only use three differentiation media supplemented with only three or two cytokines and first osteoclasts emerged already after 4 weeks. The resulting osteoclast density of 41% on average and up to 73% in some experiments is very high.

Our in-depth characterization by flow cytometry, qRT-PCR, and expression profiling showed mesodermal induction in the first step, monocyte-like cell production in the second step, and the generation of macrophages and osteoclasts in the final, third differentiation step. Terminally differentiated osteoclasts obtained by this procedure were multinucleated and displayed the characteristic podosome belt necessary for the sealing zone formation and thus the resorption process.[27]

The crucial criterion for successful osteoclast formation is bone resorption activity. Both, pits and trenches were generated by hiPSC-derived osteoclasts on dentine as well as on bovine cortical bone. Osteoclasts from BIHi004-A hiPSCs showed significantly more trenches than those from BIHi001-A and PBMCs; however, a large variability between different iPSC lines and their capacity to differentiate into specific cell types has been reported.[28] It has been demonstrated that osteoclasts making trenches reflect a more effective way of bone resorption.[19,29] Because we find that the proportion of trenches made by hiPSC-derived osteoclasts is equal or higher than for PBMCs-derived osteoclasts this highlights that iPSC-derived osteoclasts are effective at performing bone resorption. It has been shown that 67% of the variation in trenches between different osteoclast donors can be explained by the protein levels of activated cathepsin K.[30] Although we did not observe large differences in *CTSK* expression at messenger RNA (mRNA) level between PBMC-derived and hiPSC-derived osteoclasts, higher protein levels of activated cathepsin K in the latter could be a possible explanation. Moreover, it was clearly demonstrated that the level of multinucleation strongly facilitates trench-making osteoclasts, but not those that make pits. This is in line with our observation, because the increased fusion of hiPSC-derived osteoclasts correlated with a higher proportion of trenches. Recent studies suggest this might be linked to the expression of Dendritic cell–specific transmembrane protein (DC-STAMP).[31] However, the only gene known to be involved in osteoclast fusion more highly expressed in hiPSC-derived osteoclasts is *CCL2*. Again, this does not exclude differences in protein levels not correlating with mRNA levels.

To a large extent, osteoclasts derived from hiPSC lines tended to generate more "pseudoresorption", reflecting a superficial staining of the bone surface without cavitation. Thus, only mild demineralization has been switched on, but collagenolysis apparently has not. We recently described a similar behavior of *LRRK1*-deficient osteoclasts.[18] Since we observed that iPSC-derived osteoclasts often become larger than PBMC-derived osteoclasts, it is conceivable that the increased level of pseudoresorption of hiPSC-osteoclasts could be a secondary effect of very large osteoclasts having problems to polarize properly and/or to form a proper sealing zone. Interestingly, we observed that large osteoclasts generated from human HSCs showed both an enhanced resorptive activity, but also increased levels of pseudoresorption (Hennig, unpublished observations). Because hiPSC-derived osteoclasts share these characteristics with osteoclasts differentiated from HSCs, but not with PBMC-derived osteoclasts, this hints at a difference in the maturation of these cells. This phenomenon is mirrored by the production of $CD34^+$ HSC-like cells during the first days of monocyte production. In addition, although typical osteoclast marker genes such as *CTSK* were expressed at equal levels in hiPSC-osteoclasts and PBMC-osteoclasts, hiPSC-osteoclasts showed higher levels of macrophage marker genes such as *MAF* and *CSF1R*, which can be interpreted as a sign of lower maturation of these cells. It is not unusual that hiPSC-derived cells are less mature than their primary counterparts. For example, cardiomyocytes derived from hiPSCs first show characteristics typical for fetal cardiomyocytes, although the hiPSCs were generated from adult cells.[32]

To demonstrate the usability of our osteoclast differentiation protocol for functional investigations, we applied it to the patient-derived osteopetrotic hiPSC line BIHi002-A.[16] The donor was diagnosed with ARO by a chest x-ray at the age of 7 months. Before this, the failure to thrive and neurological symptoms beginning at 4 months of age were interpreted as signs of a mitochondriopathy or a lysosomal storage disease. The MRI images of the central nervous system are highly reminiscent of a case with *OSTM1* mutations described by Maranda et al.[33] Also in this case, heterotopias and global cortical atrophy were observed. Similar to our case, this patient started to have seizures at 4 months of age and died at 1 year of age. In humans as well as in mice, ("grey lethal" mutants) *OSTM1* deficiency leads to a more severe brain phenotype than loss of *CLCN7*. It is currently unknown whether the *OSTM1*-ARO developmental brain phenotype is solely due to lysosomal dysfunction because a role of this protein in cytoskeletal organization and Wnt-signaling was also discussed.[34,35] The formation of enlarged osteoclasts with enhanced multinucleation is also a typical feature of osteoclasts with both *CLCN7* and *OSTM1* deficiency.[36,37] As a possible explanation, Pata and Vacher[36] discussed the dysregulation of the calcium and NFATc1 pathway and an indirect compensation mechanism due to the resorption inability in their *Ostm1*-knockout mouse. Neutzky-Wulff et al.[37] proposed that the absence of apoptotic factors normally released during the resorption process may expand lifespan and fusion of ClC-7 deficient osteoclasts. In the light of the overlap of the cellular and clinical phenotype of *OSTM1*-deficient and *CLCN7*-deficient mouse mutants and human patients, we suggest that the main pathomechanism in both cases is primarily a defective lysosomal ion homeostasis. Possibly, an early onset of severe lysosomal perturbation during postnatal brain maturation might affect neuronal migration leading to the observed heterotopias. OSTM1 needs to bind to ClC-7 to exit the endoplasmic reticulum and for correct targeting.[21,38] Although we found that overexpressed ClC-7 harboring the mutations p.(G292E) or p.(R403Q) delivers OSTM1 to the lysosome, OSTM1 surface expression was barely detectable upon co-expression with plasma membrane-localized mutant ClC-7 (data not shown). If OSTM1 would play a role independent of ClC-7, the remaining and correctly targeted OSTM1 should be sufficient to prevent the phenotype, which is not the case.

The brain abnormalities of our patient appeared disproportionally severe compared to the degree of osteosclerosis and tardive bone marrow failure. The mutation p.(R403Q) was described in combination with the mutation p.(G521R) in another patient with global brain atrophy.[24] Because a heterozygous *CLCN7* gain-of-function mutation leading to increased lysosomal acidification and swelling was recently described that caused an exceptional neurological phenotype without bone involvement, we tested for the electrophysiological properties of the mutated ClC-7.[9] Although the severe amino acid exchange p.(G292E) completely abolished function, currents elicited by p.(R403Q) were changed in quantity (13% of WT levels), but not in quality. Because we previously found in transgenic experiments that 25% to 30% residual ClC-7 expression is needed for full cellular functionality, we assume that the overall reduced ClC-7 protein levels and the reduced currents for p.(R403Q) are far below this threshold.[39]

To address the possible role of abnormal lysosome functionality in the observed phenotypes we investigated the lysosomal pH. Lysosomal pH remained unchanged in osteopetrotic hiPSCs, and these findings correlate with previous investigations in mouse fibroblasts, neurons, and macrophages from *Clcn7*-knockout mice.[4,40] The reason for the unchanged lysosomal pH is still unclear and controversially discussed. It has been shown that other cation channels support lysosomal acidification and ClC-7 is not essential.[7,40] However, ClC-7 probably regulates lysosomal function through intraluminal chloride concentrations and impacts lysosomal ion homeostasis in general.[41–43] However, we further investigated autophagy in ARO hiPSCs, because Wartosch et al.[6] and Weinert et al.[44] reported accumulation of the autophagy marker LC3-II in *Clcn7*-deficient murine tissues. Under normal culture conditions we observed similarly elevated levels of the autophagy marker LC3-II and an increase in the autophagic flux. Under starvation, however, this difference vanished, implying similar autophagy levels at maximum stimulation. Enhanced LC3-II levels might be due to a reduced turnover of autophagosomes, as the intra-autophagosomal LC3-II is only degraded by lysosomal proteases after fusion of the autophagosome with the lysosome and it was proposed that proteins are degraded with slower kinetics in ClC-7 knockout cells.[45] Interestingly, perturbed autophagy is the basis for several neurodevelopmental disorders.[46]

In future studies, poorly understood aspects of the osteopetrotic phenotype like the enlarged osteoclasts, the unchanged lysosomal pH or the defective autophagic flux could be molecularly dissected using engineered hiPSCs. Moreover, therapeutic approaches, including the research for novel targeted therapies, could be pursued in osteopetrotic hiPSC lines like the one presented here. Our novel differentiation protocol also might prove valuable for in vitro disease modeling of other osteoclast-related pathologies.

ACKNOWLEDGMENTS

This project was part of the BCRT crossfield project GenoPro and was supported by the Berlin Institute of Health (BIH) through a BIH translational PhD grant to Uwe Kornak and Zsuzsanna Izsvák. This work was supported by the German Federal Ministry of Education and Research/German Center for Cardiovascular Research (to Lukas Cyganek), and by the German Research Foundation (SFB1002 S01 to Lukas Cyganek). This work was partly funded by the funding program of the academic grants committee of the Charité – Universitätsmedizin Berlin. Support was also provided by the Helmholtz Association through program-oriented funding and by the Federal Ministry of Education and Research, Germany, in the Programme HealthResearch (BCRT grant no. 13GW0098 and 13GW0099) and the European Community's Seventh Framework Programme under grant agreement no. 602300 (SYBIL) to Uwe Kornak. We thank Frank Konietschke and Asanka Gunawardana for their statistical advice and multiple helpful discussions. We are grateful to the BIH Core Facility Stem Cells for helpful advice and technical assistance regarding hiPSCs. We thank Jean-Marie Delaissé for inspiring discussions on osteoclasts and the initiation of a fruitful collaboration. We thank Jacob Bastholm Olesen for excellent technical assistance with the resorption analysis. We are grateful to Nico Lachmann and his team for their helpful advice regarding the initial steps of the hematopoietic differentiation process. Many thanks to Katriina Aalto-Setälä from Tampere University for providing one of the used induced pluripotent stem cell lines. The authors thank the UMG Stem Cell Unit for excellent technical support. The antibody H4A3 developed by August, J.T. / Hildreth, J.E.K. was

obtained from the Developmental Studies Hybridoma Bank, created by the NICHD of the NIH and maintained at The University of Iowa, Department of Biology, Iowa City, IA 52242. Open Access funding enabled and organized by Projekt DEAL.

Author contributions: Study design: Uta Rössler, Anna Floriane Hennig, Zsuzsanna Izsvák, Uwe Kornak. Study conduct: Uta Rössler, Anna Floriane Hennig, Uwe Kornak. Data collection: Uta Rössler, Anna Floriane Hennig, Nina Stelzer, Shroddha Bose, Johannes Kopp, Lukas Cyganek, Giovanni Zifarelli, Salaheddine Ali, Maja von der Hagen, Elisabeth Strässler, Gabriele Hahn. Data analysis: Uta Rössler, Anna Floriane Hennig, Shroddha Bose, Johannes Kopp, Kent Søe, Lukas Cyganek, Giovanni Zifarelli, Salaheddine Ali, Maja von der Hagen, Tobias Stauber, Uwe Kornak. Data interpretation: Uta Rössler, Anna Floriane Hennig, Kent Søe, Lukas Cyganek, Michael Pusch, Tobias Stauber, Manfred Gossen, Harald Stachelscheid, Uwe Kornak. Writing manuscript: Uta Rössler, Anna Floriane Hennig, Uwe Kornak. Revising manuscript content: Uta Rössler, Anna Floriane Hennig, Kent Søe, Lukas Cyganek, Tobias Stauber, Zsuzsanna Izsvák, Manfred Gossen, Harald Stachelscheid, Uwe Kornak. Approving final version of manuscript: all authors; The following individuals take responsibility for the integrity of the data analysis: Uta Rössler, Anna Floriane Hennig, Uwe Kornak.

DISCLOSURES

The authors report no conflict of interest.

PEER REVIEW

The peer review history for this article is available at https://publons.com/publon/10.1002/jbmr.4322.

DATA AVAILABILITY STATEMENT

Data are available upon request.

REFERENCES

1. Sobacchi C, Schulz A, Coxon FP, Villa A, Helfrich MH. Osteopetrosis: genetics, treatment and new insights into osteoclast function. Nat Rev Endocrinol. 2013;9(9):522-536.
2. Supanchart C, Kornak U. Ion channels and transporters in osteoclasts. Arch Biochem Biophys. 2008;473(2):161-165.
3. Chalhoub N, Benachenhou N, Rajapurohitam V, et al. Grey-lethal mutation induces severe malignant autosomal recessive osteopetrosis in mouse and human. Nat Med. 2003;9(4):399-406.
4. Kasper D, Planells-Cases R, Fuhrmann JC, et al. Loss of the chloride channel ClC-7 leads to lysosomal storage disease and neurodegeneration. EMBO J. 2005;24(5):1079-1091.
5. Kornak U, Kasper D, Bösl MR, et al. Loss of the ClC-7 chloride channel leads to osteopetrosis in mice and man. Cell. 2001;104(2):205-215.
6. Wartosch L, Fuhrmann JC, Schweizer M, Stauber T, Jentsch TJ. Lysosomal degradation of endocytosed proteins depends on the chloride transport protein ClC-7. FASEB J. 2009;23(12):4056-4068.
7. Weinert S, Jabs S, Supanchart C, et al. Lysosomal pathology and osteopetrosis upon loss of H^+-driven lysosomal Cl^- accumulation. Science. 2010;328(5984):1401-1403.
8. Ott CE, Fischer B, Schröter P, et al. Severe neuronopathic autosomal recessive osteopetrosis due to homozygous deletions affecting OSTM1. Bone. 2013;55(2):292-297.
9. Nicoli ER, Weston MR, Hackbarth M, et al. Lysosomal storage and albinism due to effects of a De Novo CLCN7 variant on lysosomal acidification. Am J Hum Genet. 2019;104(6):1127-1138.
10. Lachmann N, Ackermann M, Frenzel E, et al. Large-scale hematopoietic differentiation of human induced pluripotent stem cells provides granulocytes or macrophages for cell replacement therapies. Stem Cell Rep. 2015;4(2):282-296.
11. Cui X, Cui Y, Shi L, Luan J, Zhou X, Han J. A preliminary study on the mechanism of skeletal abnormalities in Turner syndrome using inducing pluripotent stem cells (iPS)-based disease models. Intractable Rare Dis Res. 2019;8(2):113-119.
12. Chen IP, Luxmi R, Kanaujiya J, Hao Z, Reichenberger EJ. Craniometaphyseal dysplasia mutations in ANKH negatively affect human induced pluripotent stem cell differentiation into osteoclasts. Stem Cell Rep. 2017;9(5):1369-1376.
13. Jeon OH, Panicker LM, Lu Q, Chae JJ, Feldman RA, Elisseeff JH. Human iPSC-derived osteoblasts and osteoclasts together promote bone regeneration in 3D biomaterials. Sci Rep. 2016;6:26761.
14. Neri T, Muggeo S, Paulis M, et al. Targeted gene correction in osteopetrotic-induced pluripotent stem cells for the generation of functional osteoclasts. Stem Cell Rep. 2015;5(4):558-568.
15. Grigoriadis AE, Kennedy M, Bozec A, et al. Directed differentiation of hematopoietic precursors and functional osteoclasts from human ES and iPS cells. Blood. 2010;115(14):2769-2776.
16. Hennig AF, Rössler U, Boiti F, et al. Generation of a human induced pluripotent stem cell line (BIHi002-A) from a patient with CLCN7-related infantile malignant autosomal recessive osteopetrosis. Stem Cell Res. 2019;35:101367.
17. Buchrieser J, James W, Moore MD. Human induced pluripotent stem cell-derived macrophages share ontogeny with MYB-independent tissue-resident macrophages. Stem Cell Rep. 2017;8(2):334-345.
18. Howaldt A, Hennig AF, Rolvien T, et al. Adult osteosclerotic metaphyseal dysplasia with progressive osteonecrosis of the jaws and abnormal bone resorption pattern due to a LRRK1 splice site mutation. J Bone Miner Res. 2020;35(7):1322-1332.
19. Merrild DM, Pirapaharan DC, Andreasen CM, et al. Pit- and trench-forming osteoclasts: a distinction that matters. Bone Res. 2015;3:15032.
20. Leisle L, Ludwig CF, Wagner FA, Jentsch TJ, Stauber T. ClC-7 is a slowly voltage-gated 2Cl(−)/1H(+)-exchanger and requires Ostm1 for transport activity. EMBO J. 2011;30(11):2140-2152.
21. Stauber T, Jentsch TJ. Sorting motifs of the endosomal/lysosomal CLC chloride transporters. J Biol Chem. 2010;285(45):34537-34548.
22. Klionsky DJ, Abdelmohsen K, Abe A, et al. Guidelines for the use and interpretation of assays for monitoring autophagy (3rd edition). Autophagy. 2016;12(1):1-222.
23. Takayanagi H. Osteoimmunology: shared mechanisms and crosstalk between the immune and bone systems. Nat Rev Immunol. 2007;7(4):292-304.
24. Pangrazio A, Pusch M, Caldana E, et al. Molecular and clinical heterogeneity in CLCN7-dependent osteopetrosis: report of 20 novel mutations. Hum Mutat. 2010;31(1):E1071-E1080.
25. Phadke SR, Fischer B, Gupta N, Ranganath P, Kabra M, Kornak U. Novel mutations in Indian patients with autosomal recessive infantile malignant osteopetrosis. Indian J Med Res. 2010;131:508-514.
26. Choi KD, Vodyanik MA, Slukvin II. Generation of mature human myelomonocytic cells through expansion and differentiation of pluripotent stem cell-derived $lin^-CD34^+CD43^+CD45^+$ progenitors. J Clin Invest. 2009;119(9):2818-2829.
27. Teitelbaum SL. The osteoclast and its unique cytoskeleton. Ann N Y Acad Sci. 2011;1240:14-17.
28. Ortmann D, Vallier L. Variability of human pluripotent stem cell lines. Curr Opin Genet Dev. 2017;46:179-185.
29. Søe K, Delaissé JM. Time-lapse reveals that osteoclasts can move across the bone surface while resorbing. J Cell Sci. 2017;130(12):2026-2035.
30. Borggaard XG, Pirapaharan DC, Delaissé JM, Søe K. Osteoclasts' ability to generate trenches rather than pits depends on high levels of active cathepsin K and efficient clearance of resorption products. Int J Mol Sci. 2020;21(16):5924.
31. Møller AMJ, Delaissé JM, Olesen JB, et al. Fusion potential of human osteoclasts in vitro reflects age, menopause, and in vivo bone

resorption levels of their donors-A possible involvement of DC-STAMP. Int J Mol Sci. 2020;21(17):6368.

32. Bellin M, Marchetto MC, Gage FH, Mummery CL. Induced pluripotent stem cells: the new patient? Nat Rev Mol Cell Biol. 2012;13(11):713-726.
33. Maranda B, Chabot G, Décarie JC, et al. Clinical and cellular manifestations of OSTM1-related infantile osteopetrosis. J Bone Miner Res. 2008;23(2):296-300.
34. Feigin ME, Malbon CC. OSTM1 regulates beta-catenin/Lef1 interaction and is required for Wnt/beta-catenin signaling. Cell Signal. 2008;20(5):949-957.
35. Pandruvada SN, Beauregard J, Benjannet S, et al. Role of Ostm1 cytosolic complex with kinesin 5B in intracellular dispersion and trafficking. Mol Cell Biol. 2015;36(3):507-521.
36. Pata M, Vacher J. Ostm1 bifunctional roles in osteoclast maturation: insights from a mouse model mimicking a human OSTM1 mutation. J Bone Miner Res. 2018;33(5):888-898.
37. Neutzsky-Wulff AV, Sims NA, Supanchart C, et al. Severe developmental bone phenotype in ClC-7 deficient mice. Dev Biol. 2010;344 (2):1001-1010.
38. Lange PF, Wartosch L, Jentsch TJ, Fuhrmann JC. ClC-7 requires Ostm1 as a beta-subunit to support bone resorption and lysosomal function. Nature. 2006;440(7081):220-223.
39. Supanchart C, Wartosch L, Schlack C, et al. ClC-7 expression levels critically regulate bone turnover, but not gastric acid secretion. Bone. 2014;58:92-102.
40. Steinberg BE, Huynh KK, Brodovitch A, et al. A cation counterflux supports lysosomal acidification. J Cell Biol. 2010;189(7):1171-1186.
41. Zifarelli G. A tale of two CLCs: biophysical insights toward understanding ClC-5 and ClC-7 function in endosomes and lysosomes. J Physiol. 2015;593(18):4139-4150.
42. Stauber T, Jentsch TJ. Chloride in vesicular trafficking and function. Annu Rev Physiol. 2013;75:453-477.
43. Astaburuaga R, Quintanar Haro OD, Stauber T, Relógio A. A mathematical model of lysosomal ion homeostasis points to differential effects of Cl^- transport in Ca^{2+} dynamics. Cell. 2019;8(10):1263.
44. Weinert S, Jabs S, Hohensee S, Chan WL, Kornak U, Jentsch TJ. Transport activity and presence of ClC-7/Ostm1 complex account for different cellular functions. EMBO Rep. 2014;15(7):784-791.
45. Wartosch L, Stauber T. A role for chloride transport in lysosomal protein degradation. Autophagy. 2010;6(1):158-159.
46. Teinert J, Behne R, Wimmer M, Ebrahimi-Fakhari D. Novel insights into the clinical and molecular spectrum of congenital disorders of autophagy. J Inherit Metab Dis. 2020;43(1):51-62.

Curriculum vitae

Mein Lebenslauf wird aus datenschutzrechtlichen Gründen in der elektronischen Version meiner Arbeit nicht veröffentlicht.

Complete list of publications

Rössler, U., Hennig, A. F., Stelzer, N., Bose, S., Kopp, J., Søe, K., Cyganek, L., Zifarelli, G., Ali, S., von der Hagen, M., Strässler, E., Hahn, G., Pusch, M., Stauber, T., Izsvák, Z., Gossen, M., Stachelscheid, H., Kornak, U., 2021. Efficient generation of osteoclasts from human induced pluripotent stem cells and functional investigations of lethal *CLCN7*-related osteopetrosis. J. Bone Miner. Res. Off. J. Am. Soc. Bone Miner. Res.

Impact factor 2020: 6.741

Amini, L., Wagner, D. L., **Rössler, U**., Zarrinrad, G., Wagner, L. F., Vollmer, T., Wendering, D. J., Kornak, U., Volk, H.-D., Reinke, P., Schmueck-Henneresse, M., 2021. CRISPR-Cas9-Edited Tacrolimus-Resistant Antiviral T Cells for Advanced Adoptive Immunotherapy in Transplant Recipients. Mol. Ther. J. Am. Soc. Gene Ther. 29, 32–46.

Impact factor 2020: 11.454

Howaldt, A., Hennig, A. F., Rolvien, T., **Rössler, U**., Stelzer, N., Knaus, A., Böttger, S., Zustin, J., Geißler, S., Oheim, R., Amling, M., Howaldt, H.-P., Kornak, U., 2020. Adult Osteosclerotic Metaphyseal Dysplasia With Progressive Osteonecrosis of the Jaws and Abnormal Bone Resorption Pattern Due to a *LRRK1* Splice Site Mutation. J. Bone Miner. Res. Off. J. Am. Soc. Bone Miner. Res. 35, 1322–1332.

Impact factor 2020: 6.741

Hennig, A. F., **Rössler, U**., Boiti, F., von der Hagen, M., Gossen, M., Kornak, U., Stachelscheid, H., 2019. Generation of a human induced pluripotent stem cell line (BIHi002-A) from a patient with *CLCN7*-related infantile malignant autosomal recessive osteopetrosis. Stem Cell Res. 35, 101367.

Impact factor 2018: 3.929

Acknowledgement

I am deeply grateful to my supervisor Uwe Kornak for giving me the opportunity to prepare this PhD thesis in his research lab. Thank you for the guidance and support even after two maternity leaves and the transfer of the lab to Göttingen.

I am very thankful for the opportunity to work on this exciting topic and special thanks go to Uwe Kornak, Harald Stachelscheid, Floriane Hennig and Zsuzsanna Izsvák for the design and permanent transformation of the research project. I learnt so much during my time as a PhD student and loved to work on this topic.

Gigantic thanks go to my friend Floriane Hennig. Without you the PhD time would definitely not have been the same. We shared good as well as bad times, we had so much fun and tears together. You pushed me and helped me, you kicked my ass and held my hand. This work would not exist without you.

I would like to thank all members of the research group for helping out, giving good advice, for sharing experiences and the great atmosphere in the lab and beyond. I loved working with you. Special thanks go to Guido Vogt, Daniela Keller, Michael Thelen, Namrata Saha, Johannes Kopp, Miguel Rodriguez, Alexej Knaus, Naji El Choubassi and Nina Stelzer. Thanks to Oliver Klein for great discussions about everything around and your support.

Furthermore, I thank the whole team of the BIH iPS Core Facility for working in their lab, learning everything about hiPSCs, the great atmosphere and lots of fun. Special thanks go to Janine Cernoch, Judit Küchler, Kristin Fischer, Tanja Fisch and Valeria Fernandez Vallone.

I want to acknowledge the BSRT graduate school, in particular Sabine Bartosch and Bianca Kühn, who supported this PhD project in many ways. Additionally, I'm grateful to the Berlin Institute of Health, who offered a BIH translational PhD grant to Uwe Kornak and Zsuzsanna Izsvák in order to get this project on its way.

I thank Nico Lachmann, Tobias Stauber, Kent Soe and their research groups for the great collaboration, helpful advice and sharing their experiences with me. Thanks to Asanka Gunawardana for discussing statistical analysis with me.

I would also like to thank Uwe Kornak, Floriane Hennig and Deborah Smart for reviewing my thesis and for giving creative suggestions regarding language, structure, and layout.

Finally, I wish to thank my family, in particular my parents and my husband, for their support and encouragement as well as their patience with me. Thank you for taking care of me and my kids and for giving me the time to finally complete this PhD thesis.

In deep sorrow my thanks also go to MT and his family.